Exploration of scalable industrial platforms for the commercial production of active molecules from microalgae cell walls

Submitted by

Gino Schiano di Visconte

to the University of Exeter as a thesis for the degree of

Doctor of Philosophy in Biological Sciences

June 2022

I certify that all material in this thesis which is not my own work has been identified and that any material that has previously been submitted and approved for the award of a degree by this or any other University has been acknowledged.

Acknowledgements

First and foremost, I would like to thank Algenuity Ltd for believing in me and sponsoring my PhD studies; Denis Spicer, Managing Director of Spicer Consulting Ltd and Andrew Spicer, my supervisor and CEO of Algenuity Ltd for their trust and support.

I am incredibly grateful to Professor Mike Allen for both his expertise and constant support and encouragement throughout the project and I would also like to thank my co-supervisor Dr Stephen Michell for his expertise and guidance.

I would also like to thank Gavin Lowe, Sam Sizer and Denise Pallister for their technical support at Algenuity Ltd and Dr. Alex Pudney CSO at Algenuity Ltd, Dr. Richard Smith Strain Development Manager at Algenuity Ltd, Dr. Emma Ransom-Jones, Senior Scientist at Algenuity Ltd and Dr. Aumaya Taleb, Process Development Manager at Algenuity Ltd for their expertise and constant support.

Thanks also to Dr. Stavroula Balabani, Professor of Fluid Mechanics at University College London for the access to her laboratory and equipment and Anastasia Papadopoulou, PhD student, Department of Mechanical Engineering at UCL, for the support during the sample analysis; Creative Proteomics, 45-1 Ramsey Road, Shirley, NY 11967, USA, for the EPS analysis with regard to molecular weight determination, composition and glycosidic linkage determination.

Finally, I would like to especially thank my wife Francesca Baldini, my two kids Max and Elena and my whole family who have always been there to provide moral support and a confidence boost.

Abstract

Food, nutraceutical, cosmeceutical, pharmaceutical and biomedical industries are putting significant effort into looking for new natural ingredients [1,2]. Microalgae have been recognised as potential sources of high-value chemicals, with most attention focused on antioxidants, pigments and specialty oils [3]. An under-exploited group of biochemicals produced by microalgae are extracellular polymeric substances (EPS) with hyaluronan (HA) representing one of them. Current industrial production methodologies for HA leave opportunities for the establishment of improved routes with higher molecular mass, enhanced biophysical properties, lower production costs and non-bacterial nor animal origins as key unique selling points. At present, incumbent platforms are either based upon *Streptococcus spp.* (pathogen) bacterial fermentation, modified (GM) *Bacillus subtilis* or derived from animal tissues.

Furthermore, the extraction of various economically exploitable cell components from microalgal biomass is at the core of a successful microalgal biorefinery approach, and it remains a current bottleneck for the economic feasibility of microalgal biotechnological processes [4]. Cell disruption is often required to break down the hard and complicated microalgal cell walls in order to retrieve microalgal constituents such as proteins, lipids, and polysaccharides. Viral enzymes may play a beneficial role in this scenario and might be used to facilitate genetic engineering by overcoming the cell wall barrier or for biorefinery purposes.

This project's hypothesis was that it was feasible for microalgae to produce HA. The objectives included investigating a stress-induced platform for the possible

production of HA, learning how Chlorovirus/*C. varibilis* infection leads to HA formation, improving the HA production for the latter platform and looking into intriguing enzymes that can break down polysaccharides.

This PhD project focused on exploring, characterizing and developing new platforms in order to achieve profitable industrial production of valuable compounds from microalgae and identify viral enzymes that could help with the processing of *Chlorella* cells for multiple applications. Two platforms were successfully explored for the production of valuable polysaccharides, and multiple enzymes were identified, produced, characterised and evaluated for *Chlorella* cell wall digestion to enable possible biorefinery approaches of a non-domesticated *Chlorella vulgaris* strain.

Contents

List of Illustrations

List of Tables

Abbreviations

£	pound sterling
°C	degree Celsius
µE	microEinsteins
µg	micrograms
µL	microlitres
µm	micrometre
µM	micromolar
2,3-GlcA	2,3 linked glucuronic acid residue
2-Gal	2 linked galactopyranosyl residue
2-Glc	2 linked glucopyranosyl residue
3,4,6-Gal	3,4,6 linked galactopyranosyl residue
3,4-Gal	3,4 linked galactopyranosyl residue
3,4-Glc	3,4 linked glucopyranosyl residue
3,4-GlcA	3,4 linked glucuronic acid residue
3,6-Gal	3,6 linked galactopyranosyl residue
3-Gal	3 linked galactopyranosyl residue
3-Glc	3 linked glucopyranosyl residue
3-Hexf	3 linked hexofuranosyl residue

4,6-Gal	4,6 linked galactopyranosyl residue
4-Gal	4 linked galactopyranosyl residue
4-Glc	4 linked glucopyranosyl residue
4-GlcA	4 linked glucuronic acid residue
6-Gal	6 linked galactopyranosyl residue
ANOVA	analysis of variance
BBM	Bold's basal medium
BSA	bovine serum albumin
C/N	carbon nitrogen ratio
CAPEX	capital expenditures
CAZy	carbohydrate-Active enzymes
CCAP	culture collection of algae and protozoa
CPS	capsular polymeric substances
Da	Dalton
Dm	dry mass
DMEM	Dulbecco's modified Eagle's medium
DNA	deoxyribonucleic acid
DOM	dissolved organic matter
EAscA	equivalence of ascorbic acid

EPS	extracellular polymeric substances
FBS	fetal bovine serum
FERM	fermentation media
GAG	glycosaminoglycan
Gal	galactose
GC/MS	gas chromatography/mass spectrometry
GFAT	glutamine:fructose-6-phosphate amidotransferase
Glc	glucose
GlcA	glucuronic acid
GM	genetically modified
GT	glycosyltransferase
HA	hyaluronan / hyaluronic acid
HAS	hyaluronan synthase
HCl	hydrochloric acid
HDMS	hexamethyldisilazane
HMW	high molecular weight
HSM	high salt medium
HTP	HDMS:TMCS:pyridine
ID	internal diameter

IPTG	Isopropyl-β-D-thiogalactoside
ITS2	internal transcribed spacer 2
KOH	potassium hydroxide
LED	light emitting diode
MBBM	modified Bold's basal medium
Mn	average molecular mass
MOI	multiplicity of infection
MSD	mass selective detector
mTorr	millitorr
MW	molecular weight
$NaBD_4$	sodium borodeuteride
OD	optical density
OPEX	operating expenditures
PAR	photosynthetically active radiation
PBRs	photobioreactors
PBS	phosphate buffer saline
PMAAs	partially methylated alditol acetates
PmHAS	*Pasturella multocida*'s HAS
POM	particulate organic matter

PS	polysaccharides
PUFAs	polyunsaturated fatty acids
qPCR	quantitative PCR
RCF	relative centrifugal force
RNA	ribonucleic Acid
RT-PCR	reverse transcription PCR
SAG	culture collection of algae at Göttingen University
SAMS	Scottish association for marine science campus
SDS	sodium dodecyl sulfate
SDS-PAGE	sodium dodecyl sulfate–polyacrylamide gel electrophoresis
*Se*HAS	*Streptococcal* HAS
TAE	Tris base, acetic acid and EDTA
TAP	Tris-acetate-phosphate
TBE	Tris-Borate-EDTA
TFA	trifluoro acetic acid
TFF	tangential flow filtration
t-Gal	terminal galactopyranosyl residue
t-Galf	terminal galactofuranosyl residue
t-GlcA	terminal glucuronic acid residue

TMCS	trimethylchlorosilane
TMD	transmembrane domains
TMS	per-O-trimethylsilyl
UGDH	uridine diphosphate-glucose dehydrogenase
USD / $	United States dollar

Chapter 1 - General Introduction

Part of this general introduction has already been published with me as first Author and with my supervisors as co-authors [5] (Appendix A).

1.1 Microalgal production

Microalgae are a varied collection of organisms that can grow through photosynthesis with some species also able to utilise carbon sources other than CO_2, such as simple sugars. These organisms play an important part in many ecosystems and are found all around the world in salt water, fresh water, deserts, and extreme environments. A variety of microalgae have been studied for the possibility of extracting value-added products with exceptional pharmacological and biological properties, animal and fish feed, cosmetics, chemicals and polymers, pollution management, and other applications [6].

Since 1980, when the price of crude oil hit and exceeded $100 per barrel, there has been a lot of interest in using microalgal biomass as a source of bulk, commodity chemicals. [7]. Several firms spent substantially in the subsequent decades to investigate the reality of microalgae-derived biofuels [8], originally stating that the findings were within reach. Despite bringing promise to the whole field of study in 2008, when the oil price hit its peak of $163.80 per barrel, the harsh reality of process economics and the unmet challenge of delivering the necessary scale to really impact the fuel supply chain failed to solve the underlying operational challenges with productivity and production costs. Simply put, microalgal biomass productivity was insufficient, the scales involved were inadequate, and the extraction, purification, and processing expenses were too

costly. Faced with the harsh realities of capitalism, the vast majority of enterprises involved in this arena went bankrupt or were re-positioned as producer of higher-value algae-derived goods, primarily for use as foods and food ingredients, feeds, nutraceuticals, or cosmetics [8].

A greener future inspired by microalgae is still a possible option. As the early biofuel advocates left the field, a new era of thoughtful and measured activity emerged, while biotechnology advancements have provided new and diversified economic options. The basic benefits of microalgae-based processes that sparked initial industry interest have not altered. Microalgae have simple growth requirements, requiring water, nitrogen, phosphates, and trace elements to grow, while fixing CO_2 using light energy. Because of these features, they are ideal candidates for wastewater treatment and industrial CO_2 bioremediation. However, the metabolic variety and physiological plasticity of microalgae ensure that the biomass created from their development may have additional intrinsic value in addition to the remediation activities they may perform during growth. Thus, combining these 'service value' processes with the biorefinery idea may open up new avenues for changing perceptions of environmental degradation, transforming challenges into long-term economic opportunities [9]. The extraction of numerous commercially exploitable cell components from microalgal biomass is crucial to a successfully delivered microalgal biorefinery, and remains a current hurdle for the economic viability of many microalgal biotechnological operations that attempt to use this approach [4]. Cell disruption is frequently necessary in order to retrieve microalgal components such as proteins, lipids, and polysaccharides from biomass that is encapsulated within hard and complicated

microalgal cell walls. Viral cell wall digesting enzymes may be useful in this context for biorefinery objectives for recalcitrant strains by breaking the cell wall barrier [10].

Phototrophic microalgal culture systems may be divided into two types: closed (for example vertical or horizontal tubes, flat panels, or other photobioreactors [PBRs]) and open (for instance open ponds, paddle-wheel driven raceways, and cascade raceways). Open ponds or raceways (Figure 1.1) are primarily used for wastewater treatment or feed production because they generally require less capital expenditure (CAPEX) to set up and operation expense (OPEX) to run, but they provide limited control over light, temperature and CO_2 conditions; the biomass is susceptible to external contamination or crashes due to predation and for these reasons is not suitable for pharmaceutical applications.

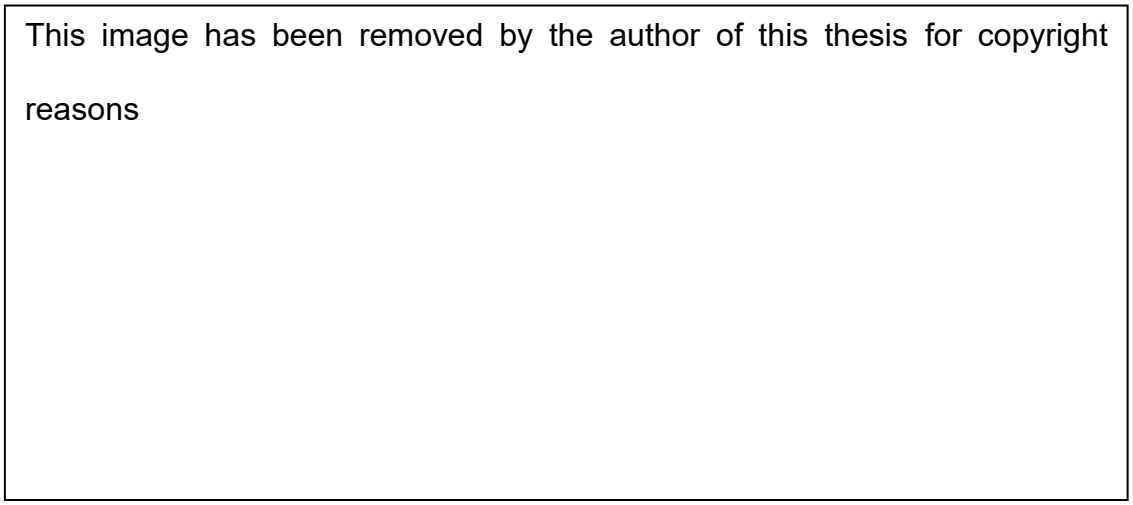

Figure 1.1. Example of open raceway pond of Earthrise in California, U.S. Taken from [11].

Closed PBRs provide increased culture stability and biomass densities, as well as decreased contamination risks, but they have higher CAPEX and OPEX. Closed systems are now the de facto systems of choice for genetically modified (GM) microalga growth due to the widely accepted necessity for contained GM

culture. Current large-scale open culturing technologies yield low density cultures (0.8–3.6 g/L) [4] and one of the key limiting variables in autotrophic development is light penetration into the culture [12]. Despite the obvious commercial risks discussed previously, academic interest has focused on improving photosynthetic efficiencies modifying the organisms or through cultivation system improvements such as simply increased mixing or decreasing the depth of the culture and thus increasing the relative surface area used for cultivation [13].

Cascade raceways are a more recently developed innovation in open production systems [13], where the design creates a shallow moving flow of culture while maintaining an extremely short light path length and achieving significantly higher biomass densities (e.g., 15–35 g/L of *Chlorella* spp. has been reported [14]). Flat panel PBRs (Figure 1.2(a)) appear to be the most productive alternative for closed culture (24 g/L of biomass for *Chlorella sorokiniana*) when compared to tubular PBRs (Figure 1.2(b)). However, these systems have very high costs and scaling issues [15]. The foam-bed PBR is a new closed system under evaluation in which algae are trapped in bubbles with a foaming agent and bovine serum albumin suspension to stabilise them; lower gas pressure is required for mixing, but the addition of a foam-breaking system is required, so overall operating costs are potentially higher, and yields are not specified as of yet [16].

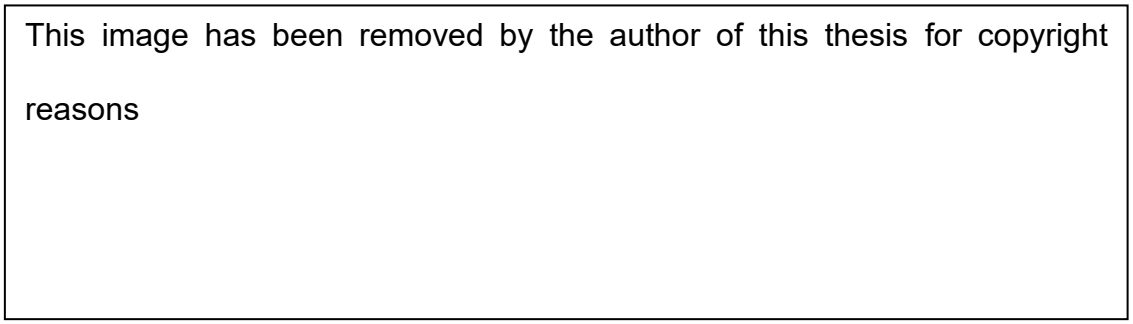

(a) (b)

Figure 1.2. (a) Example of tubular PBR, Phyco-Flow™ Serpentine PBR. Taken from [17]; (b) Example of flat panel PBR. Taken from [18].

Unfortunately, even with autotrophic production, costs are still too high for the market of low-value applications (£ 2-5 per kg) (e.g., biofuels and animal feed). Current biomass prices are still about £20–£30 per kg, supply is not stable or anywhere near enough to satisfy the demand and in order to compete with other plant sources in food, for example, it's needed to strive for £10–£15 per kg of dry biomass initially and ultimately realise future prices in the single digits to have any mainstream market impact. The main disadvantages of autotrophic production are the amount of space required for large scale production (thin layers of cultures are required for best light exposure to achieve a higher biomass density), the harvesting costs due to the low cell density, the slow growth rates of the strains (in the best conditions, doubling once in slightly less than a day), and the high energy demand required to maintain the best growth conditions controlling light exposure, temperature, pH, mixing, and CO_2 feed, all of which lead to an overall carbon positive process, unless coupled with renewable sources for power production.

The outputs of the previously discussed production scenarios are still far from the heterotrophic production systems that can be used to produce some microalgal strains at industrial scale, where biomass densities of 100 g/L dry weight and above can be routinely achieved, at which point the biomass does not need to be dewatered but can simply be dried, disrupted, or extracted, eliminating one energy-intensive step of the downstream process. Furthermore, the land and water required for a comparable production is lower through fermentation production due to the higher biomass density [19]. For this reason, research is intensifying on the hunt for microalgae strains that can grow in mixotrophic or heterotrophic environments in order to have a smoother and faster road to market and perhaps lower production costs. Coupling the process with renewable sources for power production would reduce the carbon footprint merely to the CO_2 production during fermentation and the generation of the carbon source used to feed the organisms [20].

1.2 Microalgal cell walls and cell wall products

The microalgal cell wall and all the substances that may be produced from it, including extracellular polysaccharides, are one element of the microalgae that has largely been overlooked and not fully explored [21]. The biotechnological potential of natural polysaccharides is now garnering attention as a consequence of the worldwide market's trend to shift from synthetic to natural sustainable chemicals that benefit both the consumer and the environment.

Differential expression of the large number of genes found in microalgae that code for carbohydrate-active enzymes leads to the huge diversity of cell walls' composition and structure [22,23].

Polysaccharides (PS) are long chains of linear or branched sugar monomers linked through glycosidic bonds. Depending on the composition, size, and structure, PS can have a range of physico-chemical properties including antioxidant, stabilizing, suspending, thickening, flocculating, encapsulating, emulsifying, and water retention [24]. Some PS also possess biological activities such as antiviral, anticoagulant, immuno-modulating, and antitumoral activities [25]. Due to these characteristics, PS can be used in a variety of different commercial applications, including biomedical, pharmaceuticals, cosmetics, adhesives, detergents, food additives, textiles, brewing, and wastewater treatments [24].

Natural cosmetics ingredients and formulations derived therefrom are becoming increasingly popular among both consumers and manufacturers [26]. This is driven in part by the rising global awareness of environmental and health impact in regard to products that consumer use and the source of the ingredients used to produce these products [27]. This is especially true with cosmetics. This observed shift in consumption and market focus is underpinned by the increasing amount of data that supports claims on the detrimental effects of the over-reliance on synthetic materials on health and the environment [28,29]. As a result, market trends are shifting strongly toward natural and sustainable cosmetics solutions that are related to a healthy lifestyle while also linking cosmetic product consumption to good eating habits [30] opening new opportunities for algal applications. Many new biologically active materials can also be isolated from algae (macro- and micro-algae) and employed as ingredients in cosmetics mostly for their desirable skincare properties [31]. They can moisturise the skin, improve circulation, stimulate cell renewal and metabolism, control sebaceous gland

function, regenerate tissue, have an anti-inflammatory impact, and boost skin resistance [32]. Two examples of big companies following this trend are Unilever [1] and L'Oréal [2].

1.3 Hyaluronan and its applications

Hyaluronan (HA) is a linear, polydisperse, high molecular weight (MW) (up to 10 MDa), glycosaminoglycan composed of alternating repeats of β-1,4-D-glucuronic acid and β-1,3-N-acetyl-D-glucosamine units [33] (Figure 1.3).

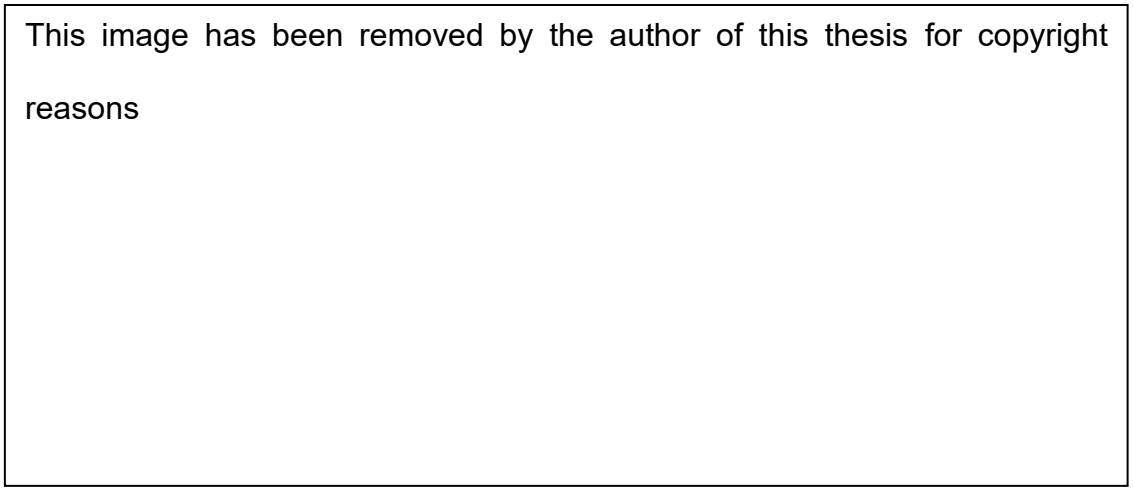

Figure 1.3. Disaccharide structure showing the β(1,3) linkage between D-glucuronic acid N-acetyl-D-glucosamine residues. Taken from [34].

Other than in vertebrates, HA is produced by some bacteria (e.g., *Streptococcus pyogenes*, *Streptococcus uberis*, *Pasteurella multocida* and *Cryptococcus neoformans*) and virally-infected *C. variabilis*. The HA-dependent capsule of group A and group C *Streptococci* is correlated with the pathogenicity of these organisms in humans and livestock, respectively, and allows the bacteria to evade the host immune system [35].

The global HA market was valued at 8.3 billion USD in 2018 and is expected to reach USD 16.6 billion by 2027 [36]. The market is witnessing rapid growth due to increasing adoption in cosmetic and aesthetic procedures with a move towards more natural materials from plants. High market growth areas include application to improve the compatibility of cardiovascular implants and to treat the increasing number of people with orthopaedic joint disorders resulting from both an ageing Western society population as well as elevated levels of obesity [36].

HA was first isolated from the vitreous humour of bovine eyes in 1934 [37]. In vertebrates, the major role of HA is to maintain the structural and functional characteristics of the extracellular matrix in vertebrates, particularly with regard to localised tissue volume regulation. HA has been found ubiquitously at different concentrations and MW in many soft tissues, especially eyes, skin and cartilage. Rheological analysis demonstrates that in water solutions, it has non-Newtonian properties even at low concentrations [38] with this property being correlated with the respective MW of the polymer. Due to this behaviour, solutions of HA of sufficient concentration and MW can serve as effective lubricants when movement is slow and shock absorbers when movement is fast [39] for instance in weight-bearing joints in mammals.

Other than its rheological properties, HA also has potent signalling properties via specific cell surface receptors. HA has been associated with contact inhibition in mammalian cells [40], modulation of the inflammatory response, limiting the diffusion of macromolecules and cells responsible for inflammation, is a key component in chronic wound healing and it also has antioxidant activity [41]. Furthermore, this molecule seems to modulate embryogenesis [42], cell

migration and adhesion, wound healing and neo-angiogenesis in mammals [43]. The various roles in morphogenesis are a result of a combination of biophysical and biochemical properties of the molecule as well as specific binding affinities to matrix proteins and cell-surface receptors.

In cells of the naked mole rat, *Heterocephalus glaber,* production of a unique high molecular weight HA (HMW-HA) has been observed. This is in contrast to other mammals, such as mouse and human, in which HA tends to be of lower comparative MW. HMW-HA leads to the activation of the early contact inhibition mechanism [44] and has enhanced anti-proliferative, anti-inflammatory and anti-metastatic properties [45]. In contrast, shorter molecules are associated with inflammation, more rapid cell proliferation and metastasis [45]. Two factors contribute to the relatively high abundance of HMW-HA in the naked mole rat: first, the naked mole rat HA synthase 2 (*HAS2*) gene encodes a unique protein variant that potentially results in altered enzymatic activity contributing to the synthesis of higher molecular weight HA polymers; and second, hyaluronidases, the enzymes that degrade HA, have very low activity in the naked mole rat's tissues [44]. Abrogation of HMW-HA in naked mole rat cells, through either gene silencing or overexpression of a HA degrading enzyme, makes them prone to tumour formation [44].

Hyper production of HA in humans, has been reported in only 1 case of a baby showing the same phenotype of Shar-Pei dogs with excessive wrinkling and folding of the skin as well as water retention in these tissues resulting in very high reported birth weights; in both cases the activity of hyaluronidase seems to be comparable with normal values, whereas the HAS activity is elevated, correlating

with an increased accumulation of HA in tissues [46]. In addition to the tissue volume changes, the HA hyper-accumulation is also correlated to recurrent episodes of fever and inflammation, and not related to either pathogenic or autoimmune causes in both dogs [47] and the reported human case [46].

HA synthases (HAS) are a family of predicted transmembrane glycosyltransferases that are responsible for the biosynthesis of HA. In contrast to previous biochemical dogma [48], which would predict that a polymer with two distinct glycosidic linkages and two substrates would result from the combined activity of at least two enzymes, all studies support the observed fact that a single HA synthase is sufficient to catalyse the biosynthesis of HA from its activated UDP-sugars. Thus, any one of the identified HA synthase enzymes is sufficient to produce HA.

HAS are grouped into 2 classes, the first class comprises processive, single domain, integral membrane proteins with the UDP-sugars added either to the reducing end or to the non-reducing end of the polymer [49–51], found in mammals, Chloroviruses and *Streptococcus*. The second class is represented by a single enzyme only (*Pm*HAS), from the Gram-negative bacterium, *Pasturella multocida*.

Crystallographic resolution of the HAS enzymes belonging to the first class has not been possible in part due to the difficulty in the isolation of this membrane-associated protein and the fact that the structure is predicted to change in relation of the state of the enzyme [50]. However, structural prediction of *Streptococcal* HAS (*Se*HAS) has been undertaken based on the structure of cellulose synthase,

an enzyme with similar activity grouped in the same family of glycosyltransferases [52].

HA synthase is predicted to contain 6 transmembrane domains (TMD) in mammals and virus and 4 in *Streptococcus* (the only known HAS to have 4 domains) (Figure 1.4). Two TMD are found at the N-terminus, and either 2 or 4 at the C-terminus of the glycosyltransferase (GT) domain [52]. The lower number of predicted TMD in *Streptococcus* could be the reason why it needs to form a dimer in order to produce a proposed channel or pore in the cell membrane through which the nascent HA molecule is translocated [52].

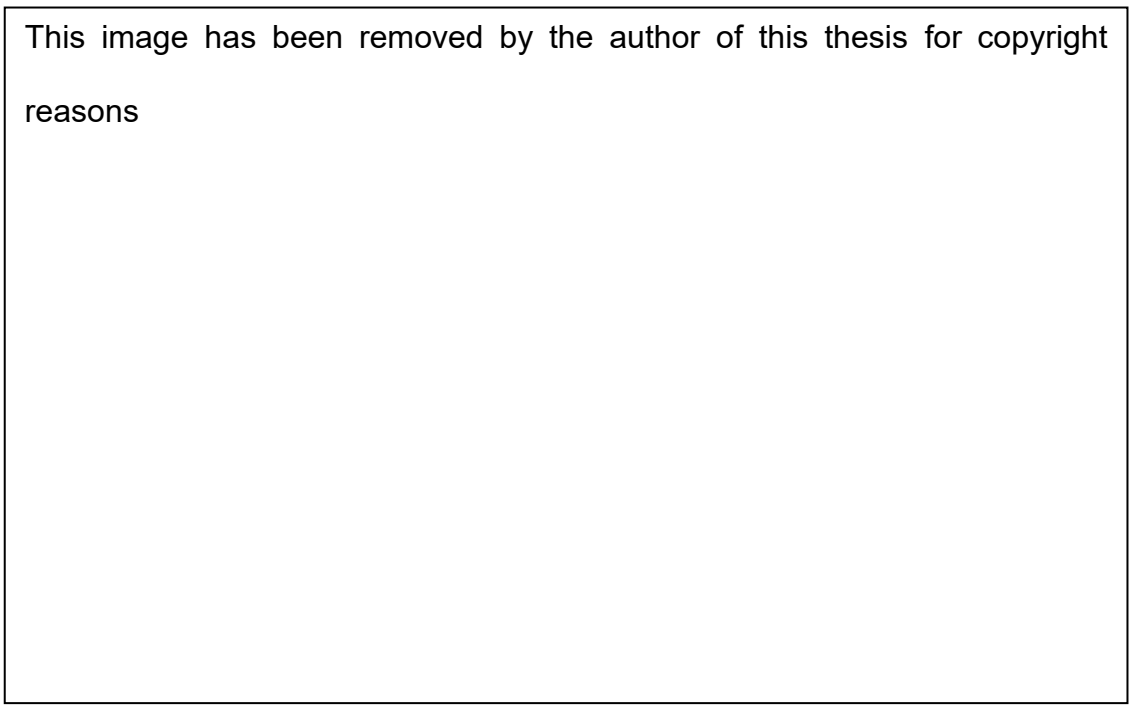

Figure 1.4. Topology of the bacterial (a) and eukaryotic/viral (b) HA synthases. The upper portion of each cartoon represents the outside of the cell membrane (indicated by the parallel lines) and the lower portion is in the cytoplasm. Taken from [53].

Crystallographic resolution of *Pm*HAS is also not available, but structural prediction has been carried out using homology modelling [54]. The membrane associated enzyme of *Pm*HAS is predicted to be composed of 3 domains: an N-

terminal domain, the UDP-N-Acetylglucosamine-transferase-domain and the UDP-glucuronic acid-transferase domain, adding the UDP-sugars at the non-reducing end of the polymer [51,54–57].

Both the HAS classes are grouped under the largest glycosyltransferase family, GT-2 in the Carbohydrate-Active enZymes (CAZy) database, together with other related enzymes including the cellulose synthases and chitin synthases [58].

HAS enzymes are subject to post-translational modifications and dimerization in mammals that control the activity of the enzyme [59,60]. Mammals express 3 forms of HAS enzymes, HAS1 produces high molecular weight HA, similar to HAS2, but is the least stable [61]. HAS3 is the most stable but produces lower molecular weight HA [61]. Mammalian HAS2 (the isoform producing high MW HA) seems to aggregate in homomeric and also heteromeric dimers with HAS1 and HAS3 affecting the activity of HAS2 enzyme, that is active also as a monomer [59]. Furthermore, ubiquitination has been observed on HAS enzymes. Deletion of one of the ubiquitination sites resulted in inactive enzymes. Co-expression of both wild type (wt) and mutated (at the ubiquitination site) enzymes, formed inactive heterodimers supporting the model that ubiquitination is necessary for HAS enzyme activity [60]. In contrast to the mammalian HAS enzymes, viral HAS doesn't seem to form dimers when expressed in *E. coli* [49].

HA MW is related to different factors. Protein sequence and structure have an impact on the HA MW, affecting the processivity of the catalysis and the strength with which the newly produced polysaccharide is bound to the enzyme [48,62–65], which, in turn, will affect the 'off-rate' or the rate of dissociation of the polysaccharide from the enzyme. Other factors that impact HA MW in bacterial

cultures include substrate availability (due to, for instance, glucose concentration in the medium) [66], fermentation conditions (dissolved oxygen, mixing rates, temperature) [67], the relative ionic availability (Mg^{2+}, Mn^{2+} or Co^{2+} ions) [68], and the lipid environment within which the enzyme is active [48,51].

Due to its unique biological and physico-chemical properties, and to its safety profile, HA and its derivatives are currently used for different applications. In ophthalmology, new longer lasting eye drops have been developed [69]. HA solutions were found to be more comfortable on the eyes due to the more pronounced pseudoplastic properties of HA solutions. In fact, the viscosity of HA solutions drops dramatically at high shear rates during blinking, causing less irritation and discomfort compared to a similar product without HA [70]. For therapeutic peptide delivery, oral administration is often limited by the instability and poor absorption of peptides in the gastrointestinal tract. Biopharmaceutical research has been conducted to deliver peptides to the systemic circulation via the nasal canal. It has been shown that high molecular weight HA (MW > 0.3 MDa) moderately enhanced the nasal absorption of drugs in rats [71]. In a dermatological context, low MW HA is used for treatment of inflammatory disorders because it is easily absorbed by the stratum corneum of the skin, while also hydrating the skin and significantly reducing wrinkle depth [72]. High MW HA, a ubiquitous component of the stratum corneum, is depolymerized into low MW HA fragments in the presence of inflammation or tissue injury. These fragments are biologically active as demonstrated by their ability to trigger built-in immune defence mechanisms, promote cytokine production and create a hydrated environment that promotes cell proliferation. Numerous medical applications, including wound care, have seen improvements as a result of

leukocyte, fibroblast, and endothelial cell migration and activation following HA application [73,74]. The use of HA for cancer therapy is also under study [75].

The cell-surface receptor CD44 is overexpressed in many tumour cells where is is associated with binding and internalisation of HA [76], as well as signalling various pathways. Based upon the observed internalisation, the CD44 route has been considered as a potential target for drug delivery of HA-coupled antitumor molecules [77]. As mentioned previously, HA has lubricating and shock-absorbing properties. Patients (human and companion animals) with osteoarthritis can be treated with intra-articular injections of high MW HA as an effective treatment that has a long-term effect, stimulating localised HA production and chondrocyte proliferation resulting in reduction of cartilage degradation and improvements in function as well as pain relief [78]. HA can also be absorbed through oral administration, and has been reported to improve skin hydration, reducing wrinkles, reducing joint pain and increasing the production of more HA by the body [79–84]. HA is currently marketed as a nutritional supplement in the USA, Canada, Europe and Asia.

1.4 Industrial production of Hyaluronan

The first industrial HA production process involved extraction from animal waste, specifically, rooster combs. Low relative concentration in the tissues, and uncontrolled degradation caused by the endogenous hyaluronidase and the harsh isolation conditions leads to the production of low yield, highly polydisperse HA [85]. Additional disadvantages of animal-derived HA were represented by the risk of biological contamination (proteins, nucleic acids and viruses infecting

animals) and by the costs for extraction and purification [86,87]. Adding in the growing trend away from animal sources of any products used in cosmetology or dermatology or biomedical devices has meant that the rooster comb source of HA is essentially irrelevant commercially. Therefore, alternative methodologies for the industrial production of HA have been developed. Currently, commercial HA is principally produced by microbial fermentation. *Streptococci* strains A and C have been the first bacteria used for HA production, with *S. zooepidemicus* and *S. equisimilis* being the most commonly used strains [85]. Optimal bacterial culture conditions to obtain HMW HA (3.5-3.9 MDa) have been determined [87]. HA yield has been optimized up to 5-10 g/L, which is the upper technical limit of the process due to mass transfer limitations caused by the high viscosity of the fermentation broth [88]. Therefore, process development shouldn't focus on increasing production, but rather should be on producing a purer HA (reduced polydispersity) with higher average molecular weight, which will affect both rheological and biological properties, and hence impact both value and applications [89]. As *Streptococci* are animal or human pathogens, producing toxins, an accurate and expensive purification of the produced HA is necessary [86]. For this reason, other microorganisms have been and are currently investigated to synthesise HA. An ideal microorganism for HA biosynthesis should be safe, without secreting any toxins and be able to produce at least 1MDa HA with low polydispersity. Since the natural HA-producing bacteria are pathogenic, genetic modification (GM) represents an interesting opportunity. HA has been synthesised by recombinant hosts, transforming them with a HAS gene and the genes encoding enzymes required for precursor formation. More than one transgene is required due to these strains not producing substrates or

producing insufficient amounts thereof. GM platforms include *Lactococcus lactis* [90], *Escherichia coli* [91], *Corynebacterium glutamicum* [92] and *Bacillus subtilis* [93,94].

1.5 Alternative *Chlorella* platform for HA production

The microalgal genus *Chlorella* has been intensively studied, with some species having been grown at industrial scale, sold commercially for decades and consumed as food and beverage ingredients as well as nutritional supplements [95]. Some products have also been used as a source of cosmetic and personal care ingredients [95]. Furthermore, members of this genus are often metabolically flexible and able to grow autotrophically using sunlight, CO_2, micro and macro nutrients and water only as well as mixotrophically and heterotrophically using simple sources of carbon. This makes them further attractive as industrially scalable organisms.

Chlorella variabilis (also known as *Chlorella* NC64A) is a freshwater, unicellular, eukaryotic, green microalga most closely related taxonomically to the more commonly studied species, *Chlorella vulgaris* [96]. *C variabilis* is often found in symbiosis within *Paramecium bursaria* (a protozoan ciliate), which affords the alga protection from viral infection as well as a measure of motility (through the symbiont) to increase the probability of access to improved or optimal light conditions, in exchange for nutrients produced from photosynthesis [97]. *Chlorella variabilis* can be grown free from its host in laboratory conditions. Its genome has been sequenced [96] and, while there is evidence of possible glucose assimilation, fermentation of this organism has not been reported in the

literature. This microalgal strain is readily infected in its free-living state by multiple viruses classified as Chloroviruses. Some of these viruses contain complex, large genomes that included genes encoding for enzymes sufficient for transferring the ability to synthesise specific exopolysaccharides to the infected host microalga. This opens up the potential for using a natural viral-algal (plant-based) platform for the scalable production of market valuable exopolysaccharides with applications in markets including personal care, health and beauty.

Paramecium bursaria Chlorella viruses (PBCV) or simply Chloroviruses, belong to the *Phycodnaviridae* family of large (175 to 190 nm in diameter) polyhedral, plaque-forming viruses. This family is composed of 6 genera, based on comparison of the DNA polymerase gene sequences: Chlorovirus, Coccolithovirus, Phaeovirus, Prasinovirus, Prymnesiovirus and Raphidovirus [98]. The viruses from the genus Chlorovirus, infect endosymbiotic green microalgae including *C. variabilis* but also *Micractinium* species (depending on the virus) commonly associated with hosts including the ciliate, *Paramecium bursaria*, the coelenterate, *Hydra viridis*, or the heliozoan *Acanthocystis turfacea* [98,99]. PBCV-1 is the model virus of the *Phycodnaviridae* family, its genome is a linear, non-permuted 330-kb double-stranded DNA molecule with covalently closed hairpin ends [100]. PBCV-1 and its close relatives infect *C. variabilis* specifically. Infected *C. variabilis* cells acquire the ability to produce HA and/or a related linear exopolysaccharide, chitin, based upon the biosynthetic machinery that is transferred into the infected cells and encoded specifically within the viral genomes [101].

1.6 Chlorovirus life cycle and HA production

To understand the potential industrial opportunity represented by the *C. variabilis*/PBCV-1 host-virus relationship, it is important to understand the infection dynamics. Studies have shown that, once the PBCV-1 viruses and the algae are mixed, the virus attaches quickly to the cell walls recognising the specific host receptor [102] (Figure 1.5), and other fibre connections form between the host cell wall and the virus capsid to stabilise the bond with the specific receptor [103].

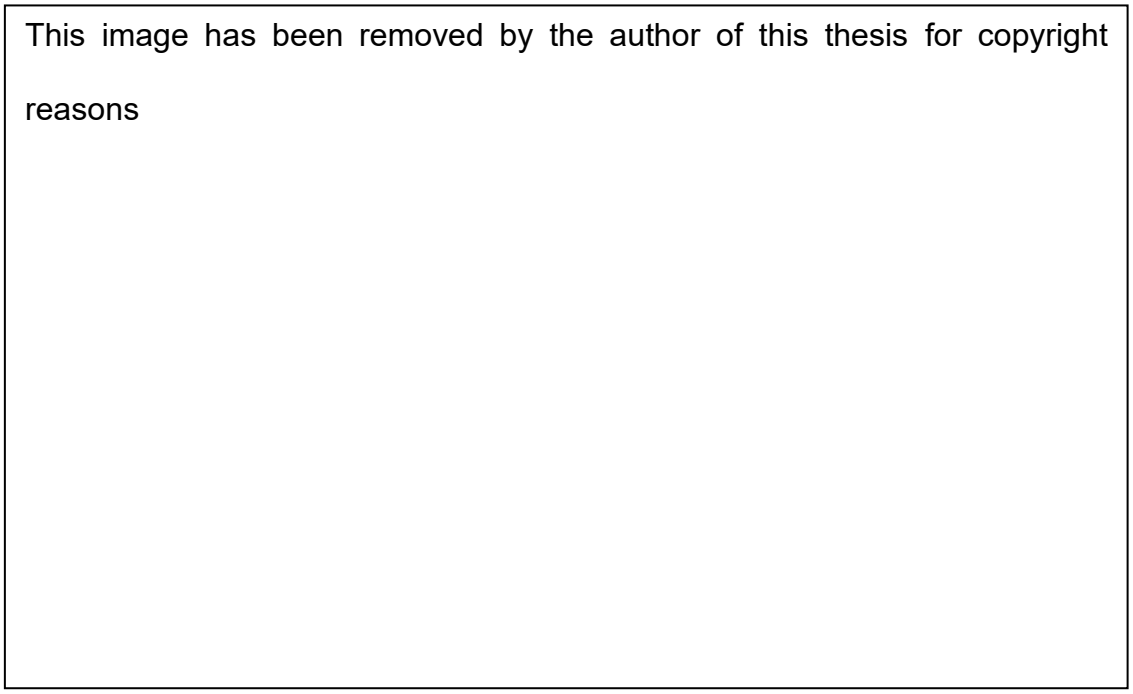

Figure 1.5. Cross section of a five-fold averaged cryo-EM image of PBCV-1 reveals a long narrow cylindrical spike structure at one vertex and the viral internal membrane (green) surrounding the viral genome asymmetrically. Taken from [104].

At least 5,000 PBCV-1 binding sites have been identified per *Chlorella* cell [105] and, for this reason, multiple virus particles can be bound to each cell. It is not clear yet if multiple infection events can happen at the same time in a single cell or what the protection mechanism might be to allow infected cells to repel

infection by other virus particles. It is possible but not yet been shown, that successful infection and viral entry activates a change in the cell surface of the *Chlorella* effectively preventing re-infection. Immediately after the attachment of the virus to the cell wall, the only enzyme that has been identified present in the virus particle with cell wall digestion activity is A561L [106], with alginate lyase activity [107]. This enzyme is delivered on the microalgae cell wall probably through the vertex protein and starts the digestion of the cell wall to access the cell membrane. The spike protein is too narrow to deliver the DNA inside the host cell so probably it is pushed aside after puncturing the cell wall. The attachment of the virus to the cell wall is reversible [108] and it has been found that virus particles also can attach to cell debris resulting from previously infected and lysed cells; these two factors could slow down the infection in cultures with very high cell density and at the same time stabilise the virus particles for long time storage, helping them to survive when there are no fresh intact cells available to infect. Once the virus reaches the cell membrane, the virus internal membrane fuses with it delivering the viral DNA genome inside the cell [109,110]. The DNA probably gets delivered in a linear form due to the small size of the pore connecting the virus and the cell and then condenses again once inside the cell to support the translocation of the viral genome into the nucleus of the host cell [104]. The membrane fusion causes rapid depolarization of the host plasma membrane, which is most likely caused by a virally-encoded K+ channel situated in the virus internal membrane [111]. The membrane depolarization could be one of the factors that inhibits multiple infections of the same cells by different viruses [112] while also facilitating the entrance of the viral DNA and proteins due to the

loss of turgor, into the host [113] with a similar mechanism compared to the inhibition of multiple fertilisations of the oocytes by the sperm cells [114].

Once the viral DNA is inside the cell, it is necessary to translocate it to the nucleus as the viral genome does not include a DNA-dependent RNA polymerase gene. The mechanism behind this translocation is undescribed at this time.

Once in the nucleus, host genome transcription decreases while viral DNA transcription starts rapidly. Reprogramming of the host transcription is still not clear, but chromatin remodelling and host chromosomal DNA degradation might be involved due to viral endonucleases and methylases packaged in the capsid [106,115–117]. Some of the first genes to be transcribed from the viral genome are those encoding enzymes involved in the synthesis of HA. Indeed, after just 15-30 min post infection, HA is already detectable on the exterior of infected cells [118]. One h post infection, the genes involved in the HA synthesis pathway are no longer transcribed [119].

Three PBCV-1-encoded enzymes contribute to the production of a linear polysaccharide consisting of alternating β-1,4-glucuronic acid and β-1,3-N-acetylglucosamine residues [101,120]. A609L and A100R genes, encode for a uridine diphosphate-glucose dehydrogenase (UGDH) and a glutamine:fructose-6-phosphate amidotransferase (GFAT), respectively. UGDH converts UDP-Glucose into UDP-Glucuronic acid, a required precursor for HA biosynthesis. GFAT converts fructose-6-phosphate into glucosamine-6-phosphate, an intermediate in the UDP-N-Acetylglucosamine metabolic pathway. A98R encodes for the HAS enzyme that is essential for HA production. All genes have been found to encode enzymes that act as enzymatically active proteins [121].

The recombinant A98R enzyme synthesises HA with an average molecular weight of 3-6 MDa [68] – this would be of high interest within a commercial context. The extracellular HA doesn't seem to have any obvious activity in the interaction between the virus and its algal host because plaque size and plaque number were not affected by testicular hyaluronidase nor free HA polysaccharide added during the plaque assay [68] (cited in this paper, reference is not available for verification). Both of these agents would have been expected to have an impact on the infection cycle if the production of HA or its presence on the host cell surface was required. HA is synthesised at the plasma membrane where the HA synthase assembles the polysaccharide through presumed alternating action on the 2 substrates [49]. The newly synthesised HA must pass through the algal cell membrane and cell wall, which includes a polysaccharide network, in which the HA could get trapped once released by the synthase. The size of the HA polymer produced could potentially be controlled by two factors: the processivity of the enzyme and the abundance of substrate precursors in the near vicinity of the active site of the enzyme. Local depletion of the substrate pool would be expected to slow and eventually stop the synthesis of the polymer.

In mammalian cells, it has been observed that enzymes with different processivity produce HA of different molecular mass; the slower the enzyme the higher the molecular mass [48,62–65]. It has been hypothesised that HA synthesis and its accumulation on the algal surface may block the uptake of virus-infected algae by the *Paramecium* in order to avoid internalisation and digestion by the *Paramecium* that would kill the viruses. Another possible explanation reported in the literature is that the *Chlorella* viruses might have another host in nature and the virus could be transmitted to the alternate host after engaging with the HA

polysaccharide on virus-infected algae [68]. The virus infected cells seem to produce some sort of signalling to which the *Paramecium* responds, moving towards them, but this signalling molecule has not been identified yet [122] ; HA could, conceivably have a role in this behavioural response as HA and also related chito-oligosaccharides are described in the literature as being active in signalling [123].

One h after infection, viral DNA synthesis begins, followed by transcription of the late genes, which include the cell wall digesting enzymes required for cell lysis and viral particle release [124]. Assembly of PBCV-1 capsomers begins in specific parts of the cytoplasm three to four h after infection [125]. At five to six h post-infection, the infected cells lyse thanks to the action of cell wall digesting enzymes, liberating approximately one thousand newly synthesised virus particles per cell, of which roughly 25% are infective [126].

1.7 Other possible applications for Chlorovirus

One of the obstacles to the mainstream industrial use of microalgal biomass is the effective recovery of intracellular chemicals [127]. Due to the recalcitrance, complexity, and diversity of the microalgal cell wall, high energy inputs or large quantities of chemicals are often necessary to extract the compounds from within the cell [127] increasing the cost of biomolecule extraction and limiting possible commercial applications by pricing the final product beyond market reach. It may be possible to develop a range of potentially industrially relevant and deployable enzymes to degrade specific microalgae cell walls in a controllable manner prior to biomass extraction and refining by gaining a deeper understanding of the role

of the specific enzymes used by Chloroviruses and related viruses to enter and exit microalgae by attacking components of cell walls. This approach could significantly reduce the amount of downstream energy and the need for harsh extraction chemicals, leading to a more environmentally friendly purification process and more favourable overall process economics.

The hypothesis explored in this project was that it was feasible for a microalgal platform to produce HA.

The objectives included:

- Investigating a stress-induced platform (*L. segnis*) for the possible production of HA;
- Learning how the Chlorovirus/*C. varibilis* infection leads to HA formation;
- Improving the best of the 2 platforms explored for HA production.

As a consequence of the Chlorovirus understanding, intriguing enzymes that can break down polysaccharides were found and further investigated for cell wall digestion.

Chapter 2 - Analysis of the *Lobochlamys segnis* platform for EPS production

This chapter was published with me as first Author and with my supervisors as co-authors [128] (Appendix B).

2.1 Introduction

Lobochlamys segnis, previously known as *Chlamydomonas segnis* [129], is a freshwater, green microalgae that was considered in the past for its fatty acid profile rich in polyunsaturated fatty acids (PUFAs) [130].

Extracellular polysaccharide production in *Chlamydomonas* strains has previously been reported [131,132]. *Lobochlamys segnis* is a microalga that is closely related to *Chlamydomonas* [129] and has been shown to produce a HA-like capsule under stress conditions [133]. To investigate this possibility, three different strains of *L. segnis* were obtained from the SAG culture collection. Of these, SAG 1.79 has previously been noted in a Canadian patent to produce a HA-like substance referred to as “Chlamyhyaluronic acid” [7], while the two other closely related strains were ordered for comparative purposes. On receipt, the identity of each strain was confirmed by 18S PCR sequencing and maintained on agar plates for several generations. Under long term cultivation conditions, the SAG 1.79 strain was confirmed to grow as mucoid colonies. In contrast, the two other strains did not exhibit the same appearance (Figure 2.1). This provided a

quick primary screening method for strains displaying EPS production, and SAG 1.79 was selected for further investigation.

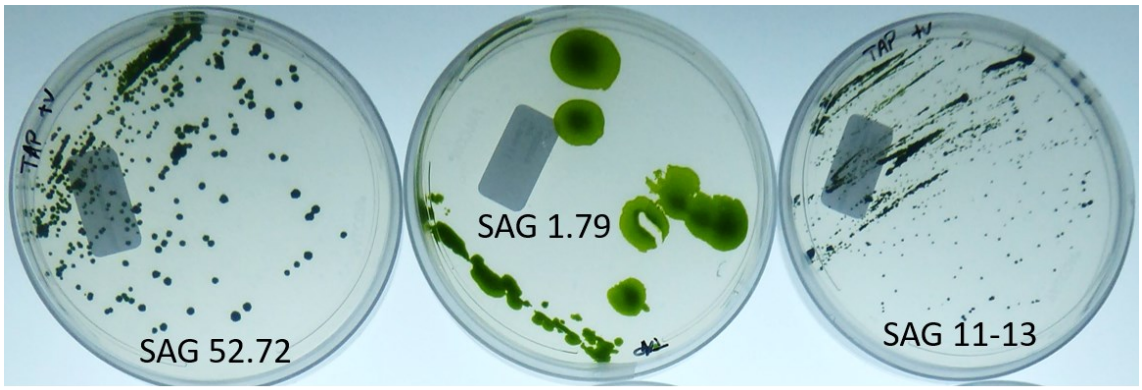

Figure 2.1. Solid medium plates showing the distinct mucoid appearance of the Göttingen University (SAG) 1.79 strain.

Under general stress conditions, such as high light intensities or nitrogen starvation, the cultivation of this species becomes difficult due to the substantial production of extracellular polysaccharides (EPS; thought to be HA or HA-like) that increase the viscosity of the culture [133]. This was considered to be a limitation during the production of PUFAs [134].

Rather than viewing EPS as a problematic by-product, this study sought to evaluate *L. segnis* as a platform for its optimised production and assessed its potential for exploitation in cosmetics and biomedical applications. The effects of culture conditions and media composition were tested in order to increase the biomass concentration in stationary growth phase. Subsequently, a panel of stress-inducing conditions were applied and the appearance of the culture was evaluated, with the aim of reaching high culture viscosity due to EPS production. Once the EPS production was increased, extraction and purification conditions were determined. Purified EPS was characterised with respect to sugar composition, molecular weight (MW), and glycosidic linkages. Rheological

properties and antioxidant activity were also determined and compared with those for HA.

2.2 Materials and methods

2.2.1 Chemicals

Culture media components were purchased from VWR international, UK. Proteinase K was purchased from New England Biolabs, UK. All other chemicals and enzymes used were purchased from Merck, UK.

2.2.2 Microalgal strain selection and determination of its growth and stress conditions

Three *L. segnis* strains were obtained from the culture collection of algae at Göttingen University (SAG) [135]: SAG 52.72 isolated in Czech Republic, SAG 11-13 isolated in United Kingdom, and SAG 1.79 isolated in Canada. All three strains were kept on Tris-acetate-phosphate (TAP) medium [136] (components in 1 L: Tris (Trizma) base 2.42 g, NH_4Cl 0.375 g, $MgSO_4*7H_2O$ 0.1g, $CaCl_2*2H_2O$ 0.05 g, K_2HPO_4 0.108 g, KH_2PO_4 0.054g, Na_2-EDTA 21.4 mg, $(NH_4)_6Mo_7O_{24}*4H_2O$ 0.35 mg, Na_2SeO_3 0.017 mg, $ZnSO_4*7H_2O$ 0.72 mg, $MnCl_2*4H_2O$ 1.2 mg, Na_2CO_3 2.32 mg, $FeCl_3*6H_2O$ 5.4 mg, $CuCl_2*2H_2O$ 0.34 mg, glacial acetic acid 1 mL, purified water up to 1 L) 1.5% agar plates and re-streaked every month.

Two media, prepared as per reference, were tested, TAP medium [136] and High salt medium (HSM) [137] (components in 1 L: NH_4Cl 0.375 g, $MgSO_4*7H_2O$ 0.1g, $CaCl_2*2H_2O$ 0.05 g, K_2HPO_4 0.72 g, KH_2PO_4 0.36g, Na_2-EDTA 21.4 mg,

$(NH_4)_6Mo_7O_{24}*4H_2O$ 0.35 mg, Na_2SeO_3 0.017 mg, $ZnSO_4*7H_2O$ 0.72 mg, $MnCl_2*4H_2O$ 1.2 mg, Na_2CO_3 2.32 mg, $FeCl_3*6H_2O$ 5.4 mg, $CuCl_2*2H_2O$ 0.34 mg, purified water up to 1 L). Three nitrogen sources were tested for TAP medium, ammonium chloride, potassium nitrate and urea all at the same molar concentration of 7 mM (urea will provide double the amount of nitrogen). Cultures were grown in Algem® HT24 photobioreactor [138] in 25 mL volume inside a 50 mL clear flask or Algem PRO photobioreactor [138] in 400 mL volume in a 1 L Pyrex Erlenmeyer flask, at 28 °C with white LED light intensity set at 200 µE photosynthetically active radiation (PAR) measuring the OD at 740 nm every 10 min. As a stress inducer, 4000 µE light intensity was applied, setting on the software red:blue:white ratio of 1:1:2 in the Algem photobioreactor until a change of the culture viscosity was observed. The mixing was set to 120 rpm with a gas aeration rate of 25 $mL*min^{-1}$ of 30% CO_2 in order to control the pH of the culture at pH 7 via computer-controlled solenoid valve. Acetic acid feeding was required to increase the carbon provided to the culture gradually as the strain doesn't tolerate too high concentrations from the beginning. One molar solution of acetic acid was prepared in purified water and used under the control of a modified version of the Algem software with a peristaltic pump [138] in order to keep the pH of the culture at 7 and with a continuous aeration rate of 50 $mL*min^{-1}$ of air.

2.2.3 Extraction of extracellular polymeric substances

Ten mL of stressed algae culture for each sample were extracted at 37 °C, except when specified, mixing with a magnetic stir bar at 120 rpm for 24 h. Extraction processes were tested independently under the following conditions:

- Lysozyme lyophilized powder from chicken egg white was resuspended at 10 mg*mL^{-1} in 10 mM Tris-HCl pH 8 immediately before use and was used at 1 mg*mL^{-1} in solution with stressed algae.
- Lyticase powder from Arthrobacter luteus was resuspended at 10 mg*mL^{-1} in 67 mM Potassium Phosphate Buffer pH 7.5 immediately before use and was used at 1 mg*mL^{-1} in the same buffer solution with stressed algae at 25 °C.
- Sulfatase powder from *Helix pomatia* was resuspended at 10 units*mL^{-1} in 200 mM Sodium Acetate Buffer, pH 5.0 immediately before use and was used at 1 unit*mL^{-1} in buffer solution with stressed algae.
- Chitinase powder from *Streptomyces griseus* was resuspended at 1 mg*mL^{-1} in purified water immediately before use and was used at 0.5 mg*mL^{-1} in solution with stressed algae.
- Proteinase K was used at 3 units*mL^{-1} in 15 mM Tris-HCl pH 7.6, 1.5 mM CaCl 0.6% SDS solution with stressed algae.
- Hyaluronidase from bovine testes was resuspended at 1 mg*mL^{-1} in 20 mM phosphate buffer, pH 7, with 77 mM sodium chloride and 0.01% BSA immediately before use and was used at 0.5 mg*mL^{-1} in solution with stressed algae.
- Sodium dodecyl sulphate (SDS) at 1% or 6% final concentration in stressed algae solution.
- Applying heat at 100 °C for 6 h or 24 h or 121 °C for 15 min every 100 mL in autoclave.
- Urea at 1 M and 10 M final concentrations in stressed algae solution.

- Potassium hydroxide (KOH) 5% final concentration in stressed algae solution.
- Sodium chloride (NaCl) 2 M final concentration in stressed algae solution.

After extraction, samples were centrifuged once at 21,000 relative centrifugal force (RCF) for 5 min with the extracted EPS present in solution in the supernatant.

2.2.4 Agarose gel electrophoresis

A TBE buffer gel was prepared with 0.5% agarose (Merck, UK) and run for 1 h at 160 V. Extracted EPS samples were prepared adding 1 volume of loading dye, composed of 2 M sucrose in TBE (1×) with 1/20 of final volume bromophenol blue, to 5 volumes of sample. The gel was equilibrated in a Petri dish at room temperature, mixing for 1 h with 40% ethanol in purified water. The gel was stained with Stains-All (Merck, UK) working solution at room temperature for 24 h; 0.1% Stains-All stock solution was prepared in formamide (10 mg in 10 mL), for working solution, 2.5 mL of stock solution, 2.5 mL formamide, 12.5 mL isopropanol, 0.25 mL of 3 M Tris-HCl pH 8.8, and 32.25 mL of purified water were mixed. The gel was de-stained with ambient light for 10 min after rinsing with water first and then with 70% denatured ethanol.

2.2.5 Filtration

An extracted sample was filtered with a glass microfiber 0.45 µm filter (Sartorius, UK). After filtration, the extracted samples were filtered with a Minimate 500 kDa tangential flow filtration (TFF) capsule (Pall Corporation) following the manufacturer’s recommendations, until reaching a reduction of volume of 90%.

Purified water was used to dilute the concentrate to the original volume, twice, in order to remove low MW contaminants and to desalt. The filtrate was collected for further processing with a 30 kDa molecular weight cut-off capsule as described for the previous filtration process.

2.2.6 High MW EPS purification with Sephacryl® size exclusion chromatography

A glass column with 46 cm length and 1 cm internal diameter was used with Sephacryl® 500-HR (Merck, UK) and 0.15 M NaCl, 0.05 M phosphate pH 7 running buffer with a flow rate of 2 mL per min; 0.3 M NaCl final concentration was added to each sample before loading on the column. One mL fractions of the elute from the column were collected and precipitated by addition of 3 volumes of acetone and centrifugation at 4600 RCF. After the supernatant was removed, the pellet was air-dried and resuspended in TBE at 4 °C overnight followed by gel electrophoresis analysis as described above. Once the fractions with the higher molecular weight product were selected, the samples were pooled and desalted with TFF as previously described.

2.2.7 Freeze dry

Purified high MW EPS was frozen at −40 °C and dried in a lab scale vacuum freeze dryer (Harvest Right, UT, US) at −5 °C heating shelf temperature, 200 mTorr cavity pressure and −40 °C cold trap temperature for 24 h in a glass Petri dish.

2.2.8 Polysaccharide MW analysis

One mL of 0.1 M $NaNO_3$ was added to the freeze-dried polysaccharide sample; it was heated up to 100 °C for complete dissolution and centrifuged for 10 min at 14,000 RCF. The supernatant was collected for analysis, with 0.1 mL injected per sample; this was performed with GPC-RI-MALS platform with the column temperature set to 60 °C, 0.1 M $NaNO_3$ mobile phase with a flow of 0.4 $mL*min^{-1}$. From the comparison of the retention time of the EPS sample with the same data from a set of standards of known MW solution, it was possible to determine the MW distribution of the sample.

2.2.9 Glycosyl composition analysis

Analysis was undertaken by combined gas chromatography/mass spectrometry (GC/MS) of the per-O-trimethylsilyl (TMS) derivatives of the monosaccharide methyl glycosides produced from the sample by acidic methanolysis [139,140]. Approximately 0.25 mg of the sample was heated with methanolic HCl in a sealed screw-top glass test tube for 17 h at 80 °C. After cooling and removal of the solvent under a stream of nitrogen, the sample was treated with a mixture of methanol, pyridine, and acetic anhydride for 30 min. The solvents were evaporated and the sample derivatized with Tri-Sil HTP (HDMS:TMCS:Pyridine) reagent (ThermoFisher Scientific, UK) at 80 °C for 30 min with added inositol as internal standard. GC/MS analysis of the TMS methyl glycosides was performed on an Agilent 7890A GC interfaced to a 5975C MSD, using a Supelco Equity-1 fused silica capillary column (30 m × 0.25 mm ID).

2.2.10 Glycosyl linkage analysis

Approximately 1 mg of the sample was treated with 0.5 M methanolic HCl for 20 min at 80 °C. It was then dried and reduction of the newly formed carboxylic esters was accomplished using 0.4 mL of a 10 mg*mL^{-1} solution $NaBD_4$ in water overnight. The sample was then neutralised with acetic acid and it was dried thoroughly and later suspended in 0.2 mL of dimethyl sulfoxide. Per-methylation of the sample was affected by two rounds of treatment, first with sodium hydroxide for 15 min and later with methyl iodide for 45 min. The sample was hydrolysed using 0.1 M TFA for 30 min in a sealed tube at 100 °C, reduced with $NaBD_4$, hydrolysed again using 2 M TFA for 2 h in a sealed tube at 100 °C and acetylated using acetic anhydride/TFA [141,142]. The resulting partially methylated alditol acetates (PMAAs) were analysed on an Agilent 7890A GC interfaced to a 5975C MSD (mass selective detector, electron impact ionization mode); separation was performed on a 30 m SP2330 bonded phase fused silica capillary column.

2.2.11 Rheology analysis

Flow sweep measurements of viscosity were implemented using Discovery HR-3 hybrid rheometer with a hard-anodised aluminium 40 mm Peltier parallel plate with Solvent Trap. The gap was set to 500 µm and the analysis was performed with samples at 25 °C with a shear rate changing between 0.1 to 1000 s^{-1} measuring 5 points per decade, with equilibrium time of 1 min. One mL of the sample was loaded and the excess was wiped out. HA standard solution was made dissolving pure 5 MDa MW HA at a concentration of 8.34 mg*mL^{-1} in purified water. *L. segnis* stressed cells were resuspended in TAP medium. *L.*

segnis EPS was extracted with heat treatment, debris was filtered, and the clear solution was concentrated with 500 kDa molecular weight cut-off membrane at about 14 mg*mL^{-1}. NaCl was added to the samples to a final concentration of 2 M to investigate the impact on the viscosity of the solution.

2.2.12 Antioxidant capacity and reducing power quantification assays

Heat extracted *L. segnis* EPS were concentrated with 500 kDa filter and freeze dried without purification in order to resuspend them in purified water at a known concentration for measurement of total antioxidant capacity and reducing power. The total antioxidant capacity was measured based on the reduction of Mo^{6+} to Mo^{5+} [143]. Aliquots of the polysaccharide solution (0.1 mL) at different concentrations (0.5%, 0.75%, 1%, 1.25%, 1.5%) were mixed with 1 mL of the reagent solution (0.6 M sulfuric acid, 28 mM sodium phosphate (NaH_2PO_4), and 4 mM ammonium molybdate). This step was followed by incubation at 95 °C for 90 min. Subsequently, the absorbance was read at 695 nm. A standard curve under the same conditions was prepared with solutions of ascorbic acid (0.005%, 0.0075%, 0.01%, 0.0125%, 0.015%) in purified water. The assays were carried out in triplicate and the results are presented as equivalence of ascorbic acid (mg EAscA*g^{-1} of sample).

The reducing power was determined according to the method on the reference [144]. 0.2 mL of EPS in purified water (1.5%, 15 mg*mL^{-1}) was mixed with 0.2 mL of 0.2 M sodium phosphate buffer (pH 6.6) and 0.2 mL of 1% potassium ferricyanide (10 g*L^{-1}). The mixture was incubated at 50 °C for 20 min. After cooling down the samples, 0.2 mL of 10% trichloroacetic acid (w/v) were added,

the mixture was centrifuged at 21000 RCF for 10 min. 0.5 mL of the supernatant were moved to a new tube and, with added 0.5 mL purified water and 0.1 mL of 0.1% of ferric chloride, samples were mixed and the absorbance at 700 nm was measured. A standard curve under the same conditions was prepared with solutions of ascorbic acid (0.005%, 0.0035%, 0.002%, 0.0009%, 0.0007%) in purified water. The assays were carried out in triplicate and the results are presented as equivalence of ascorbic acid (µg EAscA*g^{-1} of sample).

2.3 Results

2.3.1 Determination of *L. segnis* SAG 1.79 growth and stress conditions

Growth was tested in two different liquid media: HSM (no carbon source) and TAP (acetate as carbon source). Three different nitrogen sources were tested as substrate for growth at the same molarity in TAP medium: ammonium chloride (NH_4Cl), potassium nitrate (KNO_3), and urea ($CO(NH_2)_2$). Urea provides double the amount of nitrogen at the same molar concentration of the other nitrogen sources explored. The doubling times (reported in Table 2.1) as well as the cell densities at stationary phase were the same for all three conditions, as shown in Figure 2.2, suggesting that the nitrogen is not a limiting factor at stationary growth phase.

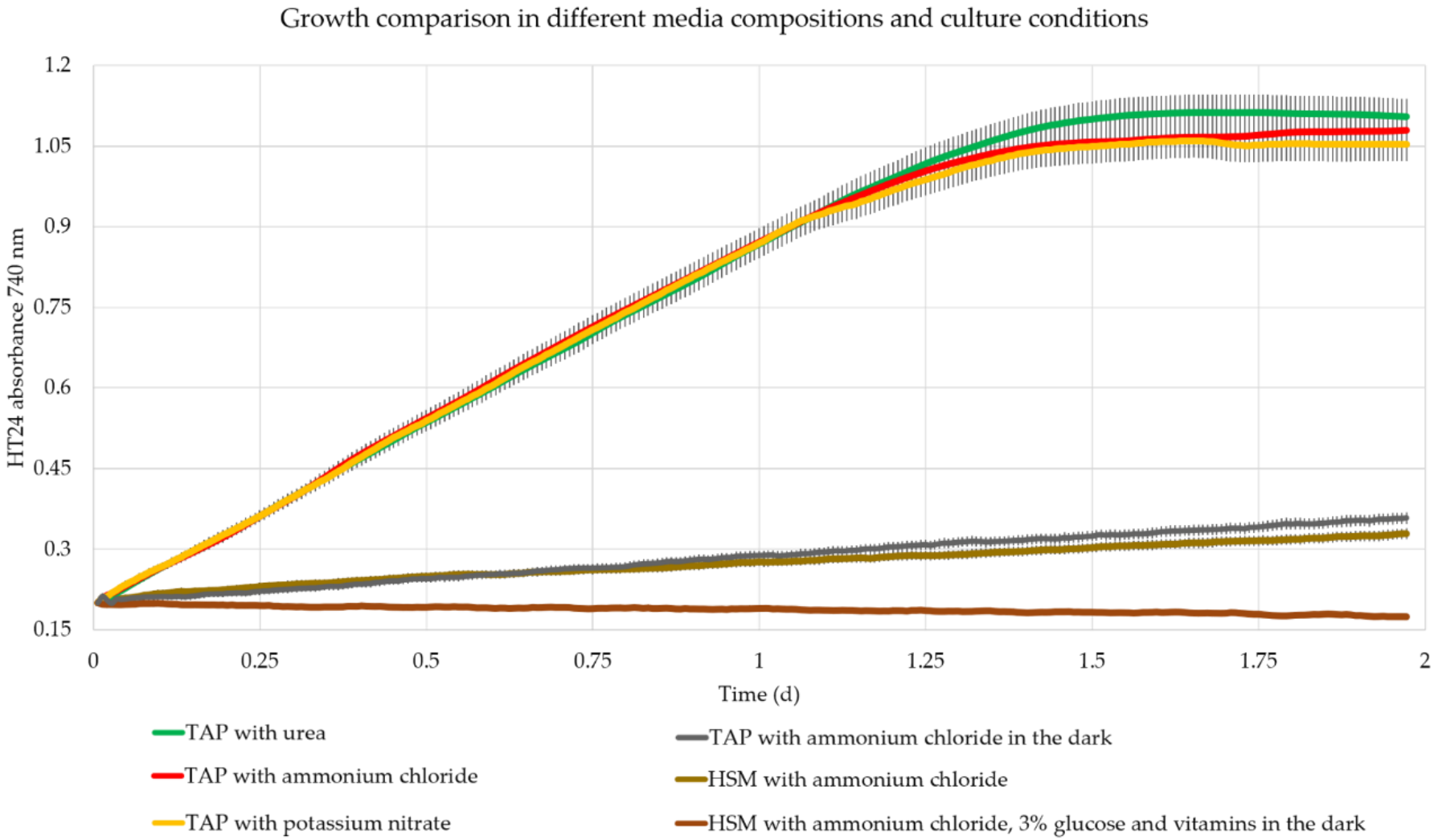
Growth comparison in different media compositions and culture conditions
HT24 absorbance 740 nm
1.2
1.05
0.9
0.75
0.6
0.45
0.3
0.15
0
0.25
0.5
0.75
1
1.25
1.5
1.75
2
Time (d)
TAP with urea
TAP with ammonium chloride
TAP with potassium nitrate
TAP with ammonium chloride in the dark
HSM with ammonium chloride
HSM with ammonium chloride, 3% glucose and vitamins in the dark

Figure 2.2. Growth comparison of SAG 1.79 in different media compositions and conditions. Each condition was run in triplicate, in this graph the mean values are plotted with standard errors displayed for each dataset. HSM, high salt medium [136]; TAP, Tris-acetate Phosphate medium [137].

Growth in the dark was also tested utilising acetate or glucose as carbon sources. As shown in Figure 2.2, SAG 1.79 was not able to utilise glucose from the medium for growth in the dark. In contrast, the strain was able to use acetate in the dark, although showing a higher doubling time (Table 2.1). This suggests that SAG 1.79 is capable of preferential mixotrophic growth using light coupled with acetate as a carbon source. Mixotrophic growth showed a doubling time that was about 1/3 compared to the growth in the dark with acetate or in the light without carbon source.

The doubling time (T_d) for each curve, summarised in Table 2.1, was calculated from data drawn from the linear portion of the growth curves (between 0.5 day and 0.75 day) using the following formula:

$$T_d\ (days) = \left(\frac{0.25\ days \cdot log_{10}(2)}{log_{10}(OD\ at\ 0.75\ days) - log_{10}(OD\ at\ 0.5\ days)} \right)$$

High salt medium (HSM) with Ammonium Chloride	Tris-acetate Phosphate medium (TAP) with Ammonium Chloride	TAP with Potassium Nitrate	TAP with Urea	TAP with Ammonium Chloride, Dark
3.32 ± 0.33	0.73 ± 0.07	0.75 ± 0.08	0.74 ± 0.07	2.10 ± 0.17

Table 2.1. Calculated Td using Algem HT24 OD readings and expressed in days for the different growth conditions.

A second trial was conducted using the Algem lab-scale photobioreactor to confirm that the lack of a carbon source was the limiting factor in increasing biomass density and to test a higher C/N ratio to stimulate EPS production by feeding the culture with acetic acid while keeping the pH constant at 7.

A few days after the culture reached stationary phase with acetic acid feeding, the Algem OD reading reached higher values compared to the cultures that were not fed with acetic acid (Figure 2.3(a)) showing high viscosity behaviour, gel like solution (Figure 2.3(b)). Centrifugation at 21,000 RCF for 5 min was not sufficient to achieve a stable cell pellet. Further, light microscopy revealed cells that appeared to be evenly spaced, as if surrounded by something not visible to the eye, which caused the cells to distribute within the culture medium as if they were kept physically apart, presumably by an extracellular capsule (Figure 2.3(c, d)) forming a physical barrier.

In an effort to visualise a hypothesised capsule around the cells, a 10 µL sample of each culture was diluted with 1 volume of India ink (Figure 2.3(e, f)). India ink is composed of small black particles resuspended in water that give a black background, and that would be excluded from areas occupied by a viscous physicochemical barrier such as that created by an extracellular polysaccharide capsule.

Using this technique, it was confirmed that, when stressed, cells were surrounded by a capsule that excluded the ink particles from the cell surface.

(a) (b) (c)

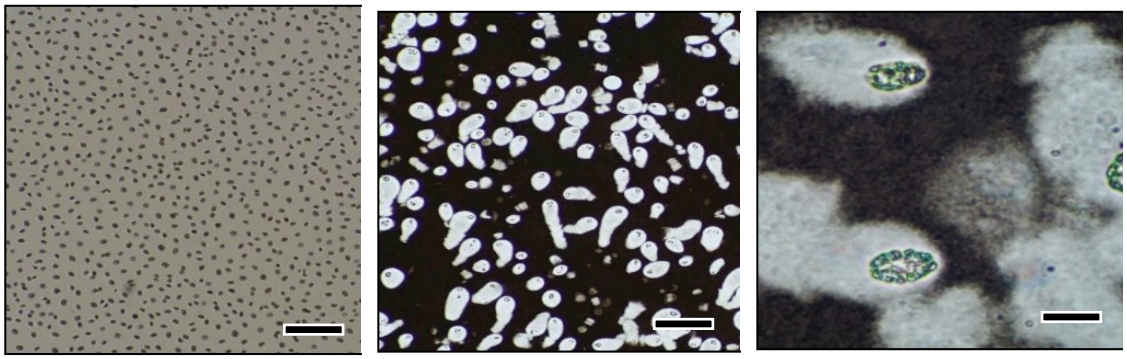

(d) (e) (f)

Figure 2.3. Visual characterisation of stressed culture. (a) Cell culture in late exponential phase; (b) stressed cell culture in late stationary phase showing suspended bubbles trapped within the viscous liquid; (c) cells in late stationary phase, 40× magnification, scale bar 10 µm; (d) cells in late stationary phase, 4× magnification, scale bar 100 µm; (e) cells in late stationary phase diluted 1:1 in Indian Ink, 4× magnification, scale bar 100 µm; (f) cells in late stationary phase diluted 1:1 in Indian Ink, 40× magnification, scale bar 10 µm.

2.3.2 Determination of extraction and purification conditions

In order to assess the nature of the capsule produced and reduce the viscosity of the culture, the stressed culture was exposed to enzymes and chemical treatments that degrade specific polymers. Susceptibility to the action of lysozyme, lyticase, sulphatase, chitinase, Proteinase K, hyaluronidase, 1 and 6% SDS, heat, urea 1 and 10 M, 5% KOH and 2 M NaCl were assessed. After the

respective treatments, samples were centrifuged at 21,000 RCF for 5 min. The presence of an obvious cell pellet was taken as an indication that the EPS was separated from the cells; this was possible after the extraction with heat, SDS, urea, NaCl and KOH, with the best result achieved through applying heat alone, 100 °C for 24 h or autoclave at 121 °C for 15 min every 100 mL of stressed algae solution at 200 kPa. Under this condition, a higher amount of the EPS was separated from the biomass compared with the other conditions. None of the enzyme digestions separated the capsular EPS from the cells nor acted to degrade it as the cells couldn't be pelleted. EPS extracted with heat was used for further evaluations and showed an apparent degradation pattern as seen through agarose gel electrophoresis in Figure 2.4.

Five hundred kDa and 30 kDa crossflow filtrations were tested sequentially for EPS purification from small MW contaminants (Figure 2.5). All the extracted EPS seemed to be bigger than 30 kDa. Due to the high viscosity and heterogeneity of the sample, filtration was not very efficient to separate high from low MW molecules. As shown in Figure 2.4, with 500 kDa filtration, most of the high MW EPS was retained, but the low MW contaminants were still present. With the 30 kDa filtration, everything was retained.

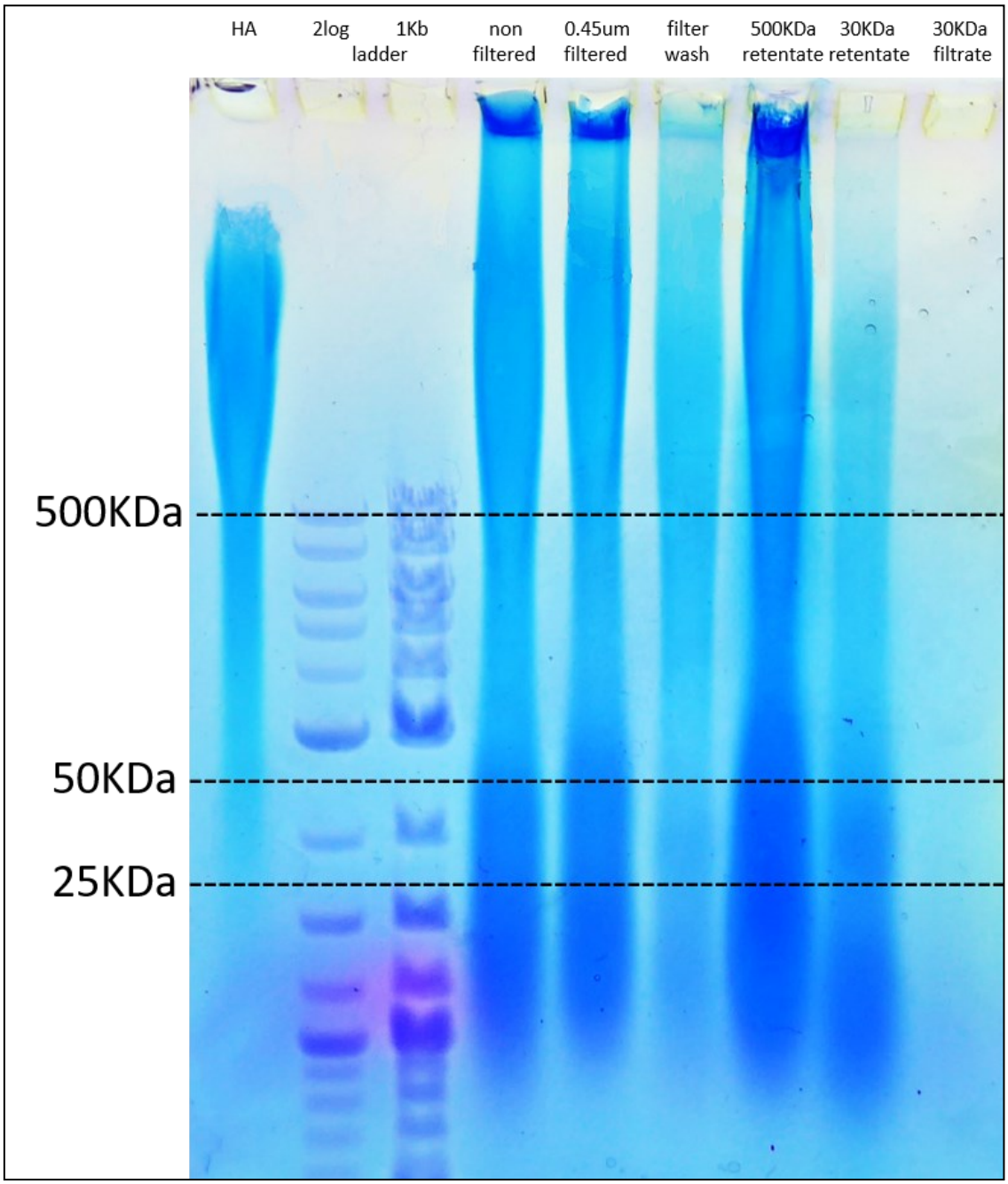

Figure 2.4. Agarose gel electrophoresis showing extracted and filtered samples. The first lane contained HA molecular weight standard, second and third lanes DNA ladders, fourth lane raw extracted EPS, fifth lane the 0.45 µm filtered EPS, sixth lane 0.45 µm filter wash, seventh lane 500 kDa retentate, eighth lane 30 kDa retentate, and the last lane contained the 30 kDa filtrate; 500 kDa, 50 kDa, and 25 kDa sizes were based on the DNA ladder that was previously compared with HA size standards.

Figure 2.5. Tangential flow filtration setup. The sample starts its journey from the "retentate" bottle, the liquid was pumped in the 500 kDa or 30 kDa cartridge measuring the pressure in order not to damage the filter. The filtrate was collected in a separate bottle and the retentate pressure was controlled with a clip in order to increase the flow to the filtrate bottle. The process was run for several min, until the retentate volume was too low for the system.

In order to purify high MW EPS from low MW EPS and contaminants, preparative size exclusion chromatography was tested. The different fractions were collected and assessed via gel electrophoresis (Figure 2.6(a)). All high MW fractions were pooled, washed, and resuspended in purified water (Figure 2.6(b)). The solution appeared viscous, colourless, clear, and free of any noticeable fragrance. After freeze-drying, the EPS appeared as a white aggregate that dissolved as soon as it was in contact with water (Figure 2.6(c)). The yield of purified EPS was about 1 $g*L^{-1}$ of stressed culture.

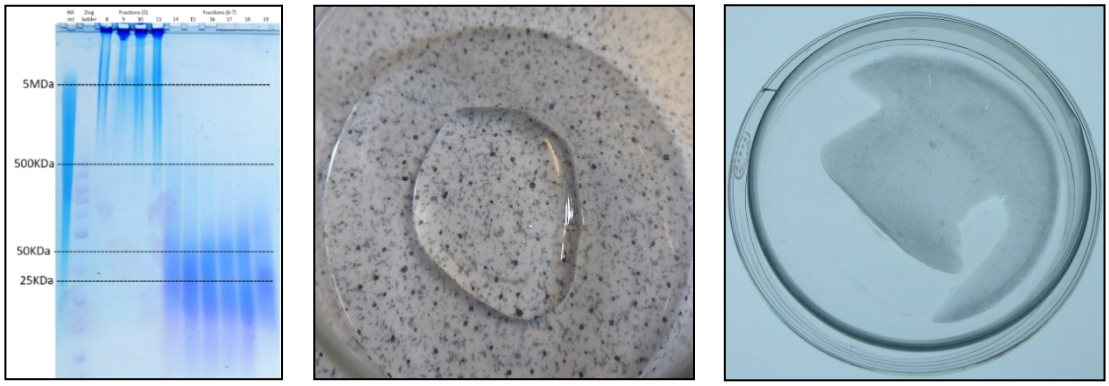

(a) (b) (c)

Figure 2.6. Size exclusion purification of high MW fractions. (a) Size exclusion fractions analysis with agarose gel electrophoresis; (b) high MW purified extracellular polymeric substances (EPS) resuspended in purified water; (c) freeze-dried high molecular weight (MW) purified EPS in a glass petri dish.

Discussion:

While heat extraction was identified as the best option for small scale extraction, translation to a larger scale may require super-heated water extraction, which is energy expensive. Since SDS, NaCl, and urea can be used to partially separate EPS from the cells, an optimised extraction carried out in conjunction with heat could be explored to lower the extraction temperature, decreasing time and costs.

2.3.3 Molecular size determination and conformation analysis

Results:

The number-average MW (Mn), used for kinetics studies and stoichiometric calculations, and the weight-average MW (Mw), used to determine tensile strength, were measured and polydispersity (Mw/Mn), that is a measure of the broadness of the molar mass distribution, was calculated.

Mn was calculated as 3.673×10^6 (±1.640%) Dalton (Da) or $g*mol^{-1}$ with a polydispersity of 2.987 (±24.970%).

The maximum MW registered was higher than 100 MDa (Figure 2.7), but the average MW was about 3.7 MDa. This suggests that the extraction protocol may degrade or fragment the EPS as well as separating it from the cells. Improvement of the extraction protocol could increase the average MW value, altering its rheological properties and potentially enabling its application in an expanded range of cosmetics, bio-medical, or food related product development opportunities.

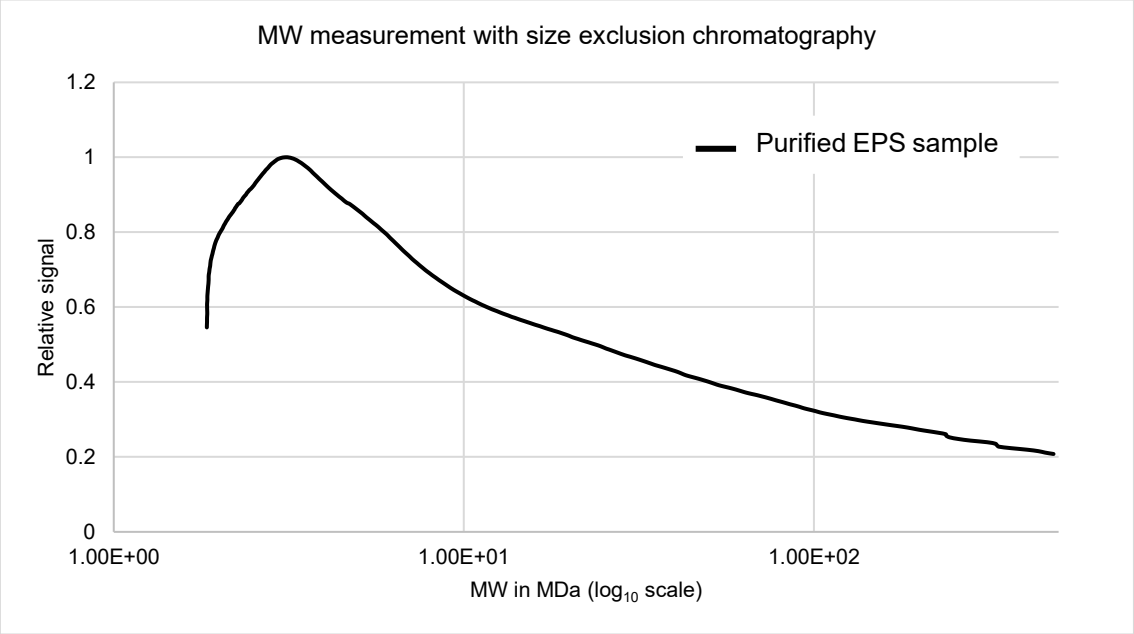

Figure 2.7. Chromatogram showing the MW distribution of the EPS with the relative signal showing the abundance relative to the molecular weight in MDa expressed in log_{10} scale.

The shape of the molecule can be assessed based on the relationship between the measured molar mass and root-mean-square (RMS) radius. A plot of the log of RMS radius in nanometres (nm) as a function of the log of the molar mass

expressed in g*mol^{-1}, called a Conformation Plot (Figure 2.8), shows the relationship between the two values.

The slope of this graph gives a good estimate of the shape. The slope calculated for this sample is 0.55, suggesting a flexible random coil structure. If the slope were about 0.33, it would have suggested a branched spherical shape, and a slope of 1 would have suggested a rigid linear rod shape [145,146].

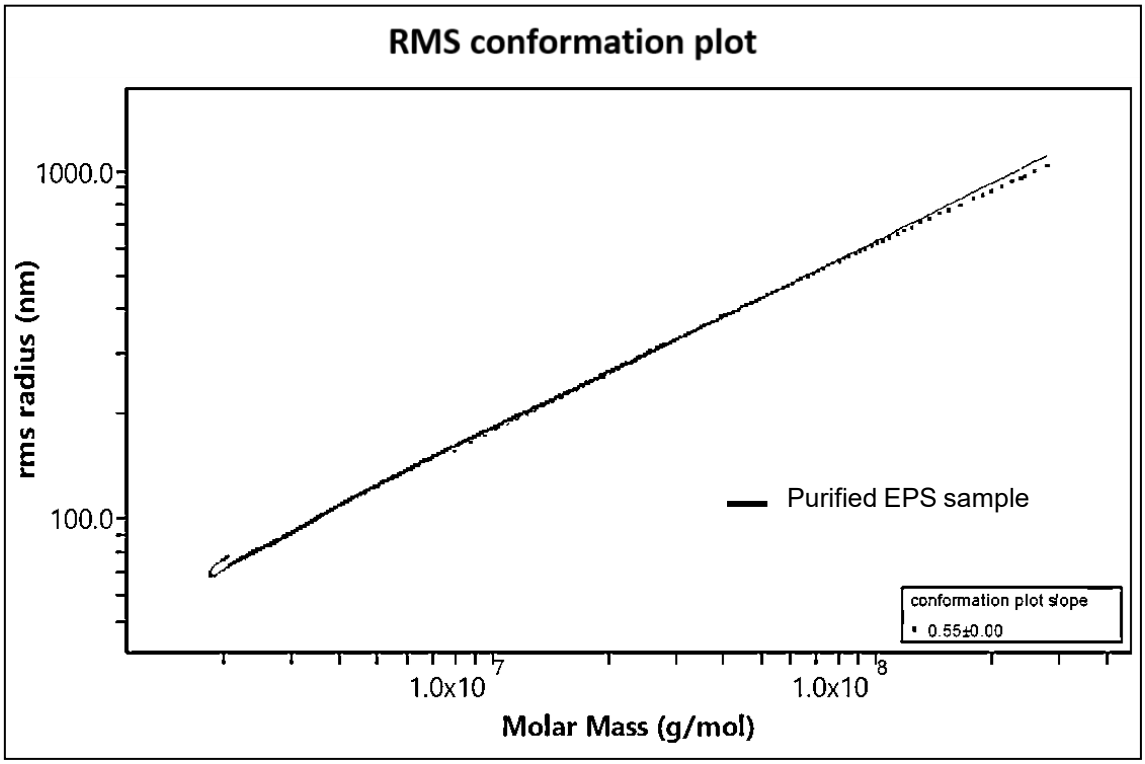

Figure 2.8. Root-mean-square (RMS) conformation plot of purified *L. segnis* EPS in relation to the molar mass.

2.3.4 Glycosyl composition and glycosyl linkage analyses

The freeze-dried sample was hydrolysed and analysed (Figure 2.9). The saccharides found in the sample were galactose, glucose and glucuronic acid along with an unidentified pyruvate containing hexose residue.

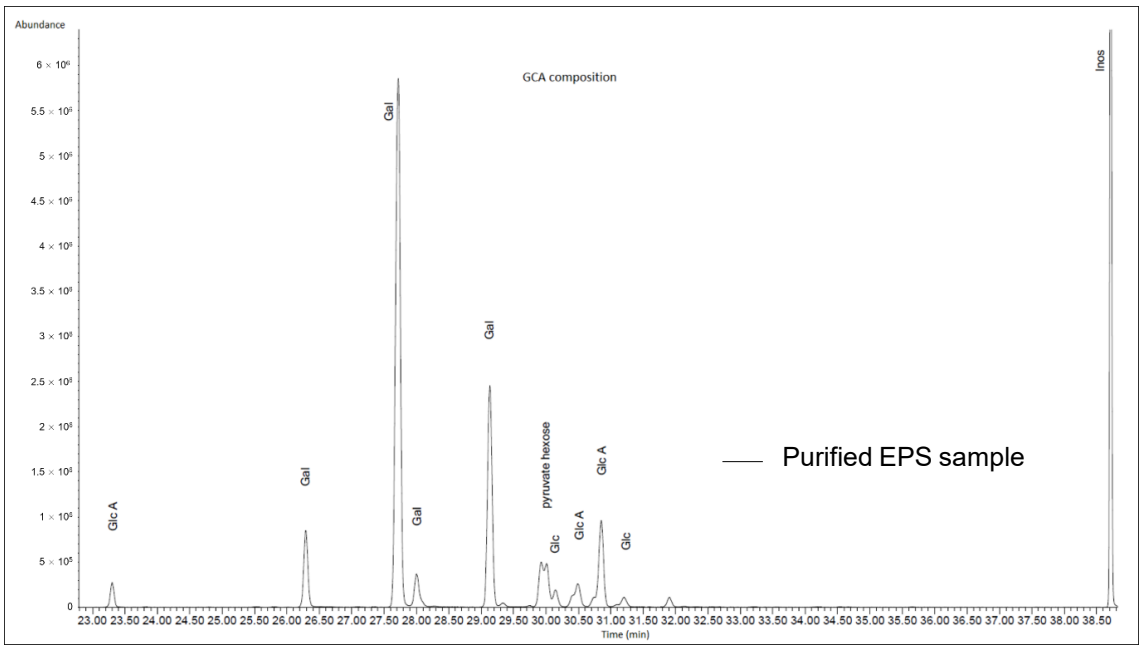

Figure 2.9. GC chromatogram of TMS derivatives of purified *L. segnis* EPS sample. Relative signal strength is represented on the Y axis relative to the retention time. Inositol used as internal standard. Glucuronic acid (GlcA); galactose (Gal); glucose (Glc).

The estimated amounts and mole percentage of each detected monosaccharide in the sample is summarised in Table 2.2.

Glycosyl Residue	Mass (µg)	Mole %
Glucuronic Acid (GlcA)	25.8	18.6
Galactose (Gal)	101.4	78.5
Glucose (Glc)	3.7	2.9
Total	130.9	100.0

Table 2.2. Glycosyl composition of purified high MW EPS reported in absolute weight and mole percentage.

Glycosyl linkage analysis was performed to identify the structure of the polysaccharide (Figure 2.10). The results, summarised in Table 2.3, are consistent with the previously reported composition data (Table 2.2). The presence of the 3,4,6 linked galactopyranosyl residue and the abundance of terminal sugars suggests that the structure of the polysaccharide is complex-branched. It is possible that some of the linkages were disrupted by the strong and non-specific extraction process. There is also no clear evidence of a regular repeat pattern of the glycosyl linkages.

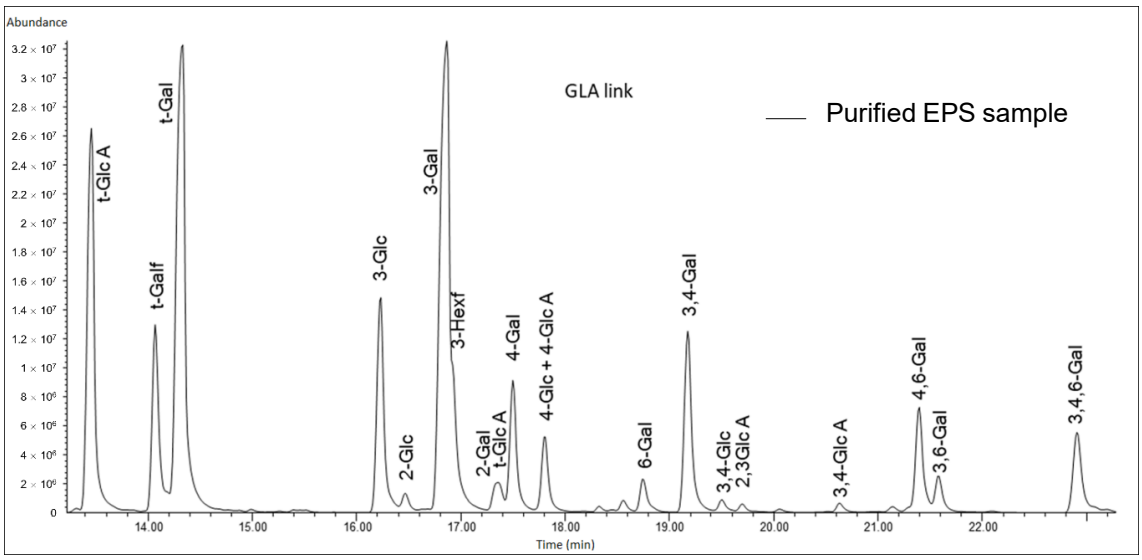

Figure 2.10. GC chromatogram of the PMAA derivatives of the sample. On the Y axis is represented the relative signal relative to the retention time. PMAA, partially methylated alditol acetates. Terminal Glucuronic Acid residue (t-GlcA); Terminal Galactofuranosyl residue (t-Galf); Terminal Galactopyranosyl residue (t-Gal); 3 linked Glucopyranosyl residue (3-Glc); 2 linked Glucopyranosyl residue (2-Glc); 3 linked Galactopyranosyl residue (3-Gal); 3 linked Hexofuranosyl residue (3-Hexf); 2 linked Galactopyranosyl residue (2-Gal); 4 linked Galactopyranosyl residue (4-Gal); 4 linked Glucopyranosyl residue (4-Glc); 4 linked Glucuronic Acid residue (4-GlcA); 6 linked Galactopyranosyl residue (6-Gal); 3,4 linked Galactopyranosyl residue (3,4-Gal); 3,4 linked Glucopyranosyl residue (3,4-Glc); 2,3 linked Glucuronic Acid residue (2,3-GlcA); 3,4 linked Glucuronic Acid residue (3,4-GlcA); 4,6 linked Galactopyranosyl residue (4,6-Gal); 3,6 linked Galactopyranosyl residue (3,6-Gal); 3,4,6 linked Galactopyranosyl residue (3,4,6-Gal).

PMAA	Mole %
Terminal Glucuronic Acid residue (t-GlcA)	14.2
Terminal Galactofuranosyl residue (t-Galf)	6.2
Terminal Galactopyranosyl residue (t-Gal)	21.8
3 linked Glucopyranosyl residue (3-Glc)	7.5
2 linked Glucopyranosyl residue (2-Glc)	0.5
3 linked Galactopyranosyl residue (3-Gal)	21.7
3 linked Hexofuranosyl residue (3-Hexf)	3.1
2 linked Galactopyranosyl residue (2-Gal)	0.8
4 linked Galactopyranosyl residue (4-Gal)	4.3
4 linked Glucopyranosyl residue (4-Glc)	2.0
4 linked Glucuronic Acid residue (4-GlcA)	0.5
6 linked Galactopyranosyl residue (6-Gal)	1.1
3,4 linked Galactopyranosyl residue (3,4-Gal)	6.9
3,4 linked Glucopyranosyl residue (3,4-Glc)	0.4
2,3 linked Glucuronic Acid residue (2,3-GlcA)	0.3
3,4 linked Glucuronic Acid residue (3,4-GlcA)	0.3
4,6 linked Galactopyranosyl residue (4,6-Gal)	3.8
3,6 linked Galactopyranosyl residue (3,6-Gal)	1.1
3,4,6 linked Galactopyranosyl residue (3,4,6-Gal)	3.6

Table 2.3. Glycosyl linkage analysis of purified high MW EPS expressed as relative percentage of each detected PMAA (partially methylated alditol acetates) in the sample.

2.3.5 Rheology analysis

Rheology is a branch of physics that studies the deformation and flow behaviour of all kinds of materials. Fluids can be classified as Newtonian (constant viscosity

independent from stress, shear rate) and non-Newtonian (variable viscosity dependent from stress, shear rate). There is interest in the cosmetic industry for low cost, naturally-sourced thickening agents that are clear, colourless and with neutral fragrance. The extracted *L. segnis* EPS sample appears to satisfy these criteria. Therefore, rheological properties of the extracted *L. segnis* EPS were explored to assess its potential for use within a cosmetics or personal care product formulation.

Non-stressed *L. segnis* culture, even at high cell density, showed a normal water-like behaviour. A few days after the culture entered stationary phase with continued acetic acid feeding, the cultures displayed higher viscosity. The viscosity of the stressed cell cultures and the extracted raw EPS were measured as explained in the materials and methods section using water (Newtonian fluid) and HA solution (non-Newtonian fluid) as standards. Extracted EPS shows a viscosity higher than water with a non-Newtonian trend at higher shear rate, similar although lower compared to the pure HA solution. Stressed algae cell cultures, at low shear rates, showed a higher viscosity compared to HA solution but it showed a different trend with the increase of the shear rate, probably due to the presence of the cells inside the EPS capsule (Figure 2.11).

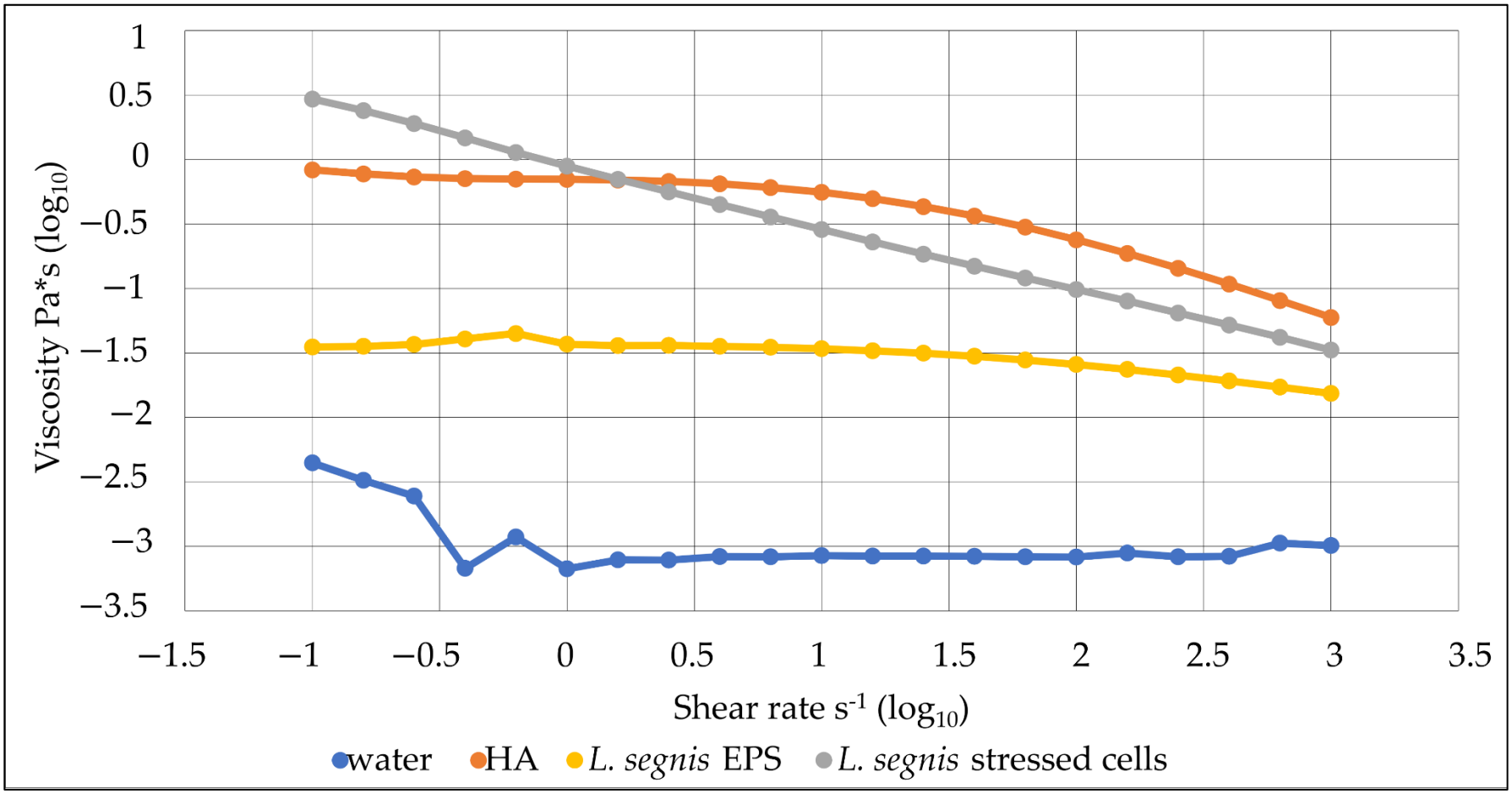
Viscosity Pa*s (log10)
1
0.5
0
−0.5
−1
−1.5
−2
−2.5
−3
−3.5
−1.5
−1
−0.5
0
0.5
1
1.5
2
2.5
3
3.5
Shear rate s-1 (log10)
water
HA
L. segnis EPS
L. segnis stressed cells

Figure 2.11. Viscosity measurement under variable shear stress of *L. segnis* EPS solutions. The viscosity is expressed in Pa*s reported on a log_{10} scale relative to the shear rate applied to the solution expressed in s^{-1} and reported on a log_{10} scale. Purified water and HA solution were reported as references to the analysed samples. Results of single measurements.

The effect of the addition of higher salt concentrations, 2 M NaCl, on the viscosity was investigated in order to further understand the behaviour of the *L. segnis* EPS under different conditions and to potentially optimize and improve the extraction protocol. In addition to salt, other compounds that could be tested for their ability to reversibly lower the relative viscosity of the solution are SDS and urea.

With NaCl addition, the viscosity of the stressed cells decreased considerably (Figure 2.12), showing a change that could impact positively upon the extraction costs, lowering the energy required for liquid pumping and mixing expenses.

In contrast, the effect on the EPS solution was milder at a high shear rate, which could be interpreted as the mixing during extraction, suggesting that optimisation and further investigation are needed to clarify the effects.

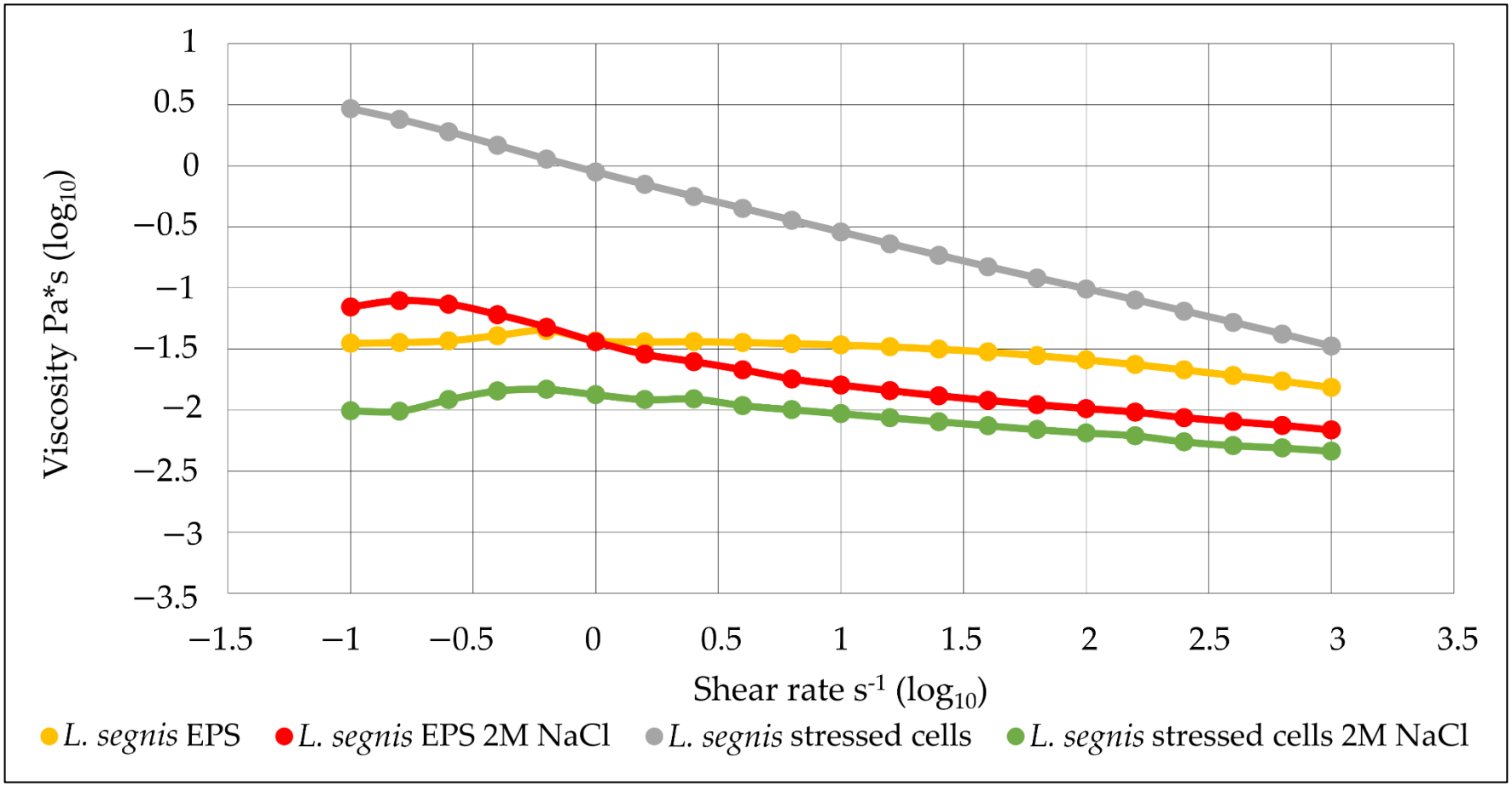
1
0.5
0
−0.5
−1
−1.5
−2
−2.5
−3
−3.5
Viscosity Pa*s (log10)
−1.5
−1
−0.5
0
0.5
1
1.5
2
2.5
3
3.5
Shear rate s-1 (log10)
L. segnis EPS
L. segnis EPS 2M NaCl
L. segnis stressed cells
L. segnis stressed cells 2M NaCl

Figure 2.12. Viscosity measurement under variable shear stress of *L. segnis* EPS solutions with added 2M NaCl. The viscosity is expressed in Pa*s reported on a log_{10} scale relative to the shear rate applied to the solution expressed in s^{-1} and reported on a log_{10} scale. Purified water and HA solution were reported as references to the analysed samples. Results of single measurements.

2.3.6 Antioxidant capacity and reducing power quantification assays

Antioxidants are usually used as preservatives in food and cosmetics and as active ingredients in cosmetics because of their skin protection properties [147–149], with ascorbic acid (vitamin C) being the most powerful, most widely used and least toxic natural antioxidant [150]. Other natural compounds with high antioxidant activity are tocopherols, carotenoids and flavonoids [150]. Total antioxidant capacity and reducing power of non-purified *L. segnis* EPS were measured with *in vitro* assays.

As shown in Table 2.4, *L. segnis* EPS sample, showed 100 times less antioxidant capacity compared to pure vitamin C. Other values are reported in the same table for reference [132,151,152].

Extract	Antioxidant Capacity (mg EAscA*g^{-1} of Dry Sample)
orange	50
spinach	0.6
red onion	0.84
tomato	8.6
Chlamydomonas sp.	5.7
HA	190
L. segnis EPS	10.0 ± 0.5

Table 2.4. Antioxidant capacity values reported in mg of equivalent of ascorbic acid (EAscA) relative to g of dry sample extracted from literature [132,151,152] for comparison with the value measured for *L. segnis* EPS.

Another way to measure the antioxidant activity of a compound is the reducing power. In Table 2.5 is shown the measured value for *L. segnis* EPS and a value from literature as reference [132].

Extract	Reducing Power (mg EAscA*g^{-1} of Dry Sample)
Chlamydomonas sp.	2.3
L. segnis EPS	0.750 ± 0.038

Table 2.5. Reducing power values reported in mg of equivalent of ascorbic acid (EAscA) relative to g of dry sample extracted from literature [132] for comparison with the value measured for *L. segnis* EPS in this study.

2.4 Discussion

The faster growth of *L. segnis* observed under mixotrophic condition suggests a synergistic effect of acetate and light, giving a higher response than an additive effect when the two were used together at the same time. The possible explanation for this behaviour could be that the strain is using acetate as carbon source through the respiration pathway producing CO_2 that may be used for photosynthesis using light [153,154].

Based on the information collected with *L. segnis* growing with equimolar quantity of urea, providing double the amount of nitrogen to the cells compared to the other nitrogen sources tested, the nitrogen content in the medium didn't not appear to be limiting the biomass density at the stationary phase; instead, the limiting factor could be the acetic acid that is the carbon source together with the CO_2 from the air. As reported in the material and method, a strong light stress was applied to the culture after it reached the stationary phase in order to stimulate the production of EPS. When this stress was applied, the appearance of the liquid culture did not change. It is reported that a high carbon to nitrogen ratio (C/N) stimulates EPS production due to nitrogen limitation [155]. In a large-scale setting, an improved heterotrophic protocol in fermenters could be more effective in optimizing *L. segnis* growth and stress conditions.

The extraction and purification methods utilised are relatively complicated and expensive with regard to materials and energy required, and could limit exploitation to high-value applications. A process to cheaply and reversibly lower the viscosity of the solution would positively influence the costs involved with this step and have a substantial impact in the overall cost of production. The high

viscosity of the stressed cells suggests that, if an improved way to extract higher MW EPS could be found, the viscosity of higher MW *L. segnis* EPS could be equivalent or even higher than that of the HA solution. There is interest in the cosmetic industry for low cost, naturally-sourced thickening agents that are clear, colourless, and of neutral fragrance [1]. The extracted *L. segnis* EPS sample could satisfy these criteria, upon further improvements, and shows potential as a future ingredient.

The fact that the EPS was able to migrate within an agarose gel electrophoresis set-up using TBE buffer suggested that it possesses a net negative charge consistent with it being a polyanion. This is similar to HA or other glycosaminoglycans [156].

Notably, N-acetylglucosamine was not detected in the sample, demonstrating that this EPS is not HA as was previously suggested [133] and is also not a glycosaminoglycan.

Antioxidants are often used as preservatives in food and cosmetics and as active ingredients in cosmetics because of their skin protection properties [147–149], with ascorbic acid (vitamin C) being the most powerful, most widely used, and least toxic natural antioxidant [150]. Other natural compounds with high antioxidant activity are tocopherols, carotenoids, and flavonoids [150]. The antioxidant activity of *L. segnis* EPS is significant and could help in cosmetic formulations, lowering the costs of other antioxidant agents that need to be added. Ingredients for food applications must have a very low manufacturing cost in order to be considered for further exploration as alternative to commonly used ingredients, and this platform requires significant development in order to achieve

this need. Furthermore, it would be a novel food ingredient that would need extensive and costly testing, projected to cost between £350,000 and £500,000 before approval. Even for cosmetic applications, the substance must be examined and certified by the Scientific Committee on Consumer Safety (SCCS) before it may be considered.

2.5 Conclusions

In this study, *Lobochlamys segnis* was investigated for the production of EPS.

The best growth and stress conditions of those tested were determined to be mixotrophic growth using acetate as the carbon source and carbon-feeding-rate controlled by pH value.

Tangential flow filtration and size exclusion chromatography proved suitable as purification techniques, which bodes well for the development of a large-scale industrial process.

Although the capsular PS produced by *L. segnis* was initially suggested to be HA, here was shown to be incorrect. While the colour of the stained product as visualised in agarose gel electrophoresis is similar to HA, when gel migration is used, the EPS products are clearly distinguishable. Indeed, the maximum MW of the purified *L. segnis* EPS measured (over 100 MDa) is vastly different from that observed for HA, 10 MDa in *Heterocephalus glaber* [157]. Glycosyl composition analysis confirmed this definitively by determining the presence of galactose and glucuronic acid with traces of glucose rather than the alternating repeats of β-1,4-D-glucuronic acid and β-1,3-N-acetyl-D-glucosamine units characteristic of HA.

The thickening property of the high MW *L. segnis* EPS is an interesting phenomenon, along with the antioxidant property and so far, *L. segnis* EPS characteristics can be considered as amenable to its use as a HA alternative. Rheological and antioxidant properties need to be more thoroughly analysed with additional characterisation for new applications being fundamental in order to fully understand and exploit the compound, together with the investigation of biocompatibility and non-toxicity of the extract. Some examples of other bioactivities that could be investigated in future are antiviral, bacteriostatic, antibiotic, mammalian cell growth stimulation, wound healing, and acting as a stabilizing agent, suspending agent, flocculating agent, encapsulating agent, emulsifying agent, and/or lubricating agent and volumizing activity.

The first objective (investigation of a stress-induced platform for the possible production of HA) was achieved. Despite the fact that *L. segnis* EPS had interesting characteristics, the hypothesis of the project (feasibility for microalgal HA production) was yet neither accepted nor rejected because the EPS was found not to be HA. Therefore, this branch of the research was not further pursued and the focus in the following chapters moved to *C. variabilis*, which is reported to produce HA following Chlorovirus infections.

Chapter 3 - Method development for the study of Chlorovirus life cycles

This chapter was published with me as first Author and with my supervisors as co-authors [158] (Appendix C). It was found that sufficiently sensitive tools to study *Chlorella*/viruses interactions for industrial applications were not available. Thus, the work in this chapter describes the development of Algem PBRs protocols to allow this work to be undertaken.

3.1 Introduction

There are a variety of tools, techniques and methodologies for characterising viruses, their life cycles, and their properties. Broadly, three main approaches are taken: direct observations derived from impact on host (such as viral plaque assay [159], infection dose (ID_{50}) [160] and immunofluorescence foci assays [161]); observations based upon specific components of the virus or infected hosts (e.g. quantification of viral nucleic acid and protein including qPCR [162], immunoblotting [163], immunoprecipitation [164], ELISA [165], mass spectrometry [166] and next-generation sequencing/metagenomics [167,168]); and, lastly, direct physical assessment/observation of whole viral particles (via flow cytometry [169], scanning/transmission electron microscopy [170] or confocal microscopy [171]).

For the microalgal viruses, the most commonly used techniques are viral plaque assay [172], transmission electron microscopy [110] and flow cytometry [173], together with mass spectrometry for metabolite analysis and next-generation

sequencing/metagenomics for genomic/transcriptomic analysis. Few generically applicable protocols have been developed that exploit monitoring of the physiological state of the host cells to learn about the presence and activity of these poorly understood yet fascinating viruses.

Previously, in order to determine Phycodnavirus host lysis and/or release time, the only possible way was to sample infected cultures at multiple timepoints and monitor visually the state of the individual infected cells or determine a virus particle count in the media. Such approaches require intensive effort and are prone to low sensitivities. They are further exacerbated by poor environmental control, variation in virus stock quality and relatively long infection life cycles.

Here, it was introduced a new method that closely monitors host health and integrity to gain new insights regarding the infection strategy of the *Chlorella variabilis* infecting Chloroviruses. This automated method exploits the continuous monitoring of infected microalgae cultures in highly controllable lab scale photobioreactors (PBR) that provide the opportunity for environmental control, technical replication and intensive monitoring, crucially, without a requirement for external intervention or disruption. In conjunction with established techniques, this novel application of PBR technology enabled an easier improvement of growth conditions and medium composition, the identification of subtle differences in virus life cycle and multiplicity of infections (MOI), a more accurate estimation of plaque forming units (pfu) released per lysed cell, the exploration of virus release strategies, as well as the investigation of the role of potential signalling molecules in controlling the virus life cycle.

3.2 Materials and methods

3.2.1 Microalgae strains, virus isolates and growth conditions

Chlorella variabilis CCAP 211/84 was obtained from the Culture Collection of Algae and Protozoa (CCAP) located at the Scottish Association for Marine Science (SAMS) [174]. The strain was maintained on Tris-acetate-phosphate (TAP) medium [136] (composition reported in Chapter 2) with added vitamins (Vitamin B1 1 mg*L^{-1} final concentration and B12 12 µg*L^{-1} final concentration) on 1.5% agar plates and re-streaked every month.

Three media, prepared as per reference, were tested: TAP medium [136] with added vitamins (composition reported in Chapter 2), high salt medium (HSM) with added vitamins [137] (composition reported in Chapter 2) and Bold's basal medium (BBM) [175] (components in 1 L: $NaNO_3$ 0.25 g, $MgSO_4*7H_2O$ 75 mg, NaCl 25 mg, $CaCl_2*2H_2O$ 25 mg, K_2HPO_4 75 mg, KH_2PO_4 0.175 g, H_3BO_3 11.4 mg, Na_2-EDTA 50 mg, $ZnSO_4*7H_2O$ 8.82 mg, $MnCl_2*4H_2O$ 1.44 mg, MoO_3 0.71 mg, $CuSO_4*5H_2O$ 1.57 mg, $Co(NO_3)_2*6H_2O$ 0.49 mg, KOH 31 mg, $FeSO_4*7H_2O$ 4.98 mg, H_2SO_4 1 mL, purified water up to 1 L) modified by the addition of 0.5% sucrose and 0.1% proteose-peptone (MBBM) [172] prepare with the recipes reported in the reference. The carbon sources tested in HSM were all at the same concentration of 3%. The nitrogen sources tested in TAP medium were normalised to the molarity of nitrogen in the media. Virus isolates PBCV-1, CviKI, IL-5-2S1, NYs-1 and MA-1D were gifted by Dr. David D. Dunigan's laboratory at the University of Nebraska-Lincoln. Virus isolate TAAS 2.1 was one of a number of viral isolates obtained from water samples taken from small ponds located in

rural New Hampshire, USA, through viral plaque assay [172] using TAP medium plates with added vitamins. Fresh viral stocks were prepared infecting *Chlorella variabilis* cultures in exponential phase (5-10×10^6 cells*mL^{-1}), and collecting the lysed culture after 24 h post infection (p.i.); viral lysates were stored at 4 °C.

Titration of the viral stocks was performed in triplicate using viral plaque assays of serial dilutions of the supernatant of lysed cells as per reference [172] using TAP agar plates with added vitamins as an alternative richer medium. By using TAP medium, *Chlorella* monolayers growing within the soft top agar greened significantly faster as compared to the more conventional published and widely used approach that uses MBBM media [172]. Results were expressed as the mean of the 3 replicates ± standard deviation, in pfu*mL^{-1}.

TAP medium [136] with added vitamins was also used for liquid cultures. Cultures were grown in Algem® HT24 photobioreactor [176] in 25 mL volume inside 50 mL clear and clean glass Pyrex Erlenmeyer flasks or Algem PRO photobioreactor [176] in 400 mL volume in 1 L clear and clean Pyrex Erlenmeyer flasks. In both cases the growth conditions were 28 °C with white LED light intensity set at 200 µE photosynthetically active radiation (PAR) measuring the OD at 740 nm every 10 min. The mixing was set to 120 rpm and gas aeration within the Algem PRO cultures was set with a flow rate of 25 mL*min^{-1} of 30% CO_2/air in small pulses (not a continuous flow) in order to control the pH of the culture at pH 7 via computer-controlled solenoid valve. All experiments were performed in triplicate.

The average growth rates of the experiment reported in Figure 3.1, were calculated between day 1 and day 2 of cultivation by subtracting the OD value at day 1 from the OD value at day 2. Dry weight (DM) was measured by centrifuging

20 mL of culture, washing the pellet with 1 mL of deionised water once and the pellet was left at 70 °C overnight with the tube open to dry. Cell count was performed manually using Olympus BH2 microscope with phase contrast 10x magnification lens, using a Neubauer cell count chamber (VWR, UK).

3.2.2 Culture crash time calculations and estimation of virus particle release per cell at lysis

The first derivatives of all curves were calculated and, based on the data collected from PBCV-1 lysis, the value of −0.006 of the first derivative, which shows the moment at which the curve has a significantly faster decrease of the OD with a p value lower than 0.05, was determined to be the start of culture crash time. The lysis time for all other virus isolates was calculated based on this assumption, and verified with microscopy monitoring where lysis time were feasible to do so. The average lysis times and the standard deviations were calculated based on 3 independent biological replicates. To calculate the number of virus particles released per cell, the following formula was used considering values of MOIs greater than 1 as MOI 1 assuming in the case of multiple infections per cell that overall virus production capacity is identical.

$$10^{n}\left(\frac{pfu}{cell}\right) = \frac{average\ culture\ crash\ time\ of\ MOI = 1}{average\ culture\ crash\ time\ of\ MOI < 1 - average\ culture\ crash\ time\ of\ MOI = 1}\sqrt{10^{-(Log_{10}(MOI<1)}}$$

For more accurate calculations, the experiment was repeated with multiple MOIs <1 and the results were plotted as culture crash time in h (y axis) against the Log_{10} of the MOI, again considering values of MOIs greater than 1 as MOI 1. The linear trendline between the points was derived and the calculated values using

the formula from the trend line were used to calculate the order of magnitude of the number of virus particles released per cell with the formula mentioned earlier.

3.2.3 Verification of the presence of signalling molecules

Spent medium was collected at 7 h p.i. from cultures infected with an MOI of 5, 10^{-4} and 10^{-6} and filtered through a 0.2 µm filter (Minisart NML Plus hydrofilic, GF+Cellulose acetate, VWR, UK) initially and 10 kDa MW cut-off PES filter (Vivaspin 20 Centrifugal concentrator, VWR, UK) afterwards, and used to resuspend the cells prior to the infection at a MOI of 10^{-4}.

3.2.4 Verification of the virus release method after infection

Three, 25 mL cultures of *Chlorella variabilis* in TAP with added vitamins in exponential phase, were infected with an MOI of 5. One-h p.i., the cells were harvested via centrifugation at 6000 × g for 2 min, resuspended in 1 mL fresh TAP medium and moved into a 2mL tube. Cells were harvested again via centrifugation at 6000 × g for 2 min and resuspended again in 1 mL of fresh TAP medium. This process was repeated 5 times and was used to remove all unbound virus particles or loosely bound particles. At the end of the 5 washes, the cells were resuspended in 25 mL fresh TAP medium and 1 mL was harvested every h for the first 7 h p.i. and after 24 h p.i. via centrifugation at 6000 × g for 2 min and filtered with a 0.45 µm filter (Minisart NML hydrofilic, Cellulose acetate, VWR, UK). 0.5 mL of each was used for the infection of a 25 mL culture and monitored in the Algem HT24.

3.3 Results

3.3.1 Growth medium improvement

The standard growth conditions for *Chlorella variabilis* are well established [172,177] and, since 1965, (MBBM) has been utilised predominantly despite supporting slow growth and low maximum culture cell densities at stationary phase. In order to improve growth rate and final cell density, two additional media (TAP and HSM) identified from the literature were therefore tested to assess their suitability to support the growth of this strain, TAP and HSM, but after subculturing *Chlorella variabilis* in these media several times, growth was observed to gradually decrease.

Through inclusion/exclusion experiments, it was subsequently identified that the presence of vitamins B1 and B12 are essential for the growth of this microalgal strain. In Figure 3.1(a) is shown the comparison between TAP and TAP+v, sub-cultured for the first time from TAP+v.

The growth rates in the two conditions tested are identical, but without vitamins, the culture reached the stationary phase at a lower cell density. In the absence of vitamins, the initial growth was supported by the residual vitamins present in the cells. In the MBBM medium the vitamins are provided by the proteose-peptone fraction, which also provides nitrogen in the form of amino acids, making the investigation of nitrogen source and optimal content challenging.

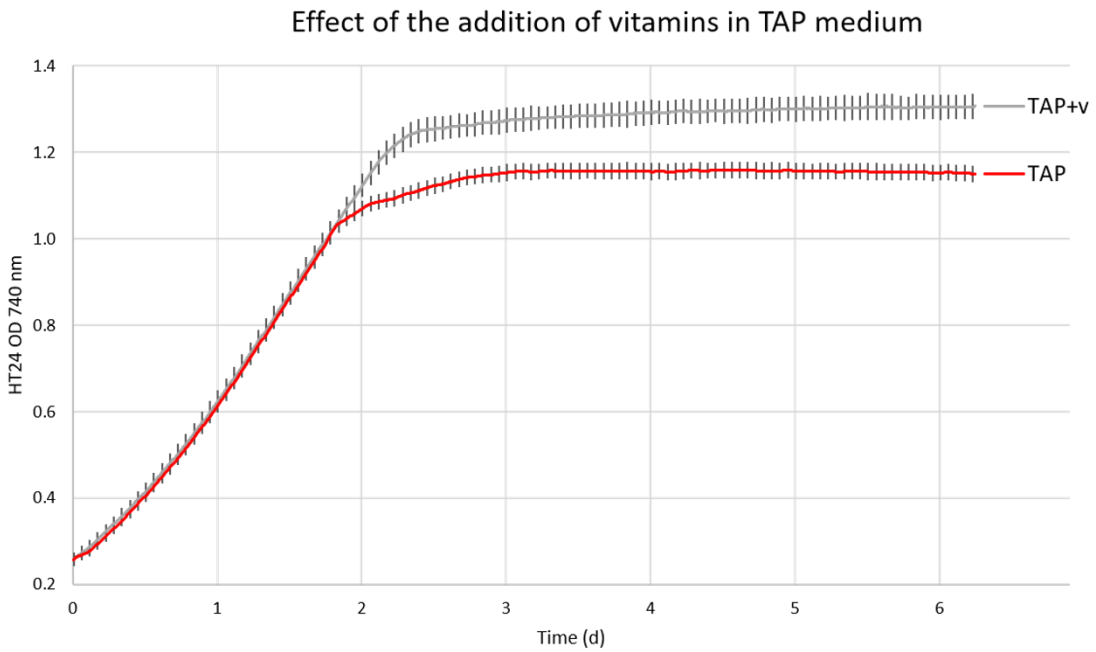
Effect of the addition of vitamins in TAP medium
HT24 OD 740 nm
Time (d)
TAP+v
TAP
1.4
1.2
1.0
0.8
0.6
0.4
0.2
0
1
2
3
4
5
6

(a)

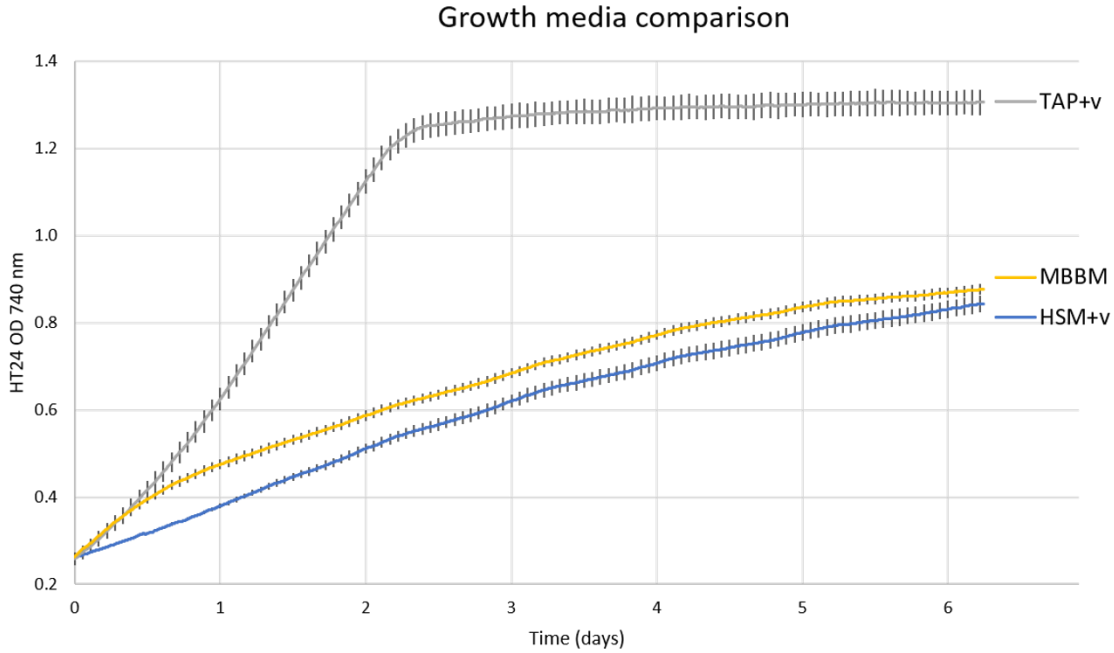
Growth media comparison
HT24 OD 740 nm
Time (days)
TAP+v
MBBM
HSM+v
1.4
1.2
1.0
0.8
0.6
0.4
0.2
0
1
2
3
4
5
6

(b)

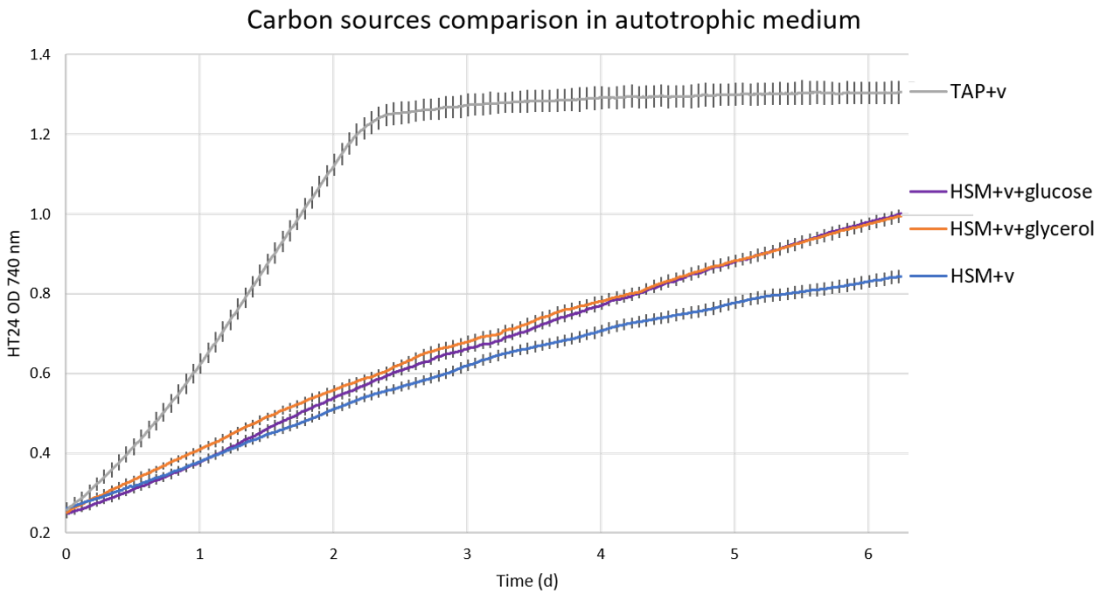

(c)

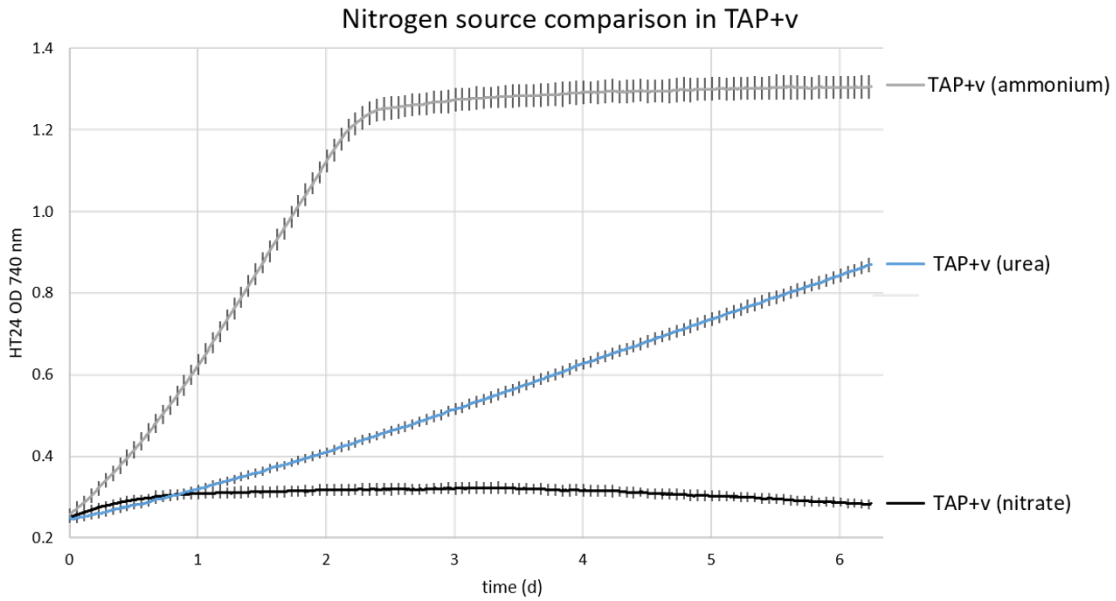

(d)

Figure 3.1. Growth of *Chlorella variabilis* in different media compositions. (a) Comparison of growth in TAP and TAP with added vitamins (TAP+v); (b) Comparison of growth in HSM+v, TAP+v and MBBM; (c) impact of carbon sources in HSM+v medium in comparison with TAP+v medium; (d) effect of nitrogen sources on cell growth in TAP+v medium. The plotted values are the mean of 3 replicates with standard deviations.

The comparison of TAP and HSM, both with added vitamins with MBBM, Figure 3.1(b), shows that the mixotrophic condition with acetate, represented by the TAP

medium, yields the highest growth rate (Table 3.1) and final biomass density. To benchmark against the acetate found in TAP medium, alternative carbon sources were investigated in HSM+vitamins (v): glucose, fructose, galactose, maltose, arabinose, lactose, sucrose and glycerol were investigated in Algem HT24 photobioreactor with mixing and without aeration. Fructose, galactose, maltose, arabinose, lactose, and sucrose had negligible impact on growth rate or final biomass. However, glucose and glycerol had a positive impact on growth rate and final biomass density achieved, but were inferior to the acetate-based TAP+v media, as shown in Figure 3.1(c).

Utilising TAP+v medium variants, (the media that resulted in the highest growth rate and final biomass density) it was investigated the impact of 3 different nitrogen sources, ammonium chloride (as in the original recipe), urea and potassium nitrate on growth (Figure 3.1(d)). The strongest growth was obtained using ammonium, but the strain was also able to process urea; however, no growth was observed on nitrate, which is the nitrogen source in the original BBM, supporting the notion that proteose-peptone is providing the nitrogen necessary for the growth of this strain when in MBBM.

The optimal media was found to be TAP with added vitamins using ammonium chloride as nitrogen source, which yielded more than 3.5 times more biomass than MBBM after 6 days and the growth rate was more than 4 times higher than that observed in MBBM. It was used TAP+v media with ammonium chloride in all the subsequent infection experiments.

Medium	Average growth rate (OD 740 nm increase*d^{-1})	Average DM measured at day 6.24 (g*L-1)
MBBM	0.112 ± 0.010	0.42 ± 0.02
HSM+v + glucose	0.162 ± 0.008	0.74 ± 0.03
HSM+v + glycerol	0.148 ± 0.009	0.73 ± 0.03
HSM+v	0.131 ± 0.007	0.34 ± 0.02
TAP (ammonium)	0.499 ± 0.025	1.37 ± 0.06
TAP+v (ammonium)	0.499 ± 0.025	1.53 ± 0.05
TAP+v (urea)	0.065 ± 0.004	0.43 ± 0.02
TAP+v (nitrate)	0.008 ± 0.001	Too low

Table 3.1. Calculated average growth rates of *Chlorella variabilis* expressed in average change in OD value per day ± standard deviation and measured DM expressed as mean ± standard deviation. All experiments were performed with 3 biological replicates.

3.3.2 Viral induced lysis at saturating MOI

Chlorella variabilis cells were cultured in TAP medium with added vitamins in Algem PRO photobioreactors and maintained in exponential growth phase, subculturing weekly starting at 10^5 cells*mL^{-1}. Cells were infected with a multiplicity of infection (MOI) of 5, i.e. 5 pfu per cell, for each of the different virus isolates. The optical densities at 740 nm of the infected cultures were automatically measured every 10 min for 16 h.

As shown in Figure 3.2 and reported in literature [126], following infection, the cells stopped growing, compared to the non-infected cultures for which the OD

increases. At differing times p.i., relative to each strain isolate, the measured OD values of infected cultures began to decrease as the cultures started crashing. All virus isolates caused a unique and reproducible absorbance profile in the host algal strain reflecting and revealing differences in their life cycle dynamic including average lytic cycle length.

Similar experiments were performed changing the MOI to 10^{-4}, namely 1 pfu per 10^4 cells to look for the impact of a lower ratio virus/algae. Culture crash times at lower MOI (10^{-4} MOI, shown in Figure 3.4) were used to gather data about the number of pfu released per cell; reasoning that the more pfu released per cell, the shorter the difference between the lysis times at the different MOIs will be.

The choice of 10^{-4} MOI is based on previous knowledge from PBCV-1 virus that releases about 200 pfu per lysed cell [126]. Under this scenario and assuming complete mixing of cultures, PBCV-1 would infect all cells in the culture within 2 viral lytic cycles and complete culture crash would be achieved within 3 lytic cycles.

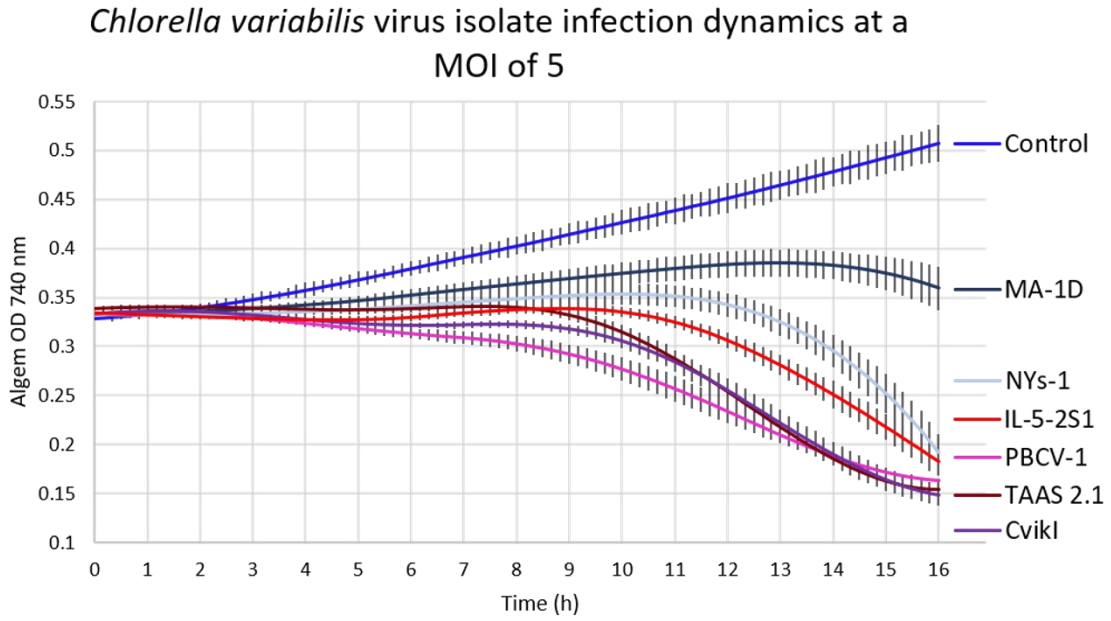

Figure 3.2. Infection of *Chlorella variabilis* cultures at a MOI of 5 with PBCV-1, MA-1D, NYs-1, TAAS 2.1, CviKI and IL-5-2S1 virus isolates and uninfected control cultures of *Chlorella variabilis* strain CCAP 211/84. The plotted values are the mean of 3 biological replicates with standard deviations.

3.3.3 Culture crash time calculations and estimation of virus particle release per cell at lysis

Three PBCV-1 infected cultures at a MOI of 5, were monitored every h with manual cell count using the microscope, up to 8 h p.i., to determine when the cells started lysing. As shown in Figure 3.3, before 7 h p.i. there was no significant difference in the relative host cell density (10^7 cells*mL^{-1}). At 7 h p.i. the culture density was lower and statistically significant when compared against previous time points of the infected culture, with a p-value lower than 0.01. After 8 h p.i. most of the cells were lysed. Based on this result could be inferred that the PBCV-1 infected CCAP 211/84 cells started to lyse after 6 h p.i. under the conditions tested.

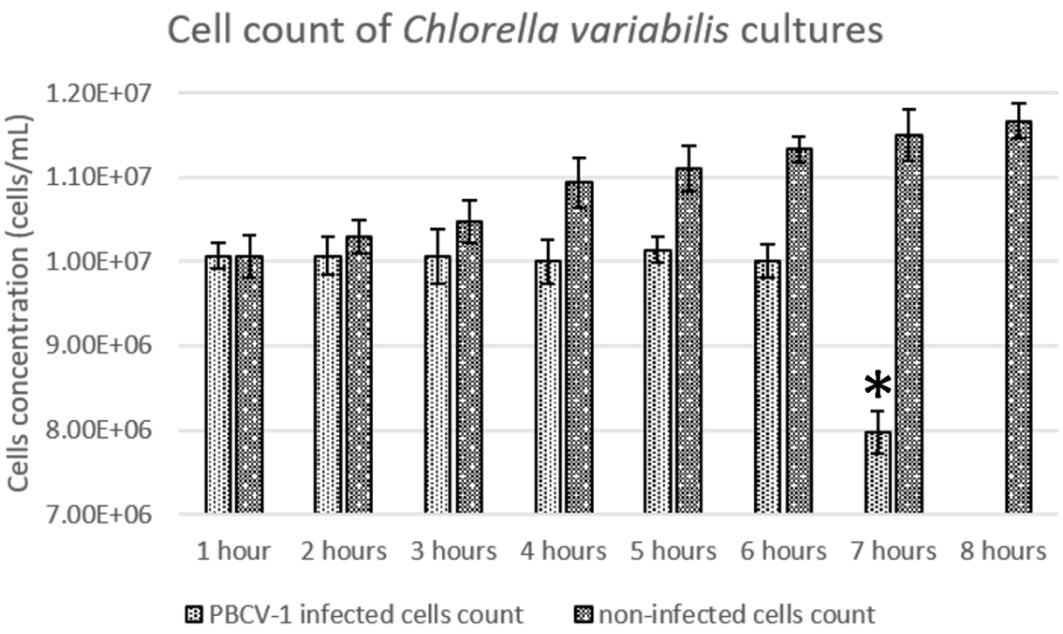

Figure 3.3. Cell count of PBCV-1 infected (lighter bar) and non-infected (darker bar) *Chlorella variabilis* cultures for the estimation of the culture crash time. The asterisk indicates statistical significance compared to the previous timepoints with a p value lower than 0.01.

The culture crash time was calculated for all conditions as mentioned in the material and methods section and reported in Figure 3.4.

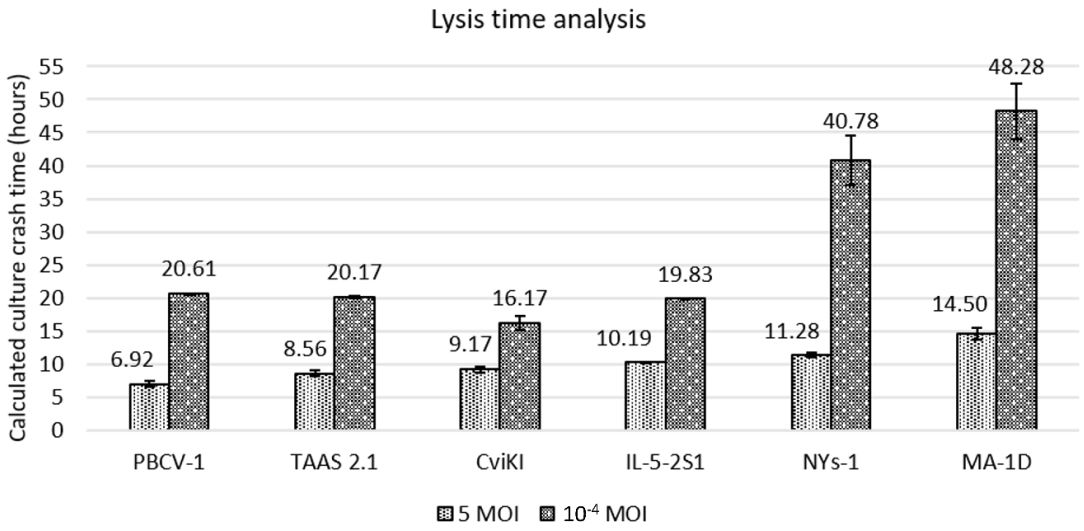

Figure 3.4. Calculated lysis time for PBCV-1, MA-1D, NYs-1, TAAS 2.1, CviKI and IL-5-2S1 virus isolates. The data represents the mean of 3 biological replicates with calculated standard deviations.

CviKI has the lowest ratio between culture crash time at the two different MOIs compared to the other viruses included in this analysis suggesting a greater stability of virus particles, faster lytic cycle at lower MOIs or largest burst size (number of virus particles released per single cell). Therefore, as the most robust and reliable virus culture system, CviKI was chosen to test further possible applications of the Algem HT24 high throughput photobioreactor. A novel approach may be used to calculate the order of magnitude of the pfu*cell^{-1} for all viral isolates. Some viruses might have a greater binding capacity to cell debris, in which case the measurement of pfu*cell^{-1} using plaque assay in the spent media would give an underestimation of the true value.

The results of the calculation for PBCV-1, for which the value is known and reported [126], and for CviKI are reported and compared to the values determined by plaque assays.

In this instance, for PBCV-1 the 2 values coincided: (200 ± 10) pfu*cell^{-1} from the plaque assay and 10^2 as the order of magnitude calculated using the culture crash times at the 2 different MOIs.

For CviKI the 2 values were different by 2 orders of magnitude: (1000 ± 200) pfu*cell^{-1} measured with the plaque assay and a calculated order of magnitude of 10^5 pfu*cell^{-1}. For confirmation of the calculated value based on the culture crash time observed, the microalgae were infected with the CviKI virus at multiple MOIs.

3.3.4 Analysis of observed culture crash time for CviKI-infection based on MOI

Microalgae cultures were infected in triplicate at saturating MOI, 2.6×10^{-2} MOI, 2.6×10^{-4} MOI and 2.6×10^{-6} MOI and monitored by growth in the Algem HT24 photobioreactor. The lysis times for all these conditions were calculated as explained earlier and the results were plotted as shown in Figure 3.5.

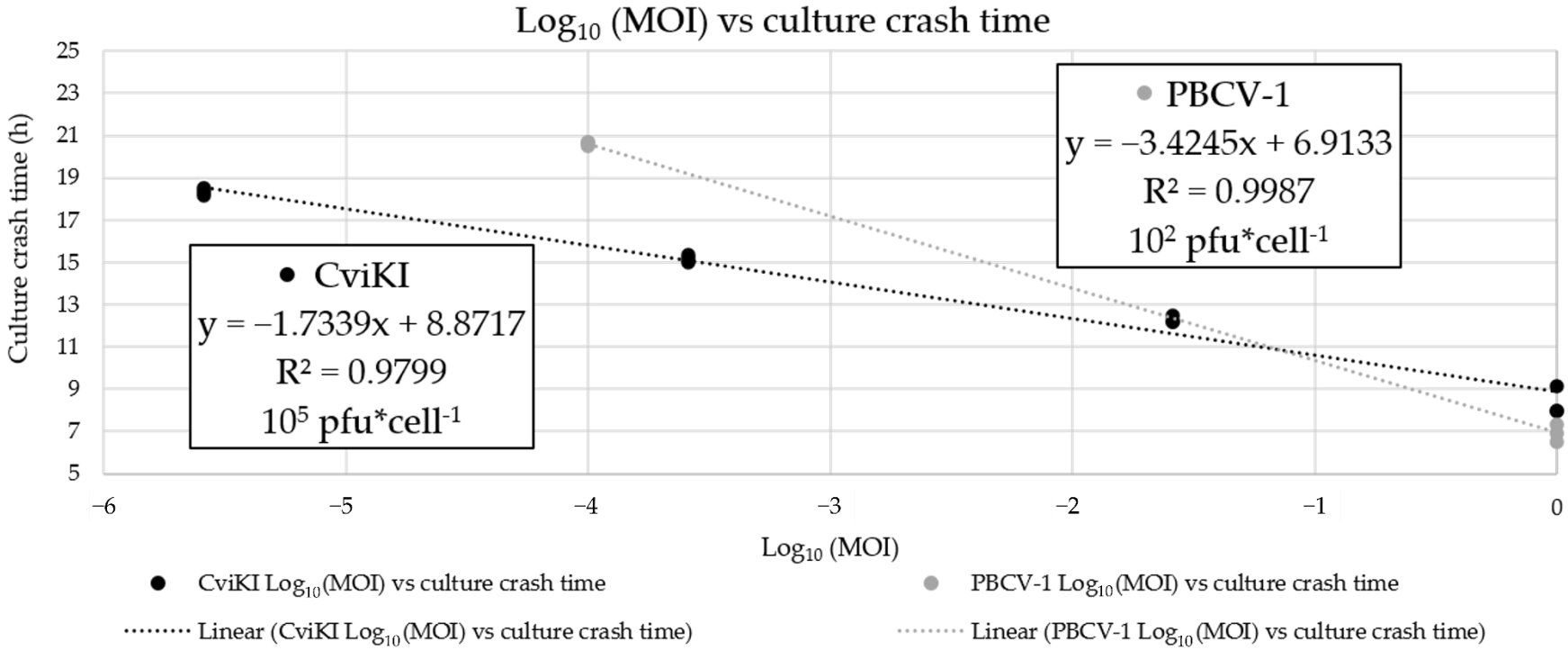
Log10 (MOI) vs culture crash time
Culture crash time (h)
25
23
21
19
17
15
13
11
9
7
5
−6
−5
−4
−3
−2
−1
0
Log10 (MOI)
CviKI
y = −1.7339x + 8.8717
R² = 0.9799
10^5 pfu*cell^-1
PBCV-1
y = −3.4245x + 6.9133
R² = 0.9987
10^2 pfu*cell^-1
CviKI Log10(MOI) vs culture crash time
PBCV-1 Log10(MOI) vs culture crash time
Linear (CviKI Log10(MOI) vs culture crash time)
Linear (PBCV-1 Log10(MOI) vs culture crash time)

Figure 3.5. Linear regression of Log_{10} of the MOIs versus the culture crash time of infected cells with PBCV-1 (grey) and CviKI (black) viruses. Linear regression equations, R^2 values, and the calculated pfu*cell-1 are reported on the graph. The data are reported as three biological replicates for each condition.

In the graph reported in Figure 3.5, a linear relationship is evident between the different conditions with an R^2 value very close to 1 (suggesting a good fit with the data). Using the equation from the trendline, the culture crash time can be determined for any given MOI. With those values, it is possible to calculate the order of magnitude of pfu*cell^{-1} and, again, the result was comparable with the previous one of 10^5 pfu*cell^{-1}, increasing the confidence that the calculated value is a good approximation because it is supported by multiple MOI conditions and multiple repeats.

This result suggests that the CviKI virus might have a higher binding affinity to cell debris compared to the PBCV-1 virus and shows that this tool could enable a new way of estimating a more accurate pfu released per cell measurement for all virus isolates.

3.3.5 Investigation of the presence of signalling molecules

Another approach for which this system could be used is the evaluation of the presence of possible quorum-sensing signalling molecules smaller than 10 kDa that could have an impact on the virus lysis cycle.

Suggestions of chemotaxis of *Paramecium bursaria* towards Chloroviruses are reported in literature [122]. Another example of signalling molecules is the production of viral-specific glycosphingolipid (vGSL) in the coccolithovirus - *Emiliania huxleyi* system [178].

Therefore, it was decided to investigate if signalling molecules from cultures infected at different MOIs could have an impact on infected cells' culture crash time. In this instance, it was investigated if the infected cells were releasing signalling molecules, the presence of which may become apparent following infection with different MOIs.

It was theorised that the release of signalling molecules could have been related to the ratio between the number of cells and the number of viruses in the culture, that corresponds to the MOI. The cultures were infected at 10^{-4} MOI and including a non-infected control. Four conditions were compared: cells resuspended in fresh medium, cells resuspended in spent medium collected from a culture infected with an MOI of 5, cells resuspended in spent medium collected from a culture infected with an MOI of 10^{-4} and cells resuspended in spent medium collected from a culture infected with an MOI of 10^{-6}.

The spent medium from all the different conditions was filtered twice. The first filtration eliminates the debris and the second stopped virus particles and any other molecule bigger than 10 kDa. The filtrate would, thus, contain any signalling molecules present, smaller than 10 kDa. The cells were resuspended in the filtered spent media prior to a new infection, to verify if the lytic cycle of the virus would change in those conditions and to confirm or disprove the presence of signalling molecules. The average growth profiles of the resultant cultures with calculated standard deviations are shown (Figure 3.6).

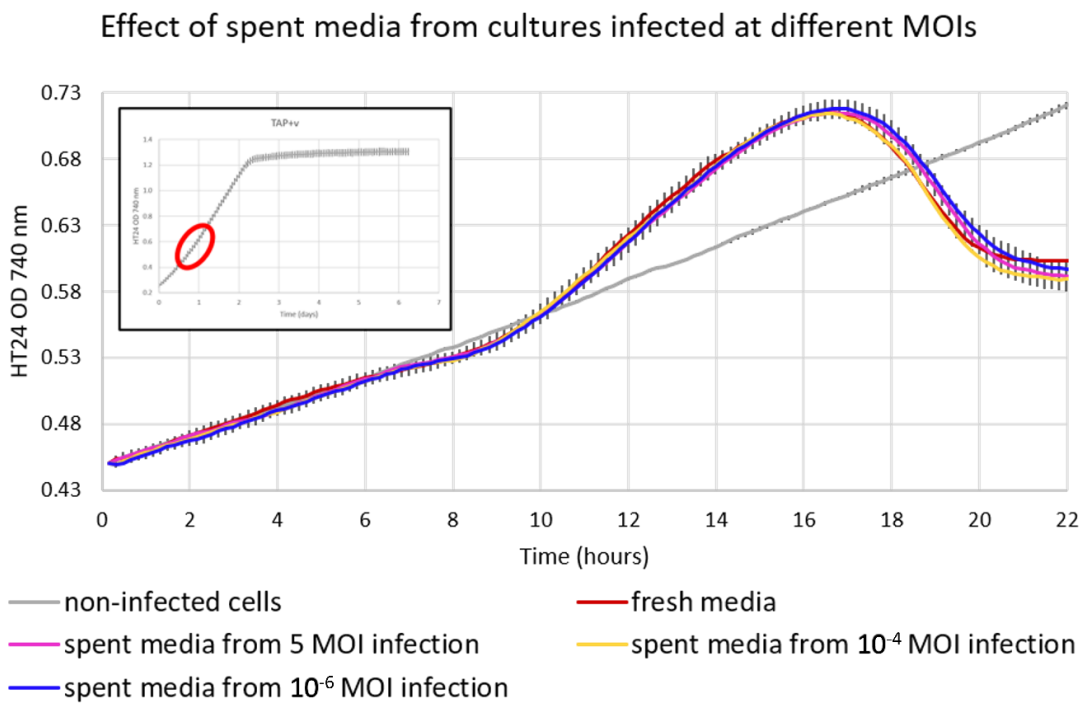

Figure 3.6. Infection of *Chlorella variabilis* cultures at 10^{-4} MOI with CviKI virus isolate and spent media from cultures infected at different MOIs, including a non-infected control. Cells were re-suspended in fresh TAP medium for no signalling molecules condition and with filtered spent medium for the other conditions as explained in the Materials and methods section. The values are the average of 3 biological replicates with standard deviations. The inset graph from Figure 3.1 on top left corner is used to highlight the scale of the closeup graph compared to the full growth of the un-infected organism, underlining that this is the fine-scale data focused on the initial part of the exponential growth.

Intriguingly in all infected states a minor decrease in OD was observed around 8 h p.i. probably due to the first round of cell lysis by the infected cells, that were about 1% of the total cell number, releasing virus particles that infected the remaining portion of non-infected cells in the culture.

More surprisingly, the decrease in OD was subsequently followed by an increase in OD above those uninfected cultures for 7-8 h prior to a rapid decrease. The reason for this could be the accumulation of viral DNA and assembled virus

particles inside the cells prior to cellular lysis which could result in a change in cell/particle volume that is detected as an increased OD. There was no significant increase in cell culture density during the increase of the OD.

This subtle pattern, which would most likely be missed without the automated nature of the sampling regime, was only observed in cultures infected at an MOI lower than 1 and it is also shown in Figure 3.7, but not present in Figure 3.2 with cultures infected at saturating MOI.

There was no significant difference between the conditions implying that neither the infected cells or the viruses are associated with quorum-sensing signalling molecules smaller than 10 kDa in any of the conditions tested.

3.3.6 Verification of the virus release method after infection

Another application of the experimental approach described herein, is the investigation of the virus release process during infection. The 3 possibilities are: i) by cell lysis, as already reported for this family of viruses [99], that is a sudden and large release of the virus particles [179]; ii) by budding, that is a slower but by the controlled (constant or otherwise) release of virus particles [180,181], or iii) a combination of both. As Figure 3.7 clearly shows, the complete removal of all virus particles, even after 5 sequential washes, proved challenging; ultimately every culture was observed to crash.

However, there was a marked difference between the infection dynamics observed from media taken 7 and 24 h p.i. Whilst 0-6 h all generated identical lytic curves, suggesting an almost identical amount of low-level cross-over

contaminating virus particles, cultures infected with media from 7 and 24 h p.i. produced a more rapid decrease in OD with discernible profiles.

At the 7 h' time point there was no evidence of lysis in the sampled cultures; it's possible that, with centrifugation, a few weaker cells with a damaged cell wall, released infective virus particles.

After 24 h p.i. the cells were completely lysed and the virus titre was the highest, as suggested by the shorter lysis profile in Figure 3.7. This result confirms that the virus release method is via cell lysis because if it had been by budding, it would be expected to see a slow but constant decrease in culture crash time and not a sudden decrease as shown after 7 h p.i.

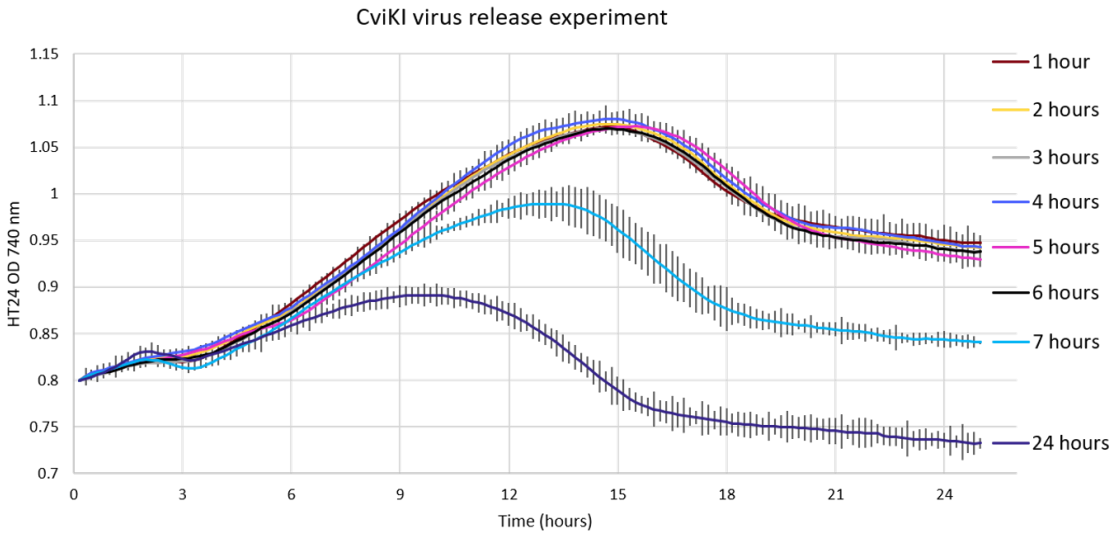

Figure 3.7. Infection of *Chlorella variabilis* cultures with filtered spent medium from previously infected cultures at 5 MOI with CviKI virus isolate sampled every h up to 7 h p.i. and at 24 h p.i. The values are the average of 3 biological replicates with standard deviations.

3.4 Discussion

The precise study of microalgae-virus infection dynamics is difficult to undertake due to long and variable infection cycles that can traverse light-dark cycles requiring prolonged and intensive sampling regimes. Every sampling intervention potentially perturbs the environmental conditions and host-virus dynamic, introducing uncontrollable variation and ultimately decreasing precision and confidence in results [158].

In this study, infected cultures were monitored continuously (every 10 min), without interruption or intervention, while agitation, light intensity and temperature were strictly controlled. The control and precision offered by the approach helped to achieve high reproducibility, enabling visualization of the subtle yet consistent differences between multiple virus isolates or of the same virus isolate under different conditions.

The virus cycle of 6 different isolates was investigated and it was determined that each had different lysis times and OD profiles following infection (i.e. phenotype), identifying PBCV-1 as the fastest virus and MA-1D being the slowest virus with regard to completing a lytic cycle under the defined condition.

The pfu*cell^{-1} released was calculated showing that the established approach could be highly valuable, especially for viruses with higher binding capacity to cell debris for which the plaque assay of the supernatant of lysed cells will underestimate and under-represent the true viral titre value. Through this new approach, CviKI virus was identified as having the smallest ratio between the culture crash time at saturating MOI and at lower MOI when compared with the other isolates. The potential biological reasons behind this observation were

explored as the order of magnitude of pfu*cell^{-1} was calculated using the culture burst times at different MOIs.

Host-virus dynamics can be complicated by the presence of signalling molecules, as has been demonstrated in the coccolithovirus - *Emiliania huxleyi* system [178]. To this end, the possibility of a similar phenomenon occurring in the *Chlorella* - Chlorovirus system was investigated. The results provide evidence that no such signalling events occur in this system.

The release of viral particles following infection was assessed through the development of a method to verify the mechanism, which was either cell burst, budding or a combination of the two. With this experiment it was confirmed previously reported findings for Chloroviruses [99], virus release initiating 6 h p.i. and being well established 7 h p.i. Crucially, early release before 6 h was not found to be a feature of the infection cycle.

Our data support a conclusion that, for CviKI, the infective virus particles released upon burst were strongly bound to cell debris which would include cell wall and cell membrane components, as 5 sequential washes were not enough to eliminate all the infective virus particles bound to the cell debris. Indeed, results indicate that even right after the wash there were still some virus particles in the medium that infected and lysed the cells (Figure 3.7). This observed phenomenon probably helps maintain the virus titre in environmental samples explaining why they have just small fluctuations over the year [104]. The implications for the virus shunt and biogeochemical cycling of this observation are unknown but it could mean an underestimation of the viral component to the particulate organic matter (POM) due to the measurement of virus just in the dissolved organic matter

(DOM) [182]. Based on what has been calculated herein, the number of infective CviKI viruses in the POM could be 100 times higher than the number of infective CviKI in the DOM.

All cultures, exposed to spent media collected from a culture displaying a synchronised-infection (washed five times to remove all unbound virus immediately following MOI 5 infection), lysed eventually (Figure 3.7); indicating a low level of transient or reversible binding of viruses to *Chlorella* cells. This means that when virus titration analysis in environmental samples are performed, the fraction of the virus that is free or unbound to cell or cell debris is quantified. Therefore, when a culture is infected with lower MOI, the pfu released per cells could be greater than what can be measured, explaining why the virus isolate is perceived to have a shorter lytic cycle at lower MOI.

This conclusion does not hold for all the Chlorovirus isolates investigated. For example, PBCV-1 at lower MOI, lysed all the cells within the expected time windows, suggesting that there are relative differences in binding affinities to cell wall components between the different virus isolates. It is reported that Chlorovirus stocks were more stable when stored with cell debris compared to filtration prior to storage [108] suggesting that storage in the presence of cell debris post lysis may act to stabilize released viral particles from degradation and inactivation. It can be speculated that the storage of Chlorovirus particles with cells debris acts to not only stabilize them but, due to a release over time in storage of those particles that are initially bound to debris and, therefore, uninfective, there is a greater stability of average pfu per sample over time. Particles that are initially uninfective within a given sample due to being bound to

cell debris are released over time and become infective, replacing free viral particles that naturally deteriorate over prolonged storage. It is the relative on-off rate of the viral particle binding to cell wall components that could underpin the difference in behaviours observed across various viral isolates. It seems that the ratio between the free virus in the supernatant and the bound virus to cell wall/cell debris is constant with an increase of both when adding more virus to the culture by cell burst suggesting multiple binding sites on the *Chlorella* cell wall [105,108].

As it was shown, the Algem HT24 and Algem PRO are powerful tools for accurate and continuous monitoring of virus-host interactions. Potentially, other lab scale photobioreactors that incorporate non-invasive continuous monitoring and precision control of parameters necessary to maintain defined growth conditions could also be used to follow microalgae viral-host interactions. Insights were gained on viral lytic cycles, mechanism of infection, stability, mechanism of virus release, quantification of pfu released per cell and possible environmental impacts.

The combination of the larger precision lab scale photobioreactor (Algem PRO) affording accurate control of multiple variables with the higher throughput system (Algem HT24) enabled a deeper understanding of viral-host biology to be gained than could have been achieved through the use of one system alone. The approach and tools validated herein could be generally applied to any algal-viral system enabling investigation into areas including but not limited to viral co-infection mechanisms, host-/virus evolution, population/community dynamics and, potentially, the impact of other microorganisms including bacteria and predators such as Paramecium on virus/host systems.

3.5 Conclusions

Algem PBRs protocols with high sensitivity were developed to integrate the variety of tools, techniques and methodologies available to characterise viruses and their possible application for industrial purposes.

Investigation into the Chlorovirus infection cycle of six different isolates revealed that each had unique lysis times and OD profiles after infection. PBCV-1 was found to be the fastest virus, and MA-1D to be the slowest virus, with regard to completing a lytic cycle under the specified conditions.

In this chapter a further step forward was achieved towards understanding Chloroviral infection. In the next chapter, the Chloroviruses will be further investigated with the final goal to achieve HA production and evaluate the platform for industrial application.

Chapter 4 - Understanding and evaluation of the *Chlorella variabilis* / Chlorovirus system for use within a novel hyaluronic acid production platform.

4.1 Introduction

Once found that the compound produced by *Lobochlamys segnis* was not HA, as described in Chapter 2, the focus of the research became the exploration of *Chlorella variabilis* following virus infection for the production of HA.

As described earlier, the current industrial approaches for HA production rely upon pathogenic or GM bacteria or extraction from animal waste. The HA yield and MW is variable between batches produced with bacteria and the polydispersity of the product is high. Furthermore, for the extraction from animal waste the cost is high and it is neither sustainable or desirable in today's market. The ultimate goal of this PhD project was to investigate and develop knowhow towards a sustainable, natural, plant-based, non-GM (the algal genome doesn't get modified but is destroyed by the virus lysing the algal cells as well – and the virus is a natural process and, per se, not defined as GM under the EU definition), hyaluronidase free, non-bacterial, non-pathogenic, toxin-free, industrially scalable platform for high molecular weight HA production with low polydispersity and high consistency between batches. To achieve this goal, it was essential that the *Chlorella* / Chlorovirus system is better understood at the biochemical and

cell biological level. To this end, virus-algal infection dynamics were investigated in Chapter 3 and other virus isolates confirmed as containing the viral HAS gene were identified in order to better understand the impact on HA production.

Approaches and tools for the quantification of the product were developed. Furthermore, the development of a heterotrophic cultivation approach (using, for instance glucose or acetate by microbial fermentation) for *Chlorella variabilis* was considered to be a potentially market unlocking milestone that could enable an industrially scalable, high-density culture with controllable algal-virus infection dynamics.

4.2 Materials and methods

4.2.1 Phylogenetic tree generation

The phylogenenies were built using Geneious v8.1.9 software (Dotmatics, USA) by comparing internal transcribed spacer 2 (ITS2) sequences (Figure 4.1) using the sequence from *Lobochlamys segnis* as outlier or the HAS/HAS2 protein sequences (Figure 4.4) with CviKI's CHS protein sequence as outlier. In the first instance, the parameters used were global alignment with free end gaps and a cost matrix with 65% similarity (5.0/-4.0). The genetic distance model used was the Tamura-Nei with neighbour-joining distance-based method. In the second case the parameters used were global alignment with Blosum62 cost matrix. The genetic distance model used was the Jukes-Cantor with neighbour-joining distance-based method.

4.2.2 Microalgae strains, virus isolates and growth conditions

Chlorella variabilis CCAP 211/84 strain and culture conditions are the same reported on section 2.2.1. *Chlorella variabilis* SAG 211-6 and *Micractinium conductrix* SAG 241.80 were obtained from the culture collection of algae at Göttingen University (SAG) [135]. *Chlorella spp.* ATCC 30562 was obtained from ATCC, USA.

4.2.3 Protein Structure prediction

The online tool RaptorX [183] was used to predict HAS protein structure using the Distance-based Protein Folding method. A Deep Learning server is used to power this website. This online service predicts the local structure, contact and distance matrix, inter-residue orientation, and tertiary structure of a protein. PyMOL software was used to visualise the predicted three-dimensional (3D) structures. Mcule's online software, 1-click-docking, was used to dock β-1,4-glucuronic acid and β-1,3-N-acetylglucosamine residues within the predicted 3D structure models of the viral HAS proteins [184].

4.2.4 Mammalian cell expression platform

ATCC, USA, provided COS-7 cells, which are modified *Cercopithecus aethiops* (African green monkey) kidney cells by transformation with an origin-defective mutant simian virus 40 (SV40), which encodes the wild-type T antigen. Expression vectors bearing an SV40 origin will therefore replicate at high copy numbers, providing sufficient minichromosomes for the expression of the encoded protein. Cell cultures were performed in cell culture incubators (Sanyo, Japan) with 5% CO_2 at 37 °C in 25 cm^2 and 75 cm^2 flasks in Dulbecco's modified

Eagle's medium (DMEM) with high glucose and GlutaMAX™ supplement (ThermoFisher Scientific, UK) with added 10% fetal bovine serum (FBS) (ThermoFisher Scientific, UK) and penicillin-streptomycin at a final concentration of 100 U*mL^{-1}. The doubling time was about 35-48 h. Every week, cells were subcultured (passaged) at a 1:10 dilution.

Cells were washed with sterile PBS to eliminate all traces of FBS-containing medium before adding 2 mL of Trypsin-EDTA (0.25%) phenol red solution (ThermoFisher Scientific, UK) and incubating for 15 min at 37 °C. To neutralise the trypsin after detachment, 8 mL of complete medium were added. In a new flask with 15 mL of fresh complete DMEM, one mL of detached cells was inoculated.

Long-term cell storage was accomplished with cells that had attained confluence in a 75 cm^2 flask. Cells were trypsin-treated as previously described, counted and resuspended at 2 x 10^6 cells*mL^{-1}. In cryovials, 0.5 mL of cells were mixed with 0.5 mL of DMEM supplemented with 20% FBS and 20% DMSO. For long-term storage, cells were frozen at -80 °C for 24 h at a rate of -1 °C per min before being placed in vapour phase liquid nitrogen at temperatures lower than -135 °C.

Using the viral genome as a template, PCR was used to amplify the HAS coding sequences (CDS) from the PBCV-1, CviKI, and NYs-1 genomes using the primers reported in Table 4.1. Amplified sequences were cloned directly as PCR products as described later. The human and naked mole rat HAS2 ORFs were designed with the NheI restriction endonuclease site added at the 5’ end region and the NotI restriction endonuclease site added at the 3’ end region of the

sequence, in each case flanking and outside the ORF, and purchased from Twist Bioscience, USA.

target template	direction	sequence (5' - 3')	annealing temperature (°C)
PBCV-1 HAS	Forward	TTGCTAGCACCATGGGTAAAAAT ATAATCATAATGGTTTCG	62
	Reverse	ATGCGGCCGCTCACACAGACTG AGCATTGGTAG	66
Nys-1 HAS	Forward	AGGCTAGCACCATGGCTGCGTC ATTTTATGTTATTTTC	64
	Reverse	ATGCGGCCGCTCACACATTTTG AATATCGACATCTG	63
CviKI HAS	Forward	TCGCTAGCACCATGGTATTTTCT TGTTTGTCATTTGTCATTTGTC	66
	Reverse	AGGCGGCCGCTCACACAGTCTG AGCATTGGTAGATG	68

Table 4.1. PCR oligonucleotide sequences used to generate the HAS open-reading frames for direct cloning. From the top: PBCV-1 HAS forward primer, PBCV-1 HAS reverse primer, NYs-1 HAS forward primer, NYs-1 HAS reverse primer, CviKI HAS forward primer, CviKI HAS reverse primer. Forward primers had the NheI restriction endonuclease site added; the 3 bases before the translation start codon and the fourth base of the coding sequence (+1) were modified to create an ideal Kozak translation initiation sequence [185], the reverse primers had the NotI restriction site added to support shuttling of resultant PCR products into expression vector.

For *in silico* cloning planning, primer design, and DNA sequence verification, Geneious v8.1.9 software (Dotmatics, USA) was used. A directional cloning approach was utilised with NheI and NotI restriction endonucleases, digesting the ORF fragments on the 5’ and 3’ ends, respectively. The expression vector used was pCI-neo which incorporates an SV40 origin of replication, allowing transient, high copy number episomal replication of the vector in COS-7 cells due to their expression of the SV40 large T antigen. This vector also includes the

cytomegalovirus (CMV) immediate-early enhancer/promoter region, which allows for robust, constitutive, transient expression, as well as the SV40 late polyadenylation signal, which improves mRNA stability. The blaM gene, conferring ampicillin resistance, and present within the pCIneo vector was used for bacterial selection. Inserts were verified by sequencing [186] before larger scale plasmid preparations were made ahead of COS-7 transfections.

The following protocol was used to transfect cloned plasmids in COS-7 cells. The day before transfection, 2.5×10^6 cells were inoculated in a 75 cm^2 flask. The next day, 10 µg of plasmid was diluted to a final volume of 300 µL in DMEM without FBS and antibiotics and 60 µL of SuperFect transfection reagent (Qiagen, UK, discontinued) was added, mixed and incubated at room temperature for 10 min. The cells were washed once with PBS and the DNA solution was mixed with 3 mL of complete media before being added to the cells. After 3 h of incubation under growing conditions, the solution was removed, the cells were washed with PBS once, and 20 mL of complete new media was added to the cells, which were then incubated under standard growing conditions. After 24 h, cells were rinsed with PBS and fresh media was added. The next day, cells were scraped from the flasks and HA was extracted twice with 50 mM Tris-HCl solution pH 7.6 sterilised by filtration through a 0.2 µm filter (Sartorius, UK). The samples were analysed through agarose gel electrophoresis as reported in 1.2.4.

4.2.5 RNA extraction and reverse transcription PCR analysis

The reverse transcription PCR analysis was repeated twice. *C. variabilis* cultures in exponential phase (5×10^6 cells*mL^{-1} in TAP medium grown for 3 days at room temperature with 200 PAR of white light) were harvested via centrifugation at

4500 x g for 10 min, resuspended at 4×10^7 cells*mL^{-1}, aliquoted in different flasks, and infected with PBCV-1, CviKI, IL-5 2S1, NYs-1, MA-1D, and TAAS 2.1 viruses separately at an MOI of 10. Samples were collected at the following intervals: 1 h, 3 h, 6 h, and 8 h. In each instance, 10 mL samples were taken, centrifuged for 5 min at 5,000 x g, and the pellets were flash frozen in liquid nitrogen in 2 mL tubes and placed at -80 °C overnight. TRIzol reagent (ThermoFisher Scientific, UK) was used to extract RNA according to the manufacturer's instructions. ThermoFisher Scientific's SuperScript IV VILO (ThermoFisher Scientific, UK) was used for cDNA synthesis, and the manufacturer's procedure was followed. The RNA control samples used to test for the presence of gDNA were not subjected to the cDNA synthesis stage.

The genes of interest were amplified by PCR with DreamTaq (ThermoFisher Scientific, UK) using a 1:100 dilution of the cDNA as the template in an iCycler Thermal Cycler System with a 96 Well Reaction Module (Bio-Rad Laboratories, UK) at an annealing temperature of 54 °C and an extension time of 45 s for 35 cycles. Table 4.2 depicts the primers used, and Table 4.3 shows the volume utilised.

template	direction	sequence (5' - 3')	annealing temperature (°C)
Elongation Factor-1a *Chlorella variabilis*	Forward	ACAAGATCAAGGGTGTGGGT	65
	Reverse	TCCAGGCCCTTGATGTTCAT	65
Hyaluronan synthase (virus alignment)	Forward	GGTTGTGTTCACTCCATTTGC	63
	Reverse	CCAATGTCCCAAAGCGTCAT	64
Chitin synthase (virus alignment)	Forward	TATCTCACAGAGGCGTCGTT	64
	Reverse	CGGAAGTCGTTTTAACCACAGT	64
UDP-glucose 6-dehydrogenase long (virus alignment)	Forward	CCGAGGCCGTCAAACTATTC	64
	Reverse	GATAATTACATCGCTCTCAGTC	60
UDP-glucose 6-dehydrogenase short (virus alignment)	Forward	GTCTTGTCTCAGGGCTGCTA	64
	Reverse	TGATAAATTTCGTCGGGGTCG	63
glucosamine-fructose-6-phosphate aminotransferase (virus alignment)	Forward	TGCAATTCACCAAAGAGCACT	64
	Reverse	GGATACAAACGGAACCTTGAC	62

Table 4.2. PCR oligonucleotide primers sequences used for RT-PCR based amplification. From the top: elongation factor 1 (EF1) forward primer, elongation factor 1 (EF1) reverse primer, HAS forward primer, HAS reverse primer, CHS forward primer, CHS reverse primer, UG6DS UDP-glucose-6-dehydrogenase short sequence forward primer, UG6DS UDP-glucose-6-dehydrogenase short sequence revers primer, UG6DL UDP-glucose-6-dehydrogenase long sequence forward primer, UG6DS UDP-glucose-6-dehydrogenase long sequence revers primer, GF6PA glutamine-fructose-6-phosphate aminotransferase forward primer, GF6PA glutamine-fructose-6-phosphate aminotransferase reverse primer.

components	For 1 sample (µL)	For 60 samples (µL)
DreamTaq 2x mastermix	5	300
Forward primer 10µM	0.05	3
Reverse primer 10µM	0.05	3
Template	1	-
Molecular grade water	3.9	234
Total volume	10	540
For each sample	10	9

Table 4.3. PCR reaction volumes.

The samples were separated followed amplification by agarose-gel electrophoresis (1% agarose gel in TAE buffer). Fragments were visualised using incorporation of Midori Green dye (Geneflow, UK) into the cast gel and imaging using a GBOX Chemi XL XT16 Imaging System (Syngene, UK) equipped with a blue light transilluminator.

4.2.6 Flow cytometry analysis of infected cells

Flow cytometry analyses were performed with a BD LSRFortessa™ Cell Analyzer. Approximately 10^5 infected and uninfected *C. variabilis* cells in 100 µL were stained for 30 min with 1 µg biotinylated HA-binding protein from bovine nasal cartilage (Calbiochem, UK) and 5 µg Molecular Probes™ Streptavidin, Alexa Fluor™ 594 Conjugate (Ex/Em maxima of ~ 590/617). After incubation, the cells were washed 3 times with PBS, resuspended in the same volume of PBS and analysed immediately [187].

4.2.7 Fermentation conditions

Fermentation was performed using BioFlo® fermenters (Eppendorf, UK) using a proprietary fermentation media (FERM) developed by Algenuity Ltd for the high productivity fermentation of *C. vulgaris*. Briefly, this fermentation medium contains glucose and was used either at 1x or at a 1:4 dilution of the FERM with distilled water. The fermentation was performed in fed-batch monitoring glucose concentration and ammonium concentration twice a day. Concentrated glucose solution was fed to keep the concentration between 10 and 30 $g*L^{-1}$; 5% potassium hydroxide solution or 5% ammonium hydroxide solution were fed to control the pH value to 6.5 ± 0.1; dissolved oxygen concentration was controlled by increasing agitation speed to keep it at 30% saturation with an aeration rate of 50% of the reactor volume per min. Agitation speed was variable and initially set at 200 rpm.

4.2.8 HA extraction and purification for gel electrophoresis

Despite the availability of a protocol for HA extraction, purification, and quantification [188], the authors failed to account for the presence of contaminants from cell wall damaged infected cells interfering with the assay that were not present in non-infected cell samples whose cell walls were still intact. As a result, the previously published approach was not implemented since it was found to overestimate the amount of HA generated by the infected cells. The extraction and partial purification techniques are a hybrid of two protocols [188,189]. At 6 h post-infection (p.i.) the infected cells were harvested by centrifugation at 4500 x g for 10 min. The pellets were resuspended in 50 mM Tris-HCl solution pH 7.6 with 0.1 percent SDS, heated to 100 °C for 5 min, and

centrifuged to remove cell debris. The extraction was done a second time with the two HA fractions combined. The majority of the cell wall contaminants were precipitated by adding 0.1 volume of 23.3% w/v NaCl solution and 0.3 volume of 2% w/v Cetylpyridinium chloride (VWR International, UK) solution to the sample, mixing thoroughly, and incubating at room temperature for 30 min before centrifugation at 4500 x g for 30 min. The supernatant was collected, 4 volumes of ethanol were added, and, following mixing, the solution was incubated overnight at -20 °C. The extract was centrifuged at 4500 x g for 30 min the next day, and the pellet was washed with cold 75% ethanol before drying at room temperature. The sample was resuspended in the appropriate volume of TBE buffer, a portion of the samples was digested with hyaluronidase solution (prepared as described in paragraph 1.2.3), and the samples were analysed using agarose gel electrophoresis as described in paragraph 1.2.4, loading 10 µL of 1 mg*mL^{-1} HA standard and 20 µL of each sample.

4.3 Results

4.3.1 Selection of the best microalgae strain for HA production

Four microalgal strains were found in the literature that could be infected by viruses generating HA: *Chlorella spp.* ATCC 30562, also known as *Chlorella variabilis* Syngen 2-3, two strains of *Chlorella variabilis* CCAP 211/84 and SAG 211-6 that are extremely closely related and may be infected by the same viral isolates, and a strain of *Micractinium conductrix* SAG 241.80 [101,190] (Figure 4.1).

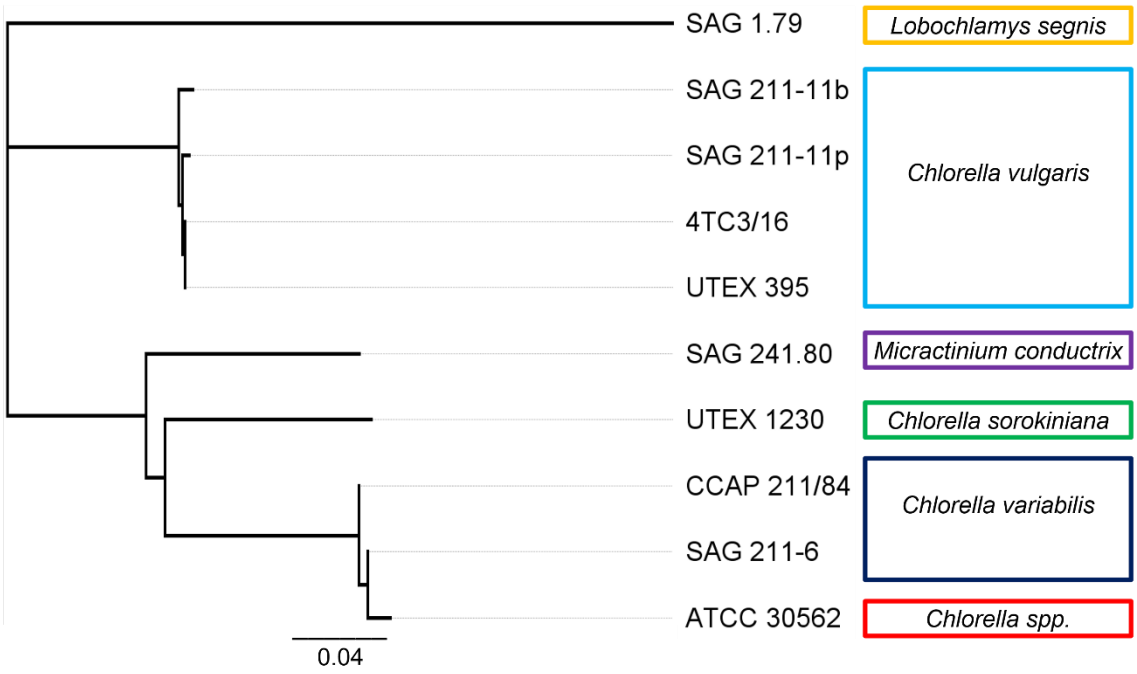

Figure 4.1. ITS2 phylogenetic tree of the strains tested using *Lobochlamys segnis* as outlier. From the bottom: ITS2 sequence from *Chlorella spp.* (ATCC 30562) in red, ITS2 sequences from *Chlorella variabilis* (SAG 211-6 and CCAP 211/84) in dark blue, ITS2 sequence from *Chlorella sorokiniana* (UTEX 1230) in green, ITS2 sequence from *Micractinium conductrix* (SAG 241.80) in purple, ITS2 sequences from *Chlorella vulgaris* (UTEX 395, 4TC3/16, SAG 211-11p and SAG 211-11b) in light blue and ITS2 sequence from *Lobochlamys segnis* (SAG 1.79) in yellow. The bar at the bottom of the figure provides a scale for the length of branch that represents an amount of genetic change of 0.04 (nucleotide substitutions per site).

The tree was built using Geneious v8.1.9 software (Dotmatics, USA) by comparing internal transcribed spacer 2 (ITS2) sequences, which is a well-known marker for eukaryotic phylogenetic investigations. The relationship based on the 18s sequences was too tight, yielding meaningless results.

Sequence comparison of the eukaryotic ITS regions is widely used in taxonomy and molecular phylogeny because it is regularly amplified due to its short size and the availability of highly conserved flanking regions; it is present at a high

copy number, making it easy to amplify; it evolves rapidly by uneven crossing-over and gene conversion and, even among closely related species, there is a great deal of variation due to the comparatively modest evolutionary pressure occurring on non-coding spacer sequences [191,192].

All four microalgae strains that have been demonstrated to be Chlorovirus hosts are closely related as reported in Figure 4.1 and were tested for growth on autotrophic and heterotrophic medium using glucose as a carbon source. The phylogeny analysis was done to confirm that the infectible species considered were closely related although they are different species and one of them is a different genus. Although SAG 211-6 and ATCC 30562 attained extremely low cell densities, all four strains were able to grow under autotrophic conditions. During the 20-day trial, CCAP 211/84 grew the fastest and reached the highest cell density (Figure 4.2).

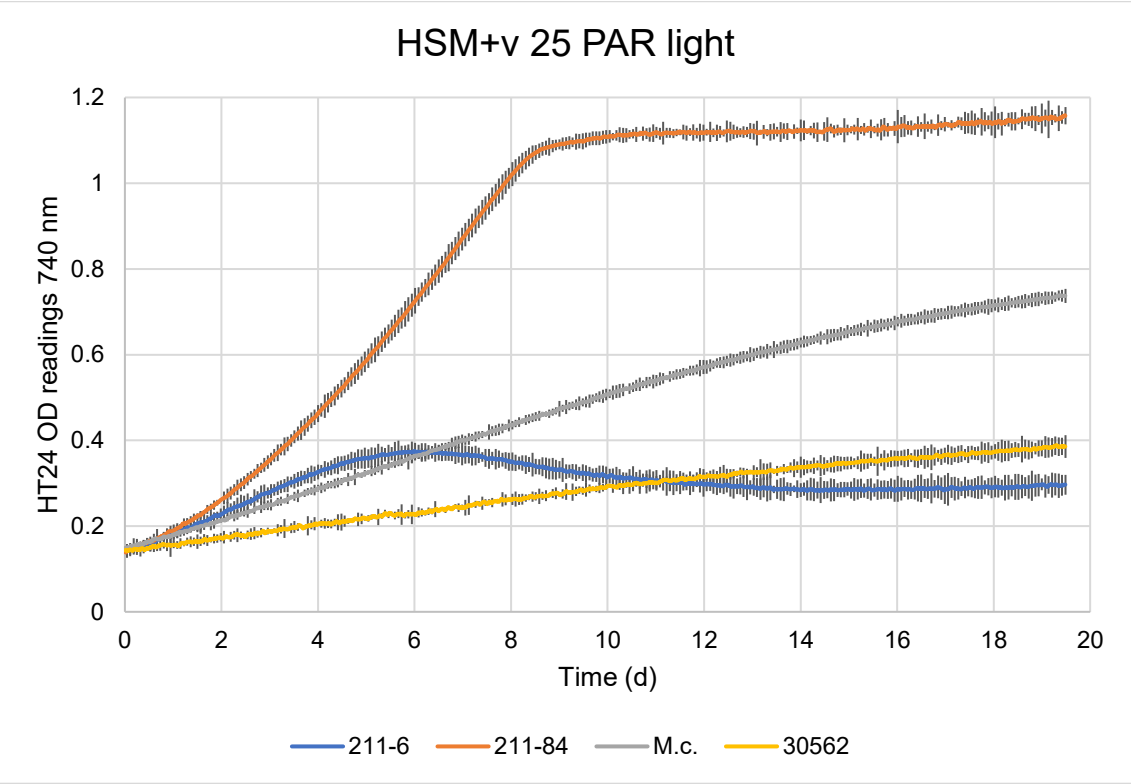

Figure 4.2. Growth comparison of infectable microalgae strains in HSM+v with 25 PAR of white LED light. The strains analysed were *Chlorella variabilis* SAG 211-6 and CCAP 211/84, *Micractinium conductrix* SAG 241.80 and *Chlorella spp.* ATCC 30562. The plotted values are the average of 3 biological replicates with standard deviations.

In media supporting heterotrophic growth, CCAP 211/84 grew over a period of 25 days after around 15 days of adaptation to the new conditions; no growth was observed in the other strains studied (Figure 4.3). Based on the findings, the CCAP 211/84 strain and the viruses infecting were studied further for HA production.

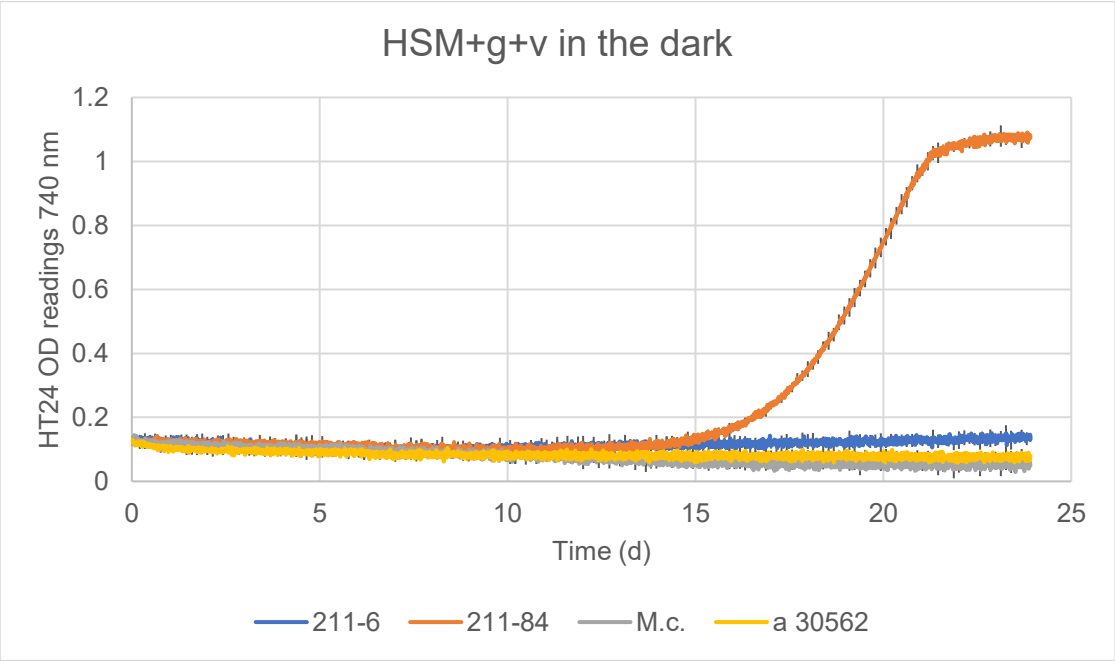

Figure 4.3. Growth comparison of infectable microalgae strains in HSM+v with added 1% glucose without light. The strains analysed were *Chlorella variabilis* SAG 211-6 and CCAP 211/84, *Micractinium conductrix* SAG 241.80 and *Chlorella spp.* ATCC 30562. The plotted values are the average of 3 biological replicates with standard deviations.

4.3.2 Comparison of genes involved in HA biosynthesis pathway between the different virus isolates

The first step to better understanding how each viral genome directs the infected microalgae to produce HA was to identify the relevant genes in each virus previously shown to be involved in the HA synthesis pathway (Figure 4.6). Genomic sequences were analysed, comparing derived copy number and primary sequence differences and building predictive models to start to better understand and identify nuances within the range of isolates available. The ultimate goal was to identify the right combination of host and viral strain to support the development of a robust industrial process for the production of HA.

As shown in Table 4.4, five sequenced virus isolates infecting *Chlorella variabilis* possess the HAS gene. Two of the five have identical primary amino acid sequences for all enzymes involved in the pathway (MA-1D and NYs-1). PBCV-1 is the only fully sequenced virus infecting *C. variabilis*, which bears the HAS gene but not the chitin synthase gene, which encodes an enzyme that shares one of the substrates used for HA synthesis and is presumed to catalyse the production of chitin or chitosan or chito-oligosaccharides by infected Chlorella [187,193]. Other viruses infecting this microalga have been isolated but not sequenced, including a proprietary novel one (TAAS2.1) from Algenuity Ltd.

Host	Viruses	HAS [1]	GFAT [2]	UDP-GlcDH [3]	CHS [4]
NC64A	AN69C		109R	384R, 487R	390R
	AR158		C132R	C413R, C729L	C128R, C418R
	CviK1	102R	105R	359R, 662L	365R
	CvsA1		064R	368R	060R, 375R
	IL-3A		104R	375R, 685L	381R
	IL-5-2s1	134L [a]	130L [b]	492R, 858L	498R
	KS-1B				
	MA-1D	485L [a]	481L [b]	355R [c], 838L [d]	362R [e]
	MA-1E		116R	396R	113L, 402R
	NE-JV-4		081R	291R	278R, 282R
	NY-2A		B143R	B465R	B132R, B472R
	NY-2B			473R, 836L	479R
	NYs-1	137R [a]	143R [b]	483R [c], 846L [d]	490R [e]
	PBCV-1	A098R *	A100R *	A609L *	

Table 4.4. HA synthesis pathway comparison of different viruses infecting *Chlorella variabilis* SAG 211-6 and CCAP 211/84 (formally known as NC64A) from available genome sequencing data. [1] Hyaluronan synthase; [2] glutamine-fructose-6-phosphate aminotransferase; [3] UDP-glucose-6-dehydrogenase; [4] chitin synthase; in the table, gene numbers are reported and R and L refer to the DNA strand orientation; different coloured text mark the parts that are were not identified or reported in [101]; [a],[b],[c],[d],[e] have the same amino acid sequence; * the expressed recombinant protein is confirmed to possess the predicted activity. Chloroviruses highlighted in yellow are the viruses considered for further analysis. The table was taken from [101] and modified.

The origin of the HAS gene in these viruses is not known but a horizontal gene transfer origin has been suggested [48]. HAS protein sequences were used for phylogenetic analyses to develop a better understanding about its inclusion in the Chlorovirus genome and to gain insight regarding its potential evolutionary history.

A BLAST search using the PBCV-1 HAS protein sequence was performed collecting the first 1000 results and producing a distance tree.

The HAS proteins of Chlorovirus infecting different microalgal strains are closely related, suggesting a common ancestor that evolved producing multiple virus isolates infecting specifically different microalgal strains.

One possibility is that this gene was acquired by infection of a different host (probably an aquatic vertebrate) by an ancestor and was lost later on in some of the viral strains. In Figure 4.4 a phylogenetic tree is shown, based on published HAS protein sequences derived from the genome sequences of virus isolates infecting the microalgae strains considered in this study with vertebrate and bacterial sequences as reference.

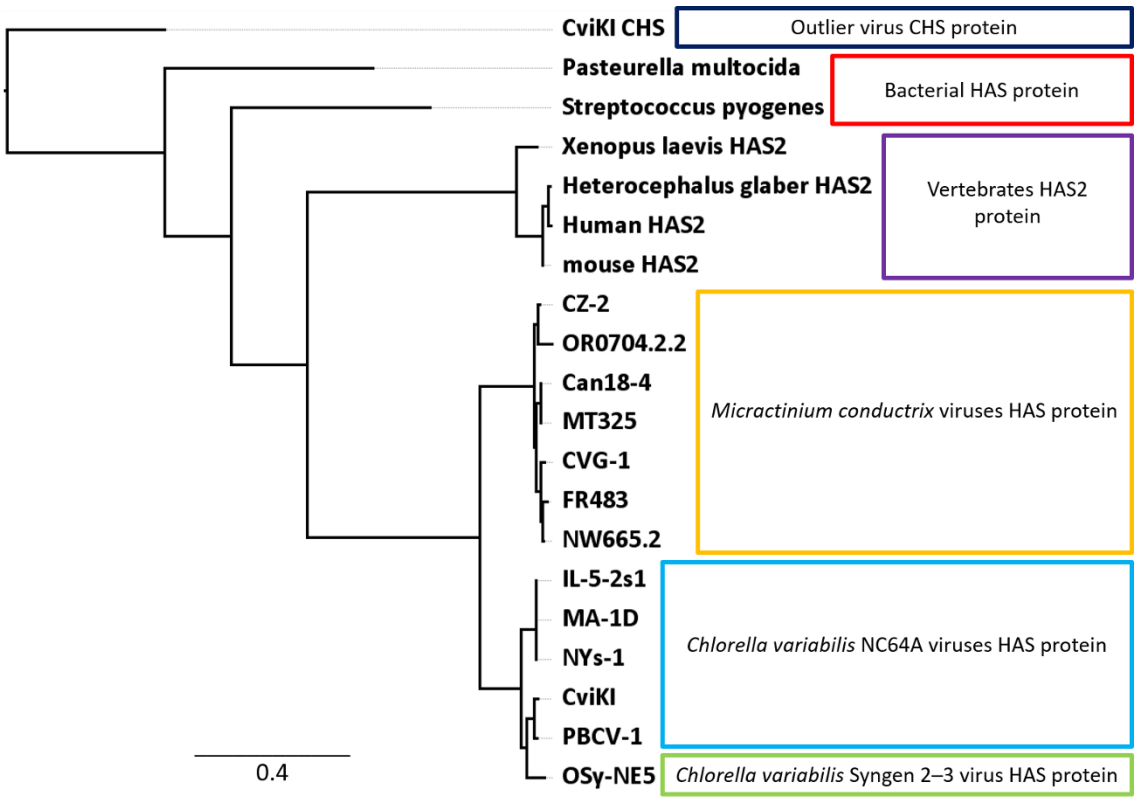

Figure 4.4. Phylogenetic tree based on derived HAS protein sequences using CviKI CHS as outlier. From the bottom: HAS protein sequence from virus infecting *Chlorella variabilis* Syngen 2-3 (ATCC 30562) in green, HAS protein sequences from viruses infecting *Chlorella variabilis* NC64A (CCAP 211/84) in light blue, HAS protein sequences from viruses infecting *Micractinium conductrix* (SAG 241.80) in yellow, HAS2 protein sequences from vertebrates in purple, HAS protein sequences from bacteria in red and CHS protein sequence from virus CviKI in dark blue. The bar at the bottom of the figure provides a scale for the length of branch that represents an amount of genetic change of 0.4 (amino acid substitutions per site).

Comparative protein sequence analysis for those enzymes involved in the HA biosynthesis pathway showed only a few amino acid differences between the different isolates (Figure 4.5). However, it is known that small differences of even a single amino acid change in these enzyme sequence could still be substantive in the relative impact on HA production including the relative HA chain length [65,194]. All virus isolates analysed except for PBCV-1, have 2 copies of the gene

encoding for the enzyme UDP-glucose 6-dehydrogenase, one with a longer amino acid sequence (denoted as ‘long’, 414 amino acids) and the other with a shorter amino acid sequence (denominated as ‘short’, 379 amino acids). The version of this gene present in PBCV-1 is the 414 amino acids long.

Viruses HAS protein sequences

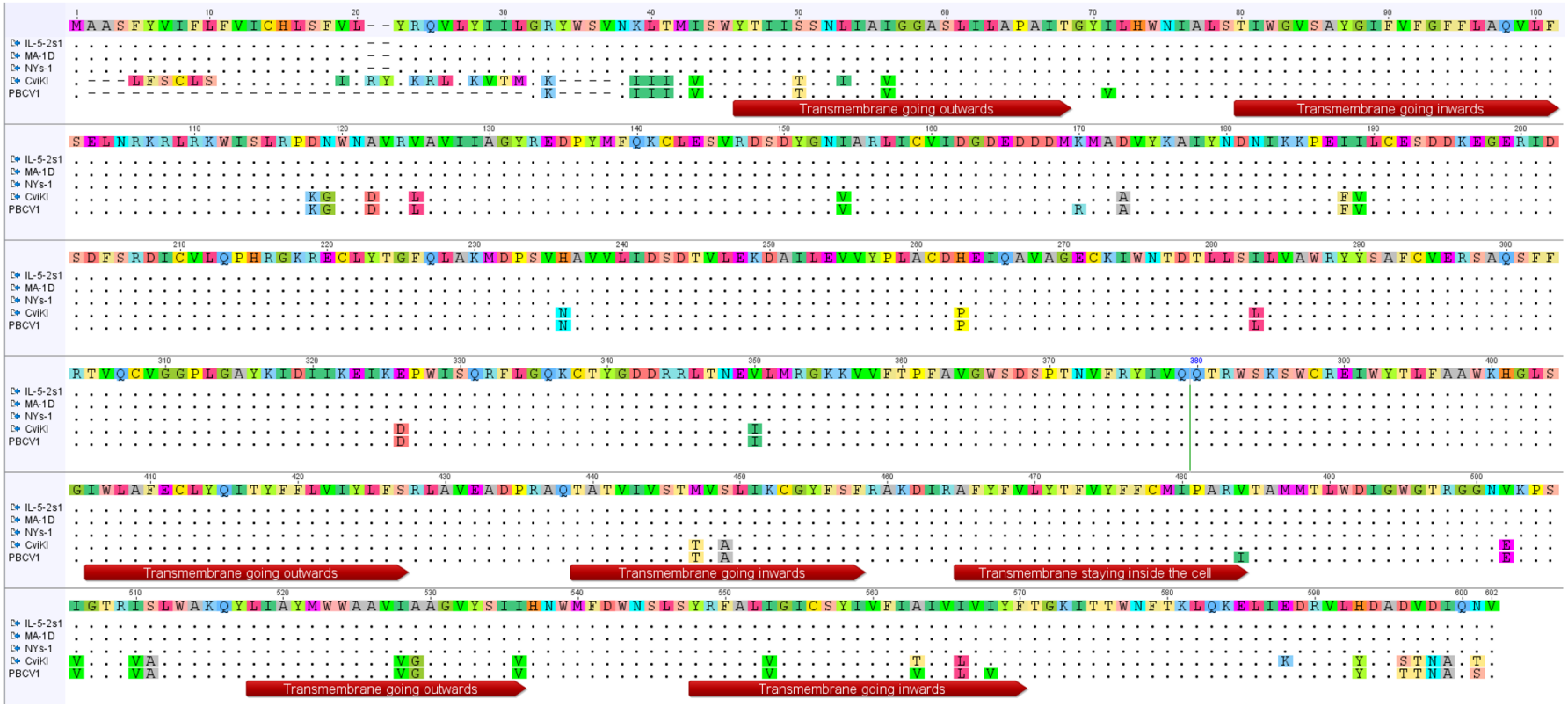

(a)

Viruses glutamine:fructose-6-phosphate amidotransferase protein sequences

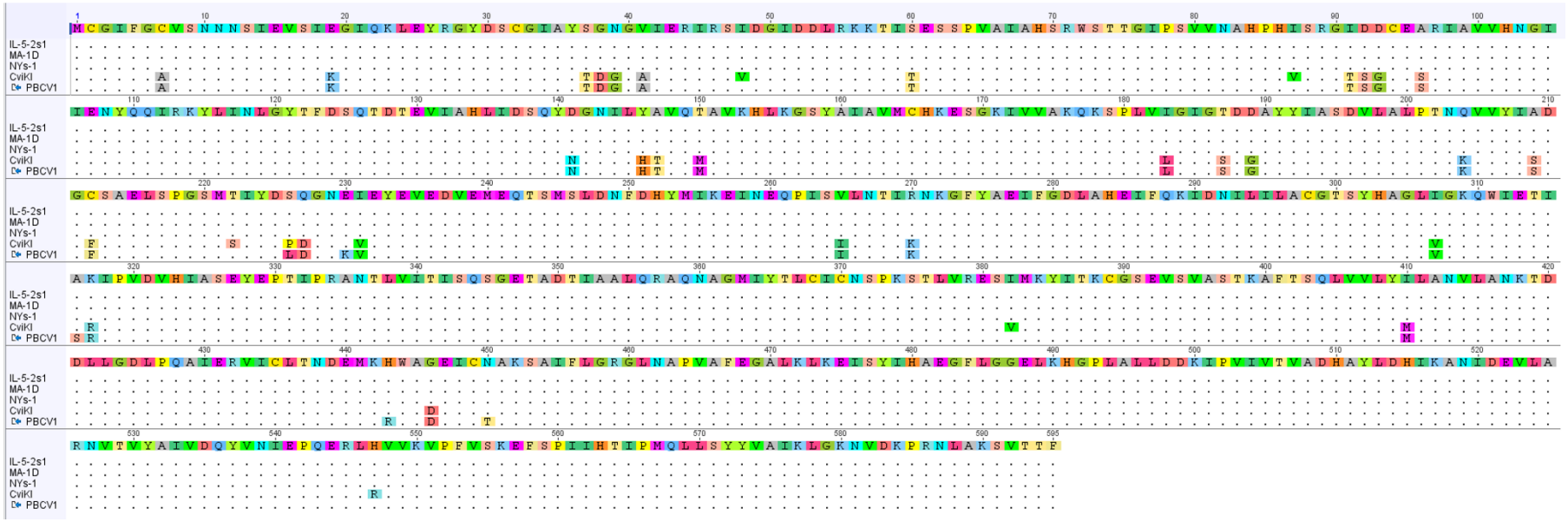

(b)

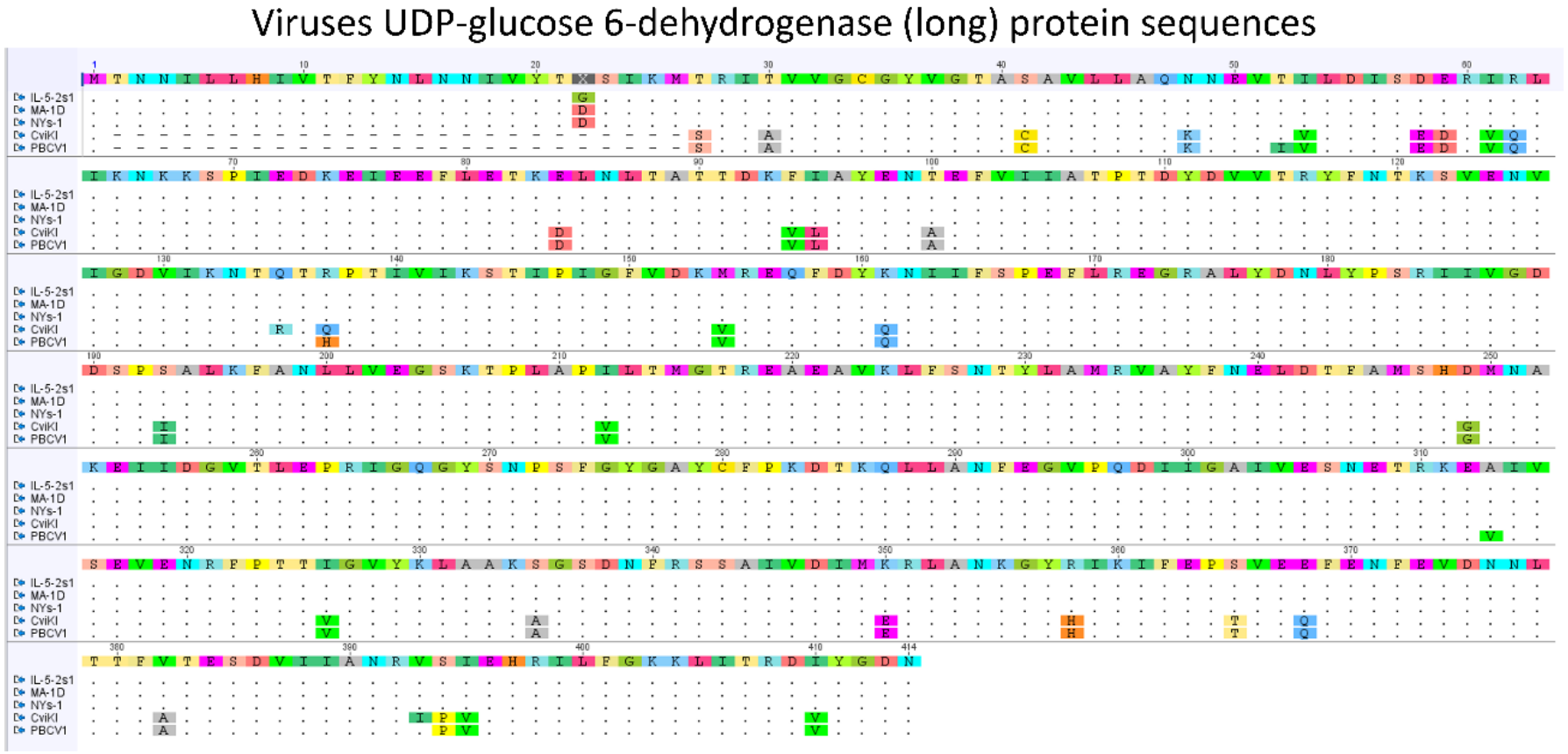
Viruses UDP-glucose 6-dehydrogenase (long) protein sequences
IL-5-2s1
MA-1D
NYs-1
CviKI
PBCV1

(c)

Viruses UDP-glucose 6-dehydrogenase (short) protein sequences

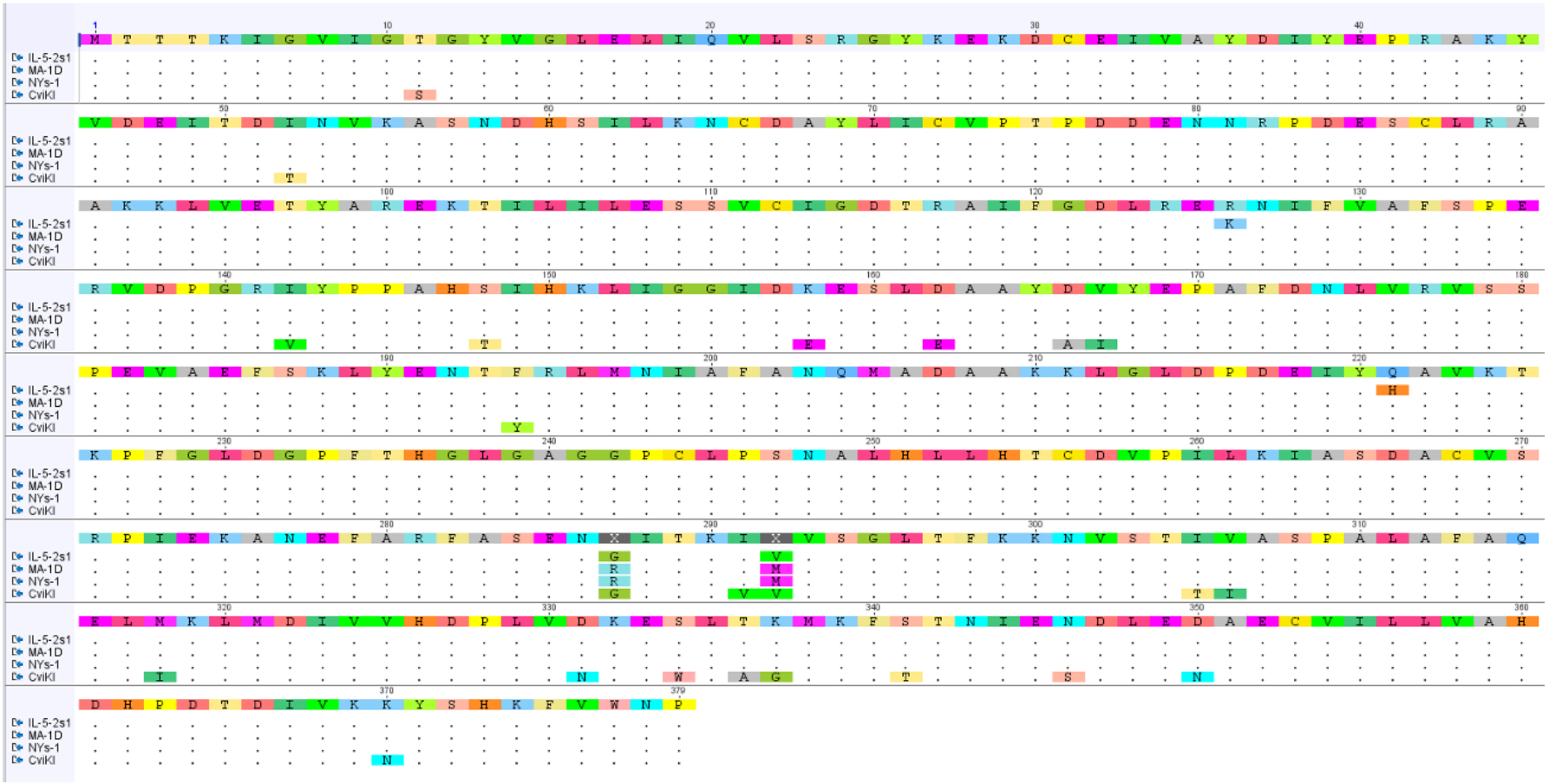

(d)

Figure 4.5. Primary amino acid sequence alignments. (a) HAS protein, (b) glutamine fructose 6 phosphate aminotransferase, (c) UDP-glucose-6-dehydrogenase (long) and (d) UDP-glucose-6-dehydrogenase (short). The order of the viral isolates in the multiple alignments is always the same (IL-5-2s1, MA-1D, NYs-1, CviKI and PBCV-1) except for the UDP glucose 6 dehydrogenase (short) in which PBCV-1 is not present because it doesn't have a copy of the gene encoding for this enzyme in its genome.

From the primary analysis of the HA synthesis pathway, it emerges that most of the steps involve a combination of viral and host microalgae enzymes, but the final and necessary step for the synthesis of the molecule is encoded by the virus alone. The other 2 enzymes involved in this pathway that are encoded by the virus are those catalysing the production of UDP-glucuronic acid and glucosamine-6-phosphate, suggesting that they could be tackling limiting steps related to substrate availability to support the final production of HA.

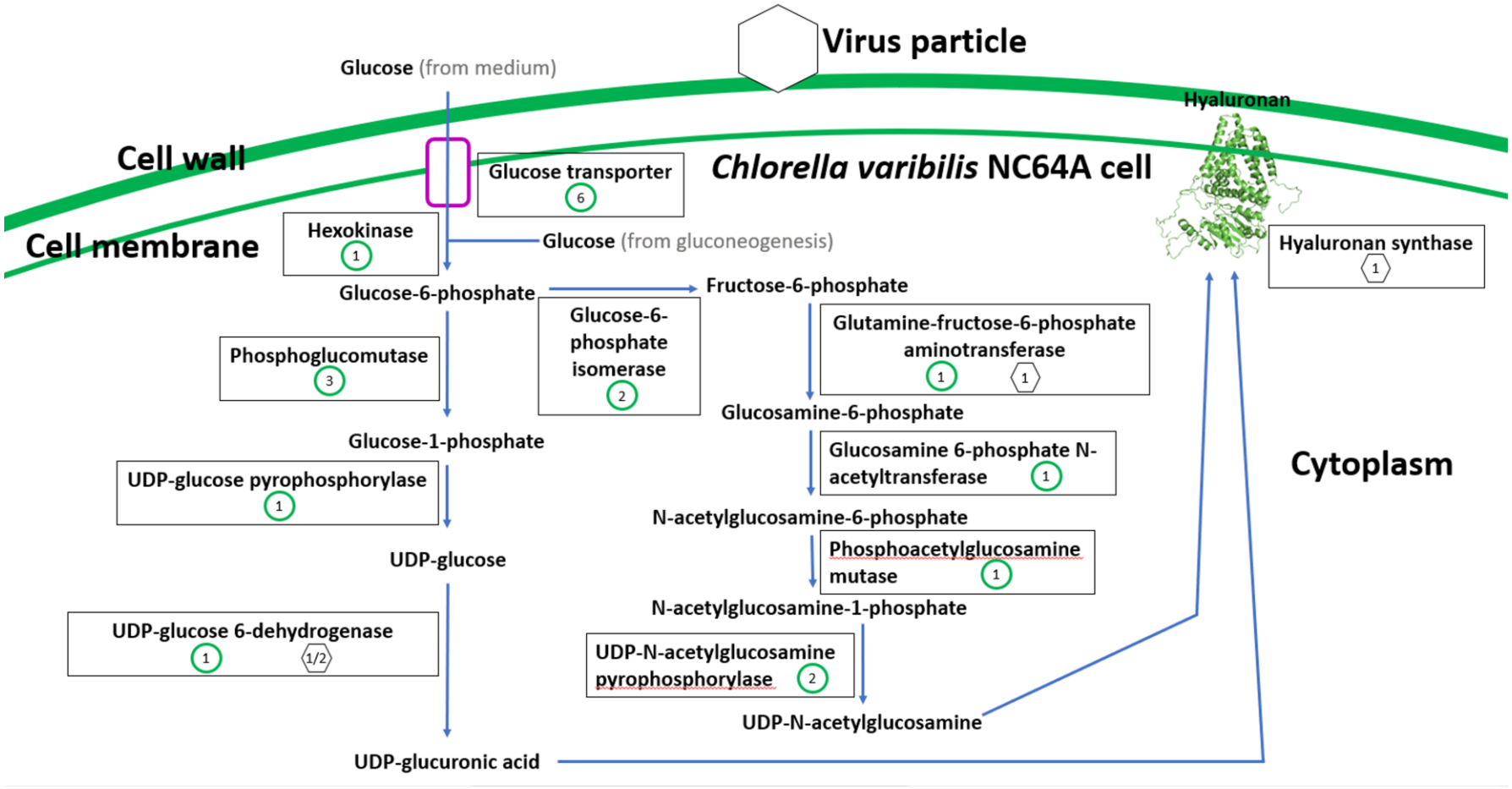
Virus particle
Glucose (from medium)
Hyaluronan
Cell wall
Glucose transporter
6
Chlorella varibilis NC64A cell
Cell membrane
Hexokinase
1
Glucose (from gluconeogenesis)
Hyaluronan synthase
1
Glucose-6-phosphate
Fructose-6-phosphate
Glucose-6-phosphate isomerase
2
Glutamine-fructose-6-phosphate aminotransferase
1
1
Phosphoglucomutase
3
Glucosamine-6-phosphate
Glucose-1-phosphate
Glucosamine 6-phosphate N-acetyltransferase
1
Cytoplasm
UDP-glucose pyrophosphorylase
1
N-acetylglucosamine-6-phosphate
UDP-glucose
Phosphoacetylglucosamine mutase
1
N-acetylglucosamine-1-phosphate
UDP-glucose 6-dehydrogenase
1
1/2
UDP-N-acetylglucosamine pyrophosphorylase
2
UDP-N-acetylglucosamine
UDP-glucuronic acid

Figure 4.6. *C. variabilis*/Chlorovirus HA synthesis pathway. The numbers in the green circles represent the number of gene variants of the enzyme in the *C. variabilis* genome and the numbers in the hexagons represent the number of the gene variants of the enzyme in the virus genome.

Isolation and crystallography analysis of the HAS protein has not been performed to date due to difficulty in isolating and purifying integral membrane proteins, keeping their structures without deformations.

In silico analysis for the prediction of protein structure was performed together with a prediction of the docking sites for the activated UDP-sugar precursors (Figure 4.7).

From structural homology modelling analysis*, Pasteurella multocida*'s HAS is predicted to have 2 distinct binding sites, one for UPD-GlcA and one for UDP-GlcNac; in all other HAS enzymes the docking sites are predicted to be located in one position within the folded polypeptide where the 2 substrates are proposed to alternate as synthesis proceeds.

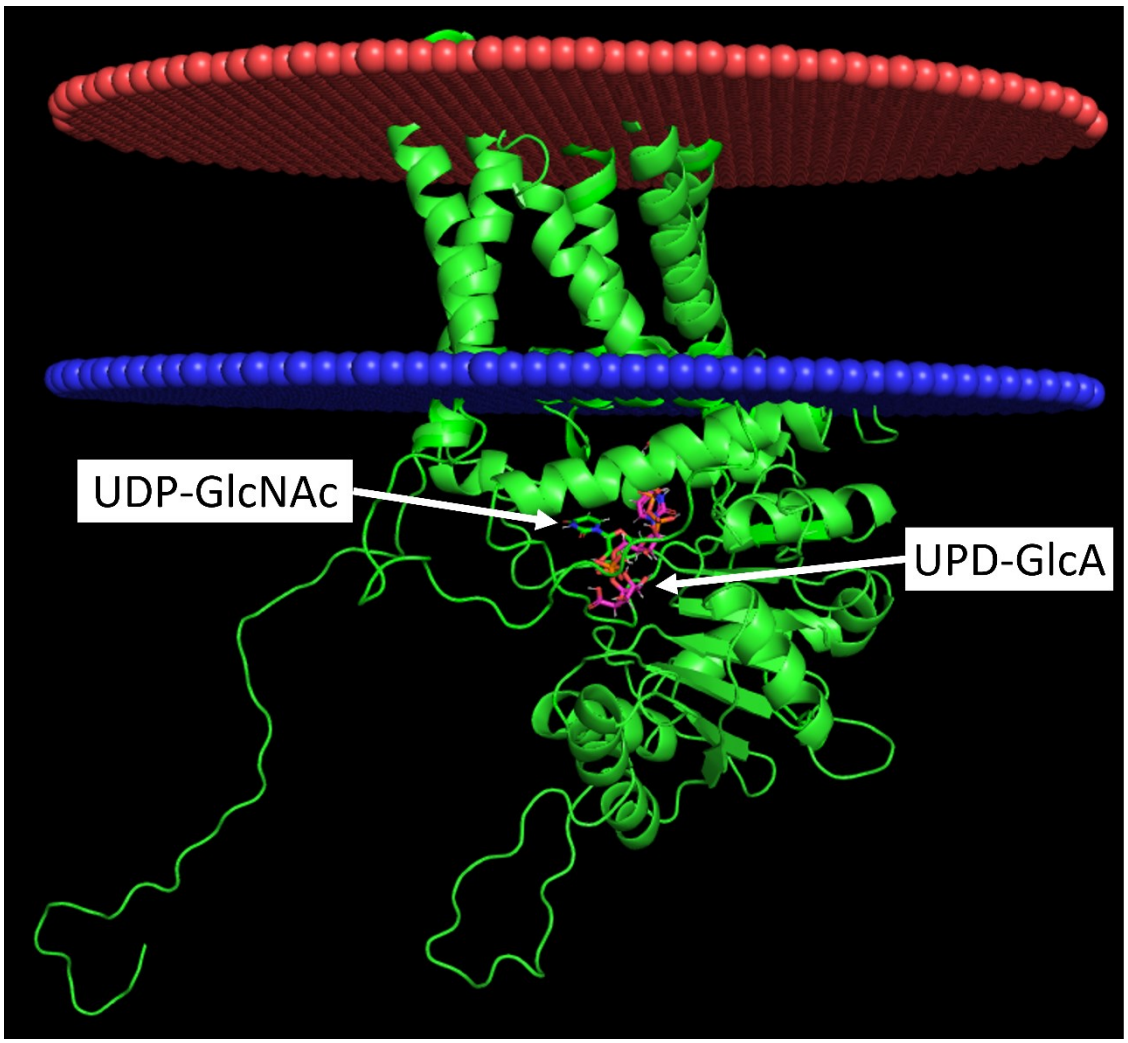

Figure 4.7. Prediction of PBCV-1 structure and position in cell membrane; the red and blue indicate the outer and inner portions of the plasma membrane respectively. UDP N-acetyl glucosamine (UDP-GlcNAc) and UDP glucuronic acid (UDP-GlcA) are pointed by the arrows.

4.3.2 Test and comparison of predicted activity of recombinant HAS proteins in COS-7 cells

This test was not intended to develop an alternative HA production platform in mammalian cells but was intended as a means to directly compare the activity of the Chlorovirus' HAS proteins with HAS from other organisms in a defined heterologous host. COS-7 mammalian cells afford the possibility of studying

heterologous HA production in a system with non-limiting precursors, with high transient expression while being free from endogenous HA production. The virus HAS protein sequences have the closest similarity with mammalian HAS2 protein so it was considered likely that viral HAS enzymes would be active when expressed in mammalian cells, drawing off of available activated UDP-sugar substrates.

The reason why mammalian cells have been preferred for this test is because neither yeast nor bacteria have all genes for precursor production so they would need to be transformed with multiple genes. Additionally, bacteria and yeasts could become pathogenic if producing HA because the immune system won't be able to recognise them as non-self, thanks to the HA coating. The ability to produce an HA capsule is correlated with pathogenicity in Streptococcal bacteria [195].

The activity of recombinant viral HAS proteins was tested in COS-7 mammalian cells in order to compare the results with previous literature data and have a system that supports high transient expression with a comparatively high throughput and turn-around time while having no reported hyaluronidase activity, abundant precursors and with undetectable endogenous HAS activity.

The transient transfection in COS-7 cells showed that the HAS2 protein from *Heterocephalus glaber*, drove the production of the highest MW HA that is reported to be up to 12 MDa [44]. Human HAS2 and PBCV1 HAS produced similar MW HA, but limited or non-visible production of HA was observed for CviKI and NYs-1 HAS in comparison with the negative control despite repeating the experiment several times. Absolute quantification of the HA's MW wasn't possible

for the small amount of HA produced in each sample for GPC-RI-MALS analysis. Therefore, agarose gel electrophoresis analysis was used to have a qualitative estimation of the MW (Figure 4.8).

Despite the significant effort to establish the mammalian cell culture laboratory, transfection of the COS-7 cells multiple times, PBCV-1's HAS gene was the only viral HAS to consistently show HA production higher than the background other than the positive controls. It was reasoned that this was most likely because the DNA sequences were not optimised for expression in mammalian cells, but the number of enzyme variants that was initially planned to be tested (13 different variants) was too large to consider genetic synthesis for all because of the high cost (about £300 per variant). Overall, this aspect of the project was required to give me the necessary experience of starting a laboratory from scratch, with all of the challenges that entails, such as health and safety procedures, researching new protocols, testing different chemicals and processes, buying needed equipment and dealing with all of the paperwork involved.

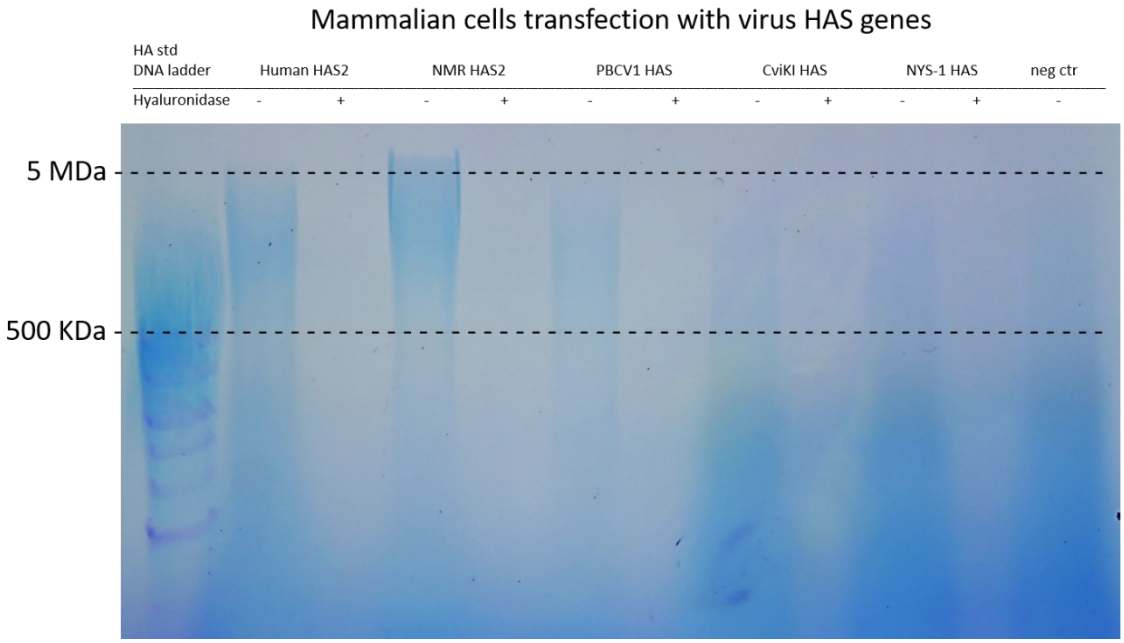

Figure 4.8. Agarose gel electrophoresis for molecular size analysis. + hyaluronidase is treated with the enzyme specific to digest HA for identification of the compound, - hyaluronidase is non-treated. NMR, naked mole rat.

4.3.3 Virus hyaluronan synthesis genes' expression analysis

To further understand potential differences between viruses across the viral life-cycle, expression of the relevant genes encoding enzymes involved in the HA synthesis pathway were investigated by reverse transcription PCR (RT-PCR) (Figures 4.9 and 4.10). No signal was detected in the cDNA PBCV-1 sample at 8 h timepoint because the cells were totally lysed by the virus.

As reported in the literature, GFAT, UGDH-L and HAS genes were expressed by *C. variabilis* infected by all strains at 1 h and 3 h timepoints and at 6 h and 8 h were not present in PBCV-1 but remained detectable in *C. variabilis* infected by the other viral strains, suggesting that the other virus strains have a longer expression of these genes or alternate RNA turnover of the transcripts. Either or both of these could, conceivably, result in an increased production of HA.

CHS and UGDH-S were expressed at all 3 timepoints in MA-1D, NYs-1 and CviKI but, surprisingly, never expressed in IL-5-2S1, even if the genes were reported to be present in the genome [98].

After further testing, the absence of the CHS and UGDH-S genes in IL-5-2S1 genome was confirmed and the distinct DNA sequence of GFAT and UGDH-L genes from the aforementioned isolate were also compared to other isolates available in the laboratory suggesting that the wrong virus stock had been sent originally, or that it had been mis-labelled when performing the genome sequencing analysis reported in literature.

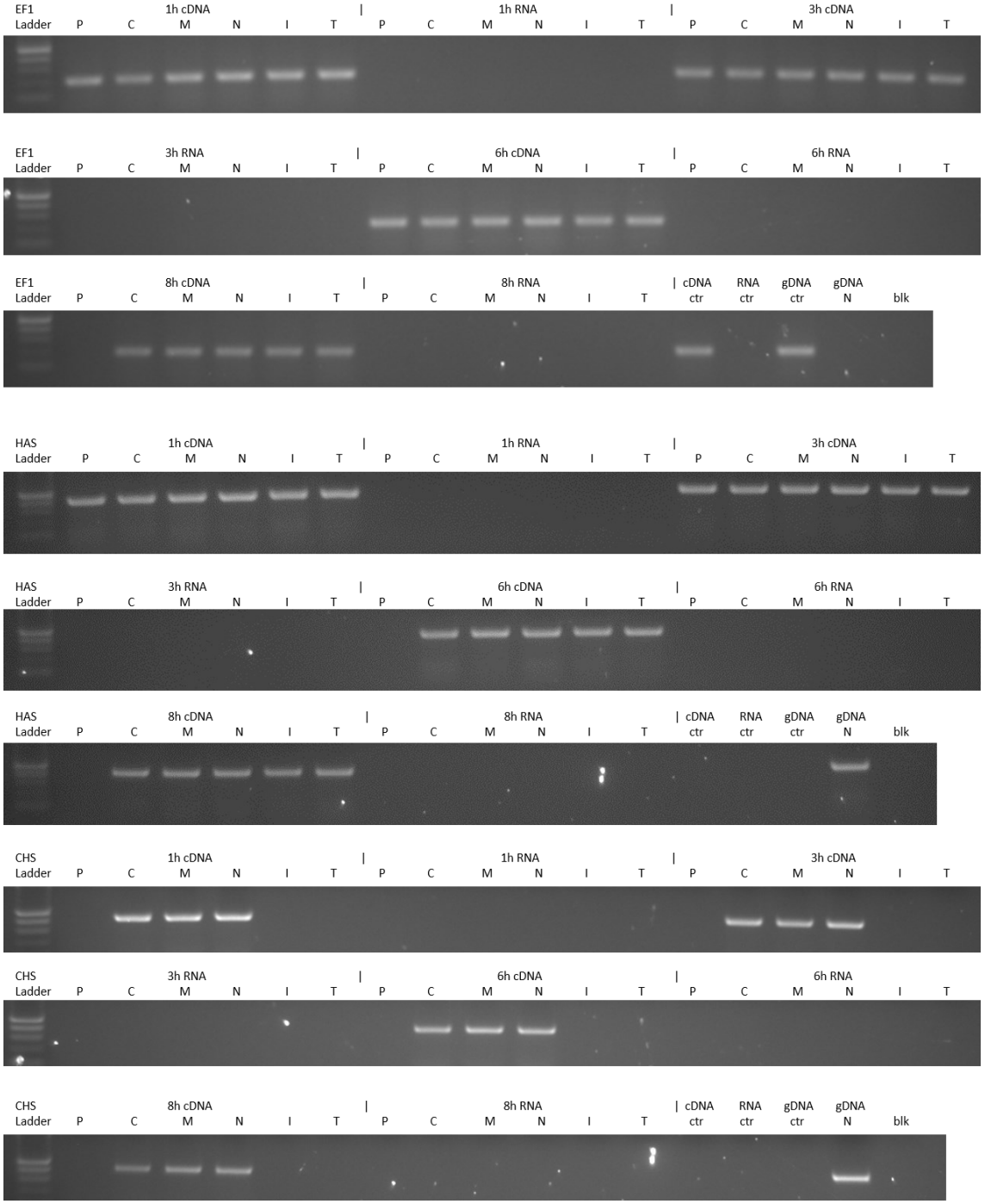

Figure 4.9. RT-PCR results of gene expression at 1-, 3-, 6- and 8-h post infection time points. EF1, elongation factor 1a gene from *Chlorella variabilis* NC64A, 200 bp band; HAS, viral hyaluronan synthase gene, 400 bp band; CHS, viral chitin synthase gene, 400 bp band; P, PBCV-1 virus; C, CviKI virus; M, MA-1D virus; N, NYs-1 virus; I, IL-5-2S1 virus; T, TAAS 2.1 virus; ctr, non-infected *Chlorella variabilis* (CCAP 211/84); gDNA ctr, genomic DNA extracted from non-infected *Chlorella variabilis* (CCAP 211/84); gDNA N, genomic DNA extracted fromNYs-1 virus.

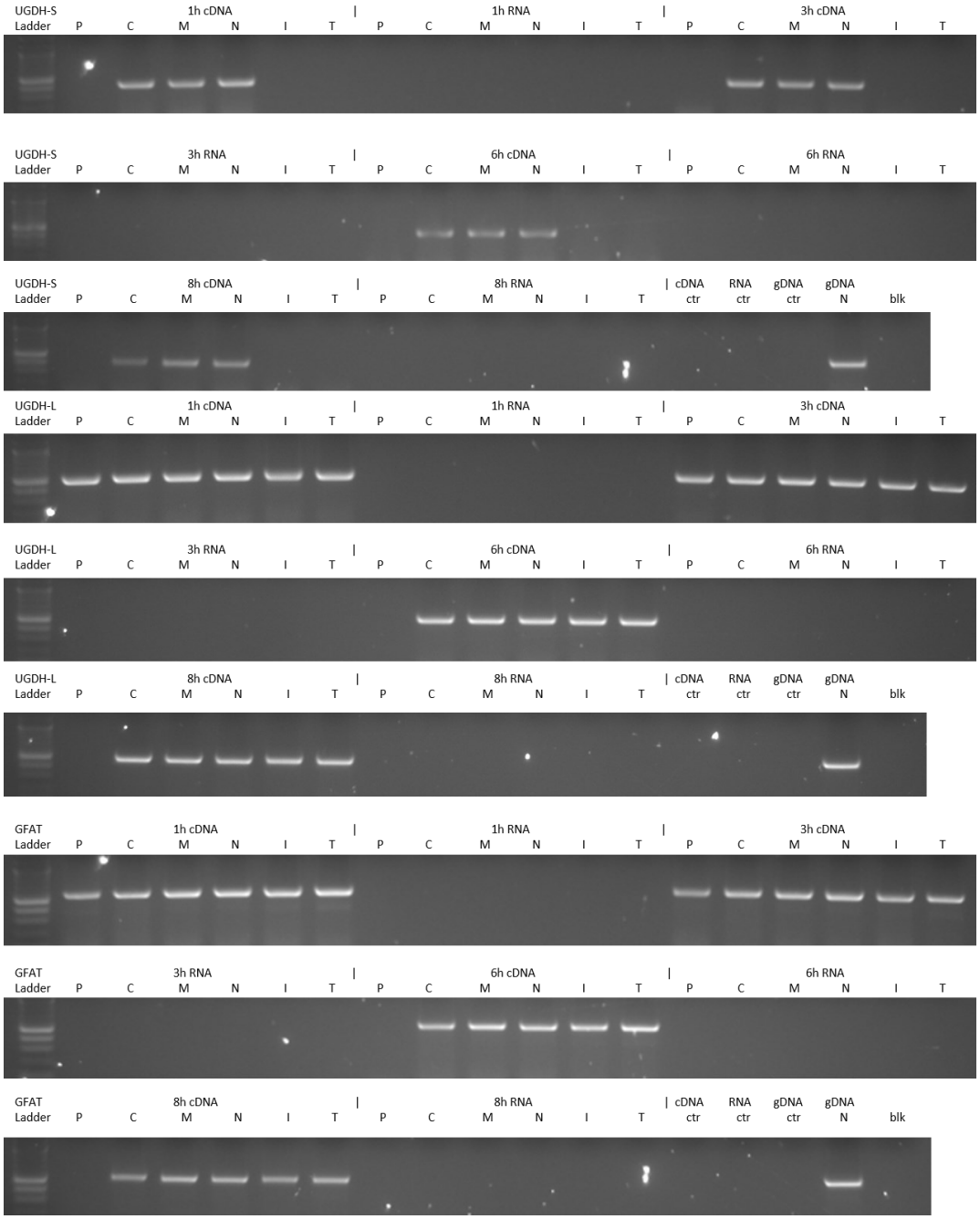

Figure 4.10. RT-PCR results of gene expression at 1-, 3-, 6- and 8-h post infection time points. UGDH-S, UDP-glucose 6-dehydrogenase shorter gene variant, 400 bp band; UGDH-L, UDP-glucose 6-dehydrogenase longer gene variant, 500 bp band; GFAT, glutamine:fructose-6-phosphate amidotransferase gene, 500 bp band; P, PBCV-1 virus; C, CviKI virus; M, MA-1D virus; N, NYs-1 virus; I, IL-5-2S1 virus; T, TAAS 2.1 virus; ctr, non-infected *Chlorella variabilis* (CCAP 211/84); gDNA ctr, genomic DNA extracted from non-infected *Chlorella variabilis* (CCAP 211/84); gDNA N, genomic DNA extracted fromNYs-1 virus.

HA and chlorophylls were measured using flow cytometric analysis using a fluorescent probe and auto-fluorescence, respectively. This analysis was performed to understand the impact of the longer gene expression in some strains and in an attempt to obtain additional data supporting the choice of the best virus strain for HA production. There was a clear shift of the majority of labelled infected sample compared with non-infected cells, confirming HA production by infected cells; not all the cells were labelled either because the cells were not all infected or the labelling protocol was inefficient (Figure 4.11).

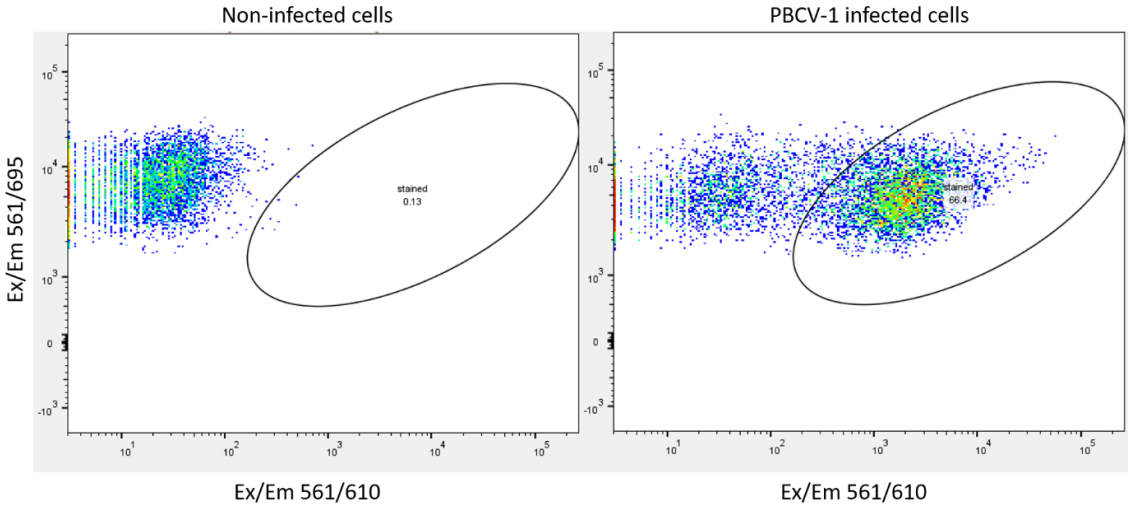

Figure 4.11. Flow cytometry analysis of HA producing PBCV-1 infected cells. Ex/Em 561/695 represent the chlorophyll autofluorescence; Ex/Em 561/610 represent the fluorescent probe used to measure HA.

Ten thousand events per replica per timepoint for all samples were analysed, 3 biological replicates for virus isolate, 1 replica for control used just as reference.

As shown on Figure 4.12(a), no statistically significant difference was found between the cell wall HA signal of cells infected by the same virus at 6 h and 8 h' time points, or by the different viruses at the same timepoint at the conditions tested. This suggests that the HA production could be restricted to the beginning

of the infection with limited differences between virus isolates and little evidence for turnover of HA on the cell surface during this time window, although the differences in the lysis cycle length between the different virus isolates shown in Chapter 3.

Chlorophyll content analysis showed the best consistency of data as a result of the direct measurement of the autofluorescence as opposed to using staining protocols for the HA measurements. The chlorophyll content appeared higher in non-infected cells (Figure 4.12(b)). There is a clear and statistically significant pattern of chlorophyll degradation for all virus isolates at each timepoint. IL-5-2S1 and PBCV-1 have the lowest chlorophyll content compared with other virus isolates. MA-1D and NYs-1 have the highest chlorophyll content from 6h timepoint, which is consistent with the longer lysis cycle data shown in paragraph 3.3.2.

Flow cytometric analysis of cell surface HA in this field is novel, not having been previously performed in microalgae cells; this approach is comparatively easy to perform, informative and powerful, owing to the number of events analysed.

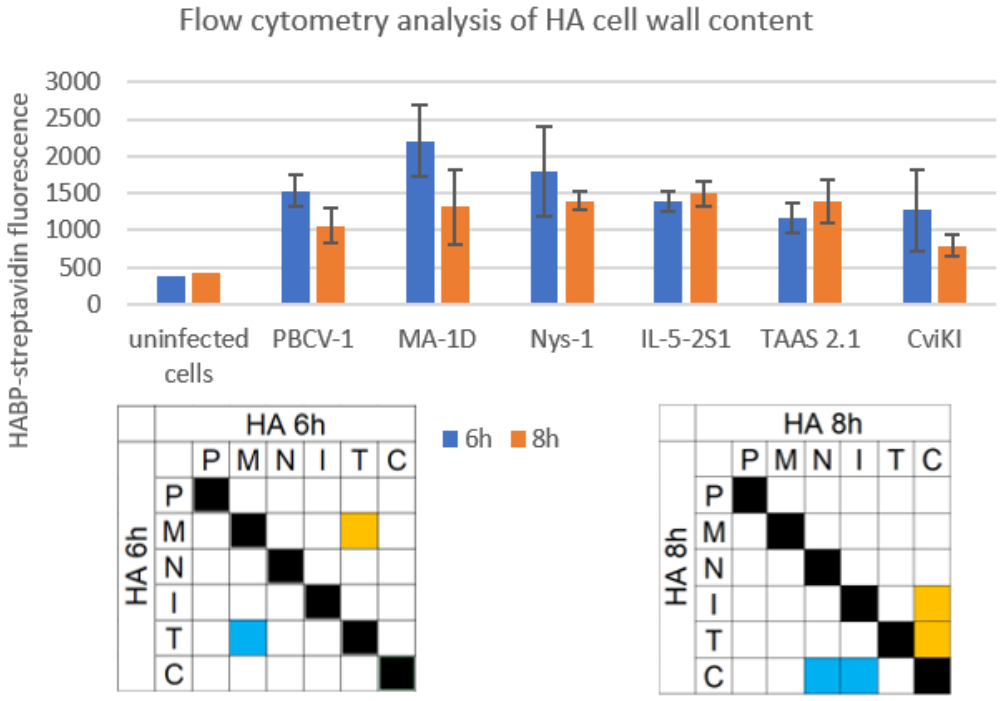
Flow cytometry analysis of HA cell wall content
HABP-streptavidin fluorescence
3000
2500
2000
1500
1000
500
0
uninfected cells
PBCV-1
MA-1D
Nys-1
IL-5-2S1
TAAS 2.1
CviKI
HA 6h
HA 8h
6h
8h
P M N I T C

(a)

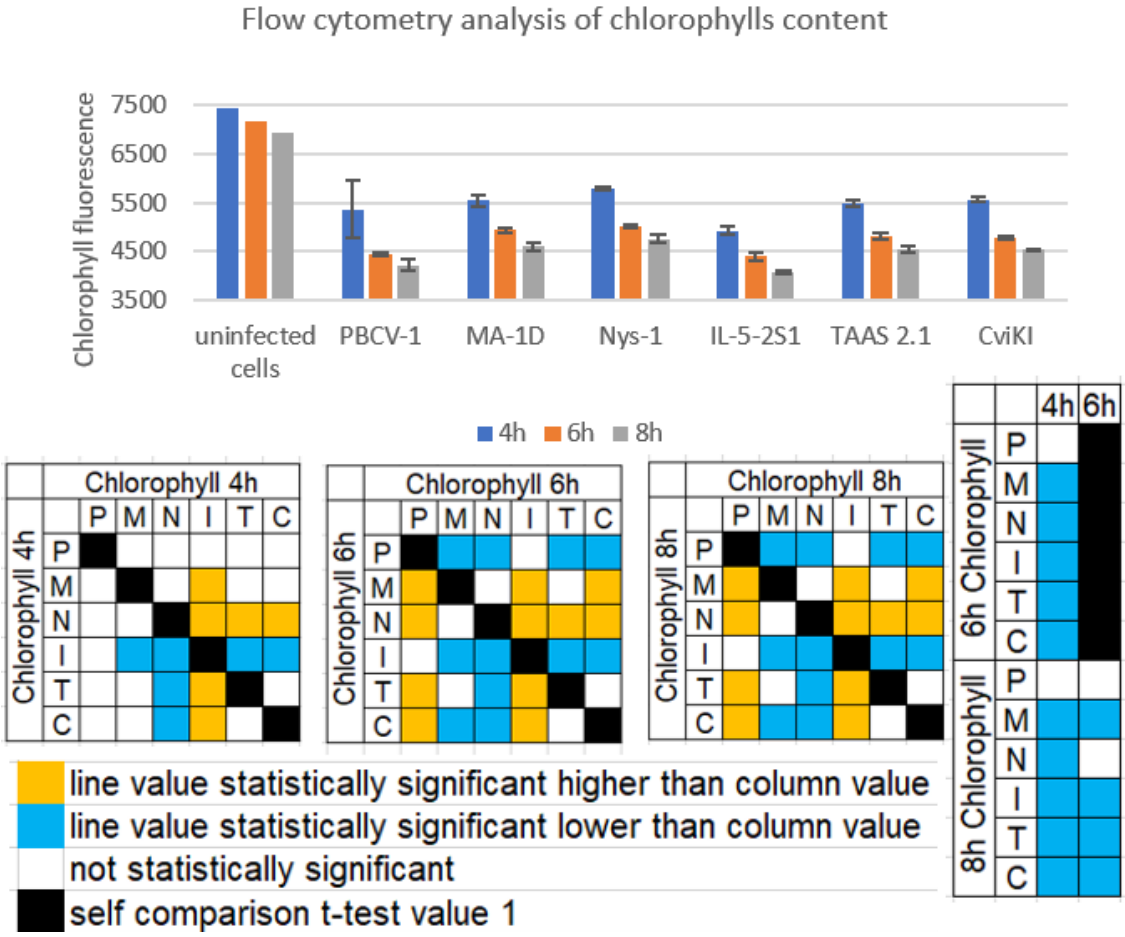
Flow cytometry analysis of chlorophylls content
Chlorophyll fluorescence
7500
6500
5500
4500
3500
uninfected cells
PBCV-1
MA-1D
Nys-1
IL-5-2S1
TAAS 2.1
CviKI
4h
6h
8h
Chlorophyll 4h
Chlorophyll 6h
Chlorophyll 8h
P M N I T C
6h Chlorophyll
8h Chlorophyll
line value statistically significant higher than column value
line value statistically significant lower than column value
not statistically significant
self comparison t-test value 1

(b)

Figure 4.12. Flow cytometric data analysis representation. The units on the histograms represent the relative fluorescence of (a) HA binding protein-streptavidin HRP, (b) chlorophyll. The colours in the squares represent the significance of the data compared between the conditions calculated with the analysis of variance (ANOVA), yellow square if the value on the line is higher than the one on the column, blue square if it is lower on the line compared to the column with a p-value of 0.05.

4.3.4 Development of a novel mixotrophic strategy for biomass production

As shown previously in Section 3.3.1. *Chlorella variabilis* CCAP 211/84 is capable to grow with the supplement of acetate.

Growth in TAP medium with added vitamins in flasks showed limited growth because of carbon limitation and pH increase due to the use of acetate in the medium. The net change in growth of the culture after around 1.6 days in Figure 4.13 shows limited carbon in the culture, as suggested by the extremely modest increase in OD over time after 1.6 days of growth with the CO_2 provided by the air supplied to the culture.

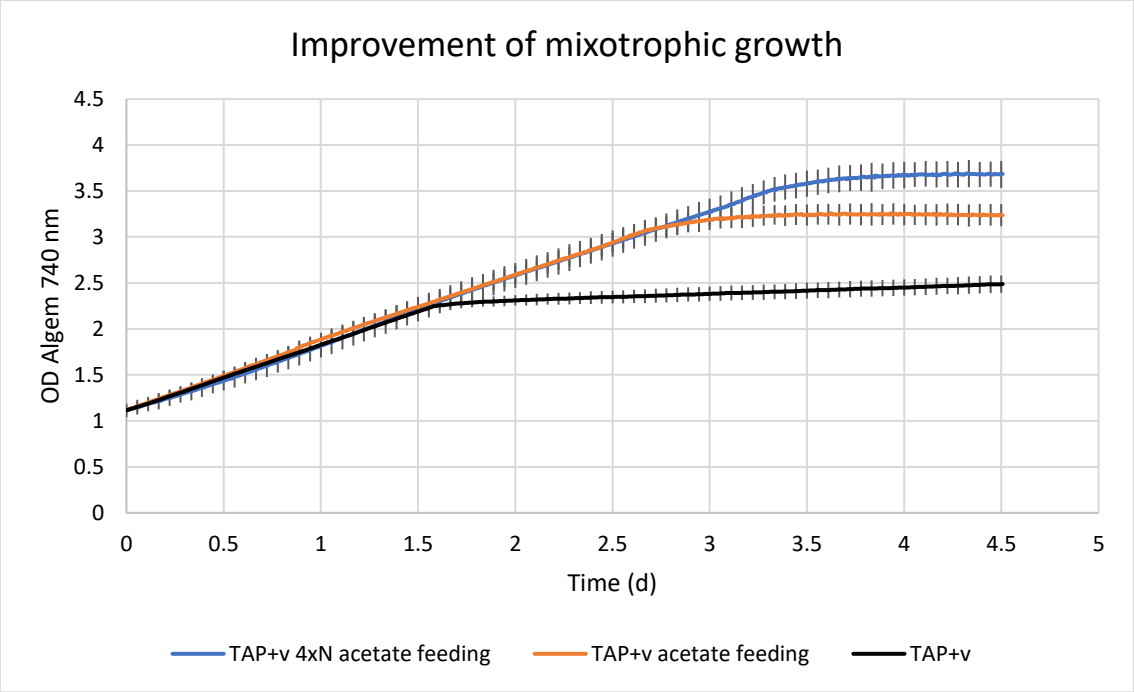

Figure 4.13. Growth comparison of *Chlorella variabilis* TAP+v under mixotrophic conditions, 500 PAR of white LED light. the three conditions compared were TAP+v, TAP+v with acetic acid feeding and TAP+v with 4 times the amount of ammonium chloride with acetic acid feeding. The plotted values are the average of 3 biological replicates with standard deviations.

To improve the cell density of the culture, the growth method developed and reported in Chapter 1 was used, providing acetic acid feeding in Algem PRO photobioreactors. This strategy was implemented in TAP medium with *Chlorella variabilis* CCAP 211/84, controlling the pH at 7, 500 PAR of white light and controlling the temperature to be stable at 28 °C. The OD measure at 740 nm of the culture at stationary phase was higher compared to the condition without feeding reaching a dry weight of (3.2 ± 0.1) $g*L^{-1}$. The limiting nutrient in this instance was the ammonium and the resultant culture was yellow because of nitrogen stress (Figure 4.14).

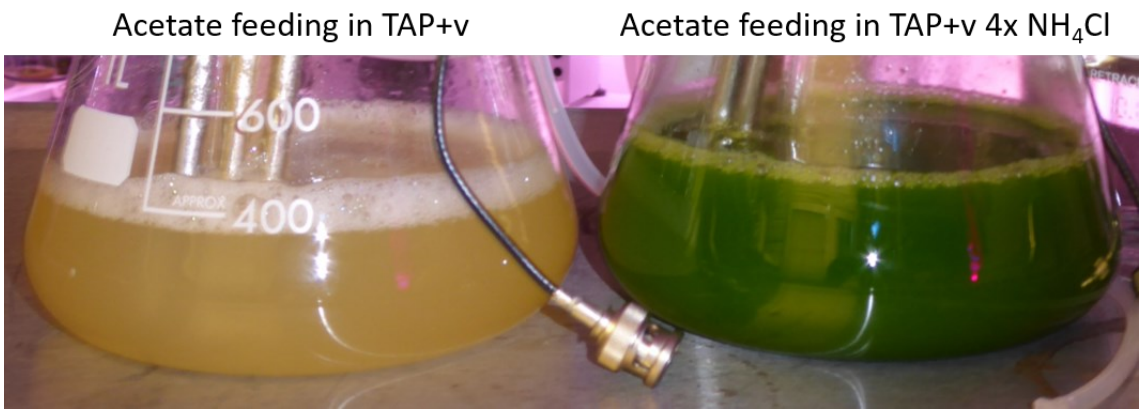

Figure 4.14. Visual characterisation of acetic acid fed cultures. On the left in TAP+v and on the right in TAP+v with the addition of ammonium chloride to reach 4 times the amount of nitrogen both at stationary growth phase after 4.5 days of cultivation.

The ammonium content in the spent medium was measured and it was zero compared to the starting concentration of (0.29 ± 0.01) $g*L^{-1}$. The culture under nitrogen stress did not undergo viral-induced cell lysis after infection by PBCV-1 virus.

To avoid the nitrogen stress and increase the biomass density at stationary phase, the nitrogen content in TAP+v was increased by 4 fold and repeated the growth with acetate feeding. Under these conditions the cultures reached higher OD values and a final dry weight of (4.4 ± 0.1) $g*L^{-1}$.

The cultures grown under this condition were infectable and the approximate HA quantification data is described in Paragraph 4.3.6.

The cell density couldn’t be increased any further. This implies that the strain's maximum potential was reached in this setup and that the limiting factors at this point were most likely light penetration (the culture was very thick and light was not penetrating in the culture, therefore not producing enough oxygen to support heterotrophic growth; a new photobioreactor shape would be necessary to

improve light penetration in the culture, for example flat panels). Gas exchange in the culture was also presumed to be limiting at high cell density, reaching the maximum achievable in the Algem based on its relatively gently circular mixing at 120rpm and gas flow rate limit of 100 cm^3*min^{-1}. It is considered highly likely that this could have been improved in a fermenter with higher gas exchange rates within the liquid but, again, the primary problem would remain to have been the degree of achievable light penetration.

4.3.5 Development of a novel fermentation strategy for biomass production in the dark

As previously demonstrated in Section 3.3.1, *Chlorella variabilis* CCAP 211/84 can grow in the dark on glucose as a substrate.

The proprietary fermentation medium (FERM) from Algenuity (Confidential) was tested for strain growth, but no proliferation was detected during a 2-week period.

HSM, an autotrophic medium with additional glucose and vitamins (HSM+g+v), demonstrated reduced growth in the dark due to resource limitation (nitrogen stress) and extreme pH drops, most likely for acid and CO_2 generation.

Controlling the pH with potassium hydroxide (KOH) solution and mixing at 200 rpm with air supply in HSM+g+v was used to assess growth in the fermenter. After 19 days, the growth stopped, reaching a maximum of 5.6 $g*L^{-1}$ dry cell weight (DM) (Figure 4.15).

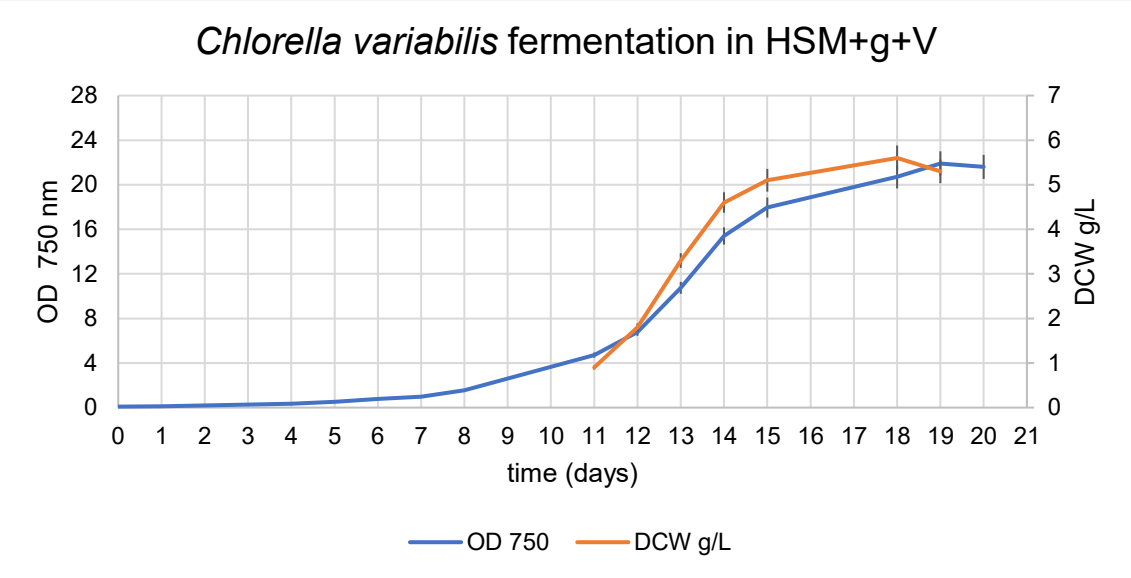

Figure 4.15. Culture density in HSM+v with added 1% glucose in the dark expressed in OD at 750 nm, blue curve with values on the left axis and dry cell weight in g*L^{-1}, orange curve with values on the right axis. One biological replicate and one sampling for each timepoint, multiple measurements of the same sample (technical replicates).

When the compositions of HSM+g+v and FERM were compared, it was noted that the nutrients in the FERM were higher than HSM+g+v, allowing for high biomass density during fermentation and, most likely, overwhelming the cells when the culture density was low. As a result, various dilutions of FERM were trialled, and a 1:4 dilution of the medium with water found to cause the algae to grow well and attain a greater ultimate biomass density in the flask when compared to growth in the same circumstances but with HSM+g+v.

As a result, the algae were grown in flasks with ¼FERM to increase the inoculum for the fermenter and accelerate the fermentation process.

The second attempt in the fermenter was carried out with ¼FERM, controlling the pH using ammonium hydroxide (NH_4OH) solution feed to also avoid nitrogen stress, 200 rpm mixing, and air supply with daily glucose and ammonium

monitoring and feeding (glucose was maintained between 1 and 30 g*L^{-1}, ammonium was maintained between 20 and 200 mg*L^{-1}). This time, growth ceased after 16 days, with a maximum of (22 ± 1.2) g*L^{-1} DM (Figure 4.16).

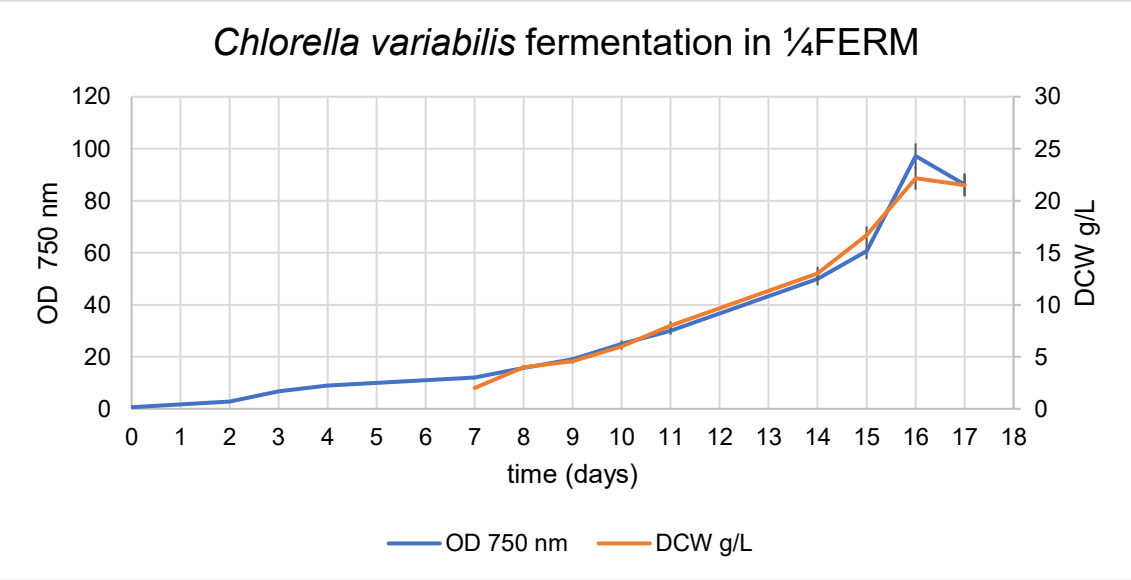

Figure 4.16. Culture density of CCAP 211/84 cultivated in ¼FERM in the dark expressed in OD at 750 nm, blue curve with values on the left axis and dry cell weight in g*L^{-1}, orange curve with values on the right axis. One biological replicate and one sampling for each timepoint, multiple measurements of the same sample (technical replicates).

A third and final trial was carried out under the same conditions as the second trial, with a greater inoculum to minimise the lag phase of growth, with daily glucose and ammonium monitoring and feeding (glucose was kept between 10 and 30 g*L^{-1}, ammonium was kept between 400 and 800 mg*L^{-1}). After the cell density reached roughly 10 g*L^{-1} DM (day 8 of fermentation), a concentrated FERM solution was added to the culture to attain the FERM composition. This time, growth terminated after 13 days, with a high of (33.4 ± 1.6) g*L^{-1} DM. (Figure 4.17).

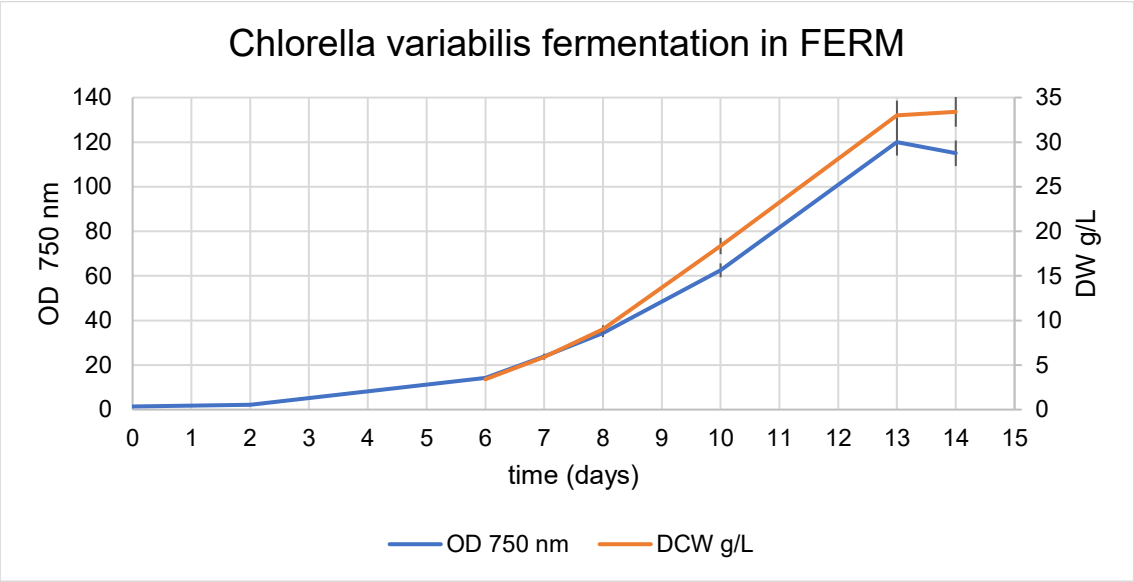

Figure 4.17 Culture density in FERM in the dark expressed in OD at 750 nm, blue curve with values on the left axis and dry cell weight in g*L^{-1}, orange curve with values on the right axis. One biological replicate and one sampling for each timepoint, multiple measurements of the same sample (technical replicates).

Under identical circumstances, Algenuity's proprietary *Chlorella vulgaris* strain, 4TC3/16, can achieve 120 g*L^{-1} DM and over, implying fermentation limitations for the CCAP 211/84 *Chlorella variabilis* strain. Performance variances occur within the same species, as demonstrated by the comparison of the two *Chlorella variabilis* strains described at the beginning of Chapter 2 (CCAP 211/84 and SAG 211-6). Most likely the strain's maximum result under these conditions was achieved.

The results obtained with heterotrophic growth were extremely promising and completely novel, as nothing comparable could be found in the literature.

The purpose of increasing biomass density was to improve HA synthesis following viral infection. As a result, the cultures were evaluated for infection and lysis.

When cultures grown in flasks under heterotrophic conditions in the dark (maximum of 5×10^7 cells*mL^{-1}) were infected with PBCV-1 virus, lysis occurred within the predicted time period, indicating that the different growth condition had no effect on the cells' infectibility, an excellent outcome for the project's continuation.

However, once very high cell densities were achieved in fermenters (over 10^9 cells*mL^{-1}, about 100 times the cell density achieved in flasks), the infection did not result in a culture crash, even after several days post infection, and only a limited decrease in cell number was measured, which could also be due to cell decay.

In Chapter 2, it was investigated the infection kinetics of six virus isolates at low cell density and obtained consistent results.

The infection dynamics of a culture 100 times denser than the conditions explored in Chapter 2, might be considerably different, and the dispersion of virus particles could be inhibited even with intense mixing (up to 500 rpm in the fermenter). Given that up to 5,000 viral binding sites per cell are available [105], the number of virus particles required to completely infect and lyse the high-density culture could be up to 10^{13} pfu*mL^{-1} (over 10^9 cells*mL^{-1} multiplied by 5,000 binding sites per cell), and an average viral stock reaches a maximum of 10^{10} pfu*mL^{-1} in laboratory conditions, theoretically, it should be used 1 L of virus stock to infect each mL of culture, which is an unscalable condition and loses the point of achieving denser cultures.

Because of the high density, viral particle dissemination in the culture is likely to be limited. Thus, when a cell releases newly created virus particles, they may

bind to cell debris and only the 0-6 cells surrounding the lysed cell, limiting viral diffusion and the formation of new virus particles. After three days in stationary phase, the cells can no longer multiply, preventing viral infection and the production of new virus particles. Hence, if the virus spreads too slowly within the culture, the culture crash may be avoided. This environment is most likely unfavourable to viral growth, which keeps the culture from collapsing following infection.

Lysis was obtained in tests using concentrated artificial cultures of cells in the exponential growth phase for lysis in fresh media. It's probable that the unsuccessful culture crash was caused by a combination of poor viral spread and cells under stress.

The stationary phase culture from fermentation was diluted in fresh media, and no growth was observed, most likely due to the cells' inability to return to the growth phase after prolonged stress.

It is likely that a sweet spot may be established in order to accomplish total culture infection for HA generation, but this proved difficult to identify due to the complex dynamics induced by the cell density. Ideally, the culture should be infected at some point during the exponential phase in order to achieve total infection and HA production (which could be monitored with flow cytometry) close to the end of fermentation, at which point the intact biomass could be harvested and potentially used for cosmetic applications, personal care, or as a scaffold for mammalian cells attachment. Due to a lack of time and equipment, it was decided not to pursue it further based on the data on HA production of the artificially concentrated cultures described in the next paragraph.

4.3.6 Analysis of HA production of infected algae

The major problems for large scale production of HA from microalgae were yield, MW and polydispersity. In paragraph 3.3.2 was shown that the enzymes present in the Chloroviruses produce high MW HA with a possible maximum of 5 MDa. In this chapter, the results of experiments to increase product yield were described. It was theorised that the limited yield of HA from the infected microalgal cultures was due to the low cell density of the culture reported in Table 2.1. For this reason, new growth protocols were developed in order to improve the biomass density prior to infection.

Quantification of HA was possible in the past combining size exclusion chromatography and the use of radioactive isotopes for the detection of the HA. The use of radioactivity was not possible in the laboratory in which the experiments were performed due to health and safety considerations and lack of available equipment.

Several purification protocols have been tested including precipitation protocols and size exclusion chromatography but the very low quantity of HA generated for each sample compared to the high amount of polysaccharide contaminants from the algae made it unfeasible for this application. For this reason, absolute quantification of the HA was not possible – for instance, contaminants were reacting with the chemicals for HA quantification making it unfeasible.

In order to have an estimate of the HA produced under the different conditions, agarose gel electrophoresis was used with a known amount of HA standard with similar molecular weight used as reference, normalising it by DM of the algal culture.

Artificially concentrated cultures were made by removing part of the medium in order to simulate a high-density culture and quantify the HA produced under those conditions. High mixing of the culture was needed for the virus spread and infection of the majority of the cells prior to HA extraction. This was tested with cells grown in both acetate feeding and glucose fermentation.

The cultures were concentrated in order to have about 11 $g*L^{-1}$ DM in 10 mL of TAP and 33 $g*L^{-1}$ DM in 10mL ¼FERM. The cells were infected with saturating MOI of MA-1D virus that gave the possible highest yield in the flow cytometry analysis although the values were not statistically significant, shown in paragraph 3.3.3, harvested after 6 h and extracted as explained in paragraph 3.2.8. Considering that the HA standard loaded was resuspended at 1 $mg*mL^{-1}$ and 10 µL were loaded in the gel, and that 20 µL of the samples were loaded, the sample bands shown in Figure 4.18 are about 5 µg with small differences between the 2 conditions in terms of MW and yield. The total volume of the extracted samples from the ¼FERM and TAP+v were 400 µL and 200 µL respectively. Based on these data the total estimated yield of HA for the samples are about 0.6 $mg*g^{-1}$ of DM for ¼FERM and about 0.9 $mg*g^{-1}$ of DM for TAP+v.

As it is visible in Figure 4.18, the ¼FERM sample holds a higher quantity of low MW (lower than 50 kDa) polysaccharides contaminants compared to the TAP+v+4xN sample probably due to the presence of glucose in the medium inducing a higher production of polysaccharides [196,197]. The gel was stained with StainsAll and different molecules are stained with different colours, blue colour indicates negatively charged polysaccharides, red colour indicates nucleic acids.

The confirmation of the identified material as HA was determined by the specific digestion with hyaluronidase enzyme, which will only degrade HA and not related polysaccharides.

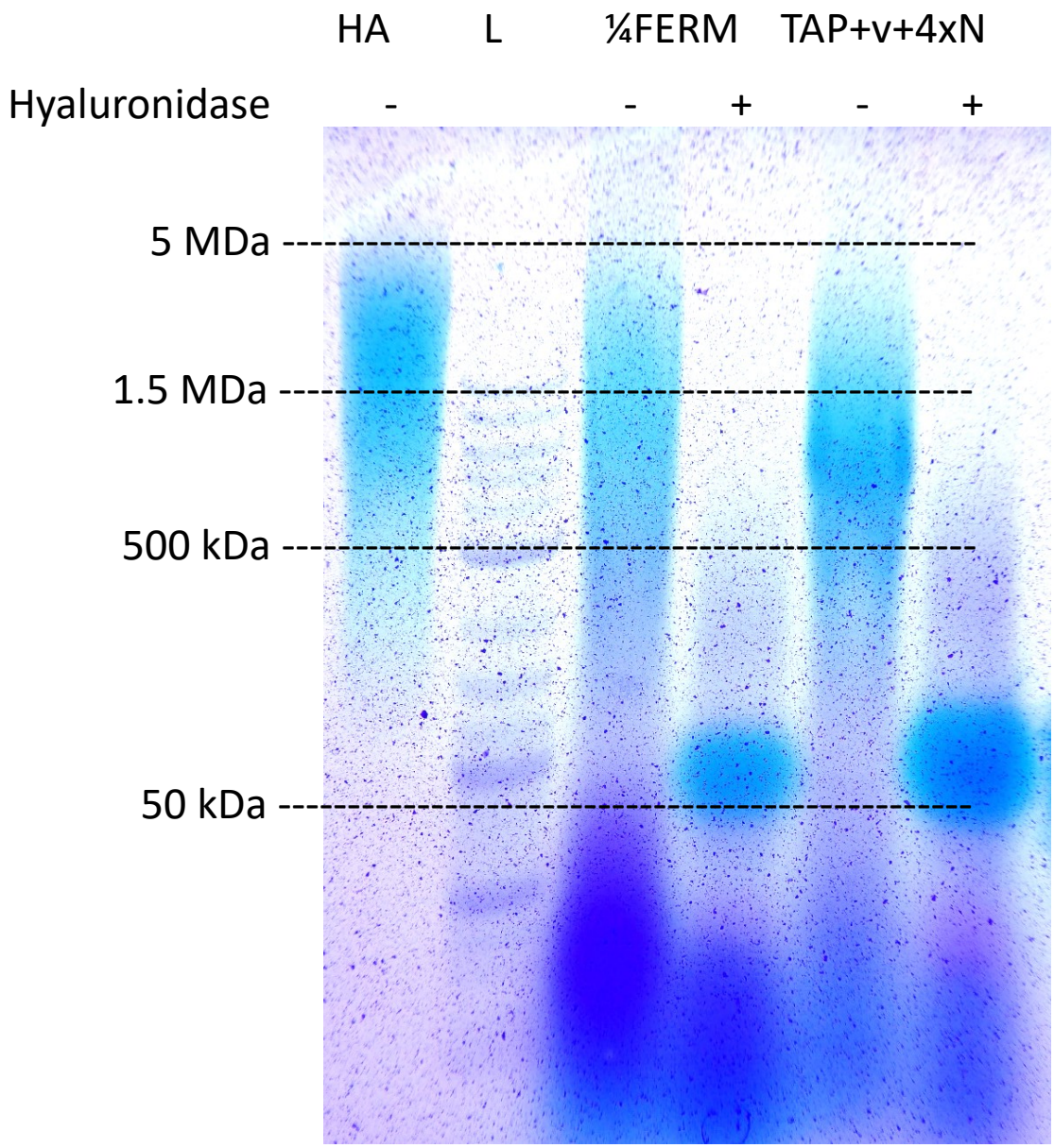

Figure 4.18. Agarose gel electrophoresis showing extracted and semi-purified samples. The first lane, HA standard; second lane, HA molecular weight standard and 2log DNA ladder; third lane, semi purified extracted HA from a concentrated culture in exponential phase grown in ¼FERM and infected with MA-1D virus; fourth lane, hyaluronidase digested semi purified extracted HA from a concentrated culture in exponential phase grown in ¼FERM and infected with MA-1D virus; fifth lane, semi purified extracted HA from a

concentrated culture in exponential phase grown in TAP+v+4xN and infected with MA-1D virus; sixth lane, hyaluronidase digested semi purified extracted HA from a concentrated culture in exponential phase grown in TAP+v+4xN and infected with MA-1D virus.

A very approximate comparison with bacterial platforms producing HA can be undertaken. The yield of HA in bacteria is about 5 $g*L^{-1}$ of culture produced in a one-day fermentation [198]. The maximum theoretical (theoretical because it couldn't be infected once the culture reached the maximum cell density) yield of HA in the microalgae platform with fermentation is about 20 $mg*L^{-1}$ (0.6 $mg*g^{-1}$ DM and assuming 33 $g*L^{-1}$ DM biomass) in about 13 days (13 days of fermentation and 6h of infection). Only considering the HA production, assuming a similar fermentation cost per day of fermentation for both bacterial and microalgal platforms and a similar cost for both platforms for extraction and purification of the product, the cost for the HA production from the microalgae platform would be about 3250 times higher compared to the bacterial platform {[(5,000 mg (bacterial HA per litre of culture) / 20 mg (microalgal HA per litre of infected culture] x 13 (days of microalgal growth)}.

The cost of production under mixotrophic conditions in TAP medium would be even higher than the fermentation cost due to the need for LED lighting, the large area necessary for tubular photobioreactors, the temperature control and the lower cell densities achieved.

4.4 Discussion

Commercial HA is currently produced by microbial fermentation of pathogenic or GM bacteria [198] and a more natural source of HA would be readily accepted by

the market if the purity, price, and sustainable production were comparable to the present platforms [36].

In this chapter, the possibility of producing HA from microalgae after infection with a species-specific virus was investigated. A variety of microalgal species, growth conditions, and viral isolates were studied. Viral HAS activity was confirmed by expression in mammalian cells, demonstrating the potential for high MW HA generation under optimum conditions.

Novel mixotrophic and heterotrophic protocols for high density biomass production were established and refined, yielding maximal biomass densities of 4.4 $g*L^{-1}$ and 33 $g*L^{-1}$, respectively, previously unreported in the literature.

When microalgae were cultivated with glucose (a precursor of the substrates for HA synthesis), the compound had a maximum MW of around 5 MDa, and when grown with acetic acid as a carbon source, the molecule had a lower MW and presumably a lower polydispersity with an increased production of 1 MDa in size. More accurate measurements of MW and polydispersity were not possible due to the very low productivity and purity of HA.

Despite the significant advancements, the estimated production per day is approximately 3250 times lower when compared to existing known bacterial platforms [198].

Chlorella extracts are currently used in cosmetics, including in combination with HA [199]. This might be a potential application to simplify product formulation while removing the usage of HA produced by GM or pathogenic bacteria, thus

opening up a new market opportunity following further improvement of the platform.

4.5 Conclusions

In this chapter, two objectives were completed as it was shown how the Chlorovirus/*C. variabilis* infection leads to HA formation and novel mixotrophic and heterotrophic protocols were developed for the production of *C. variabilis* biomass prior to Chlorovirus infection.

The hypothesis explored in this project about the feasibility of a microalgal platform to produce HA was validated, as shown in this chapter. Unfortunately, it can't be exploited industrially because of the lower yields and higher costs compared to bacterial platforms already established.

As a result of a better understanding of how Chloroviruses enter the microalgal cell to infect and burst the cell for the release of new virus particles, intriguing enzymes that can break down cell wall polysaccharides were discovered and investigated for cell wall digestion in Chapter 5.

Chapter 5 - Investigation of the activity of cell wall degrading enzymes from PBCV-1 as enabling tools for biotechnology applications in *Chlorella*.

5.1 Introduction

Biomass downstream processing improvement is essential for biomolecule production in *Chlorella* strains and cell lysis is a major obstacle to driving the cost down for most microalgae applications with product recovery [127].

The knowledge gained from a better understanding of Chloroviruses paves the way for commercial applications. The Chloroviruses have evolved to both enter and exit *Chlorella* cells and utilise a range of enzymes to perform these processes in the life cycle. Using these enzymes to learn more about *Chlorella* cell walls and how they might be penetrated brings up new possibilities for biotechnology-based applications targeting Chlorella.

As shown in Figure 4.1, *Chlorella variabilis* is closely related to other *Chlorella* species, therefore the activity of the identified cell wall digestion enzymes was investigated on multiple *Chlorella* strains across several identified species.

Several studies have been published on *Chlorella vulgaris* cell wall polysaccharide composition [200,201], the cell wall structure visualized with spectroscopy techniques [127,201] and the identification of enzymes with growth inhibition or cell wall degradation activities [127,202–204]. Despite all of these efforts, the structure and composition of the cell wall remains unclear, frequently

as a result of the analysis of strains that were mistakenly classified as *Chlorella vulgaris*.

In regards to cell wall degradation, the enzymes used are often commercial enzymes, able to degrade compounds similar to ones that were theorised to be present within the cell wall of *Chlorella vulgaris*, but probably due to the difference in the structure of the substrates or the organisational complexity and access as determined by the cell-wall architecture, these enzymes have a limited effect [204].

Chlorella vulgaris is closely related to *Chlorella variabilis* (NC64A or CCAP 211/84), the subject, along with the Chloroviruses, of earlier chapters. Chloroviruses produce a cocktail of enzymes that are able to degrade the *Chlorella variabilis* cell wall from the outside, to allow virus entry, and from the inside to release the newly assembled virus particles. The genes encoding the enzymes responsible for cell wall degradation activities have been identified in the Chlorovirus genomes and their subcellular location and site of action - produced within the infected host cell for lysis, or stored in the virus for infection - have been determined [107,205–207]. It is possible to prepare a crude cocktail containing all these enzymes from lysed *Chlorella* cells, able to digest the cells walls, in order to test the activity on different *Chlorella* species.

Although the infection of *Chlorella vulgaris* by these viruses is not possible due to the specificity of the viral spike protein in recognising specific cell surface determinants, the cell wall degrading enzymes produced by these viruses have been reported to have an effect on the cell wall of *Chlorella vulgaris* and other related species (non-specific activity) [208].

These enzymes have already been identified and tested for their activity [206–208], but no one has, to date, considered their potential enabling application for cell wall disruption using a combination of these enzymes.

The focus of this work was on a proprietary strain of *Chlorella vulgaris* named 4TC3/16, which was used to investigate the action of the crude infected cell extract from PBCV-1 virus in terms of growth inhibition and cell wall degradation. In addition, the activities of six components of the crude PBCV-1 enzyme preparation were examined by expressing each enzyme in recombinant *E. coli*.

Six enzymes with possible cell wall degradation activity were previously identified from PBCV-1 virus and similar viruses (Table 5.1). (In this work, the nomenclature of the genes encoding the enzymes of interest is based on their given names within the PBCV-1 genome).

Enzymes with presumed cell wall degradation activity	Description of the enzyme's activity
A94L	Beta-1,3-glucanase, acting either to degrade cell wall of C*hlorella variabilis* or degrade a storage polymer in the cells in order to free energy for virus multiplication [205].
A181/182R	The enzyme has 2 domains, one with endo-chitinase activity and the other exo-chitinase activity. This enzyme is not easily expressed in *E. coli* [206,207].
A215L	The enzyme was shown to have algal-lytic activity confirmed in this work, but the substrate of the enzyme is not clear with regard to the sugar released by the enzyme [208].
A260R	Endo-chitinase with a proven activity [206].
A292L	Chitosanase, present in multiple viruses that infect *Chlorella* species [206].
A561L	Enzyme with algal-lytic activity, but like A215L the substrate of the enzyme is not clear as for the sugar released by the enzyme, but has been found that the domain with the activity of interest relies just in the C-terminal portion of the protein [107]. For this reason, an N-terminally truncated version of the enzyme was expressed.

Table 5.1. List of enzymes with possible cell wall degradation activity identified from PBCV-1 virus and similar viruses with the description of the enzyme's activity.

On the basis of the information gathered by breaking down the cell walls with all possible combinations of the enzymes, a better understanding about the composition of the cell walls was achieved. Comparison of the activity of these enzymes on microalgae strains, defined closely related *Chlorella* species for classification purposes and implemented a protocol to derive viable cells with

altered cell walls in order to develop a procedure for stable transformation of the 4TC3/16 strain of *Chlorella vulgaris*.

5.2 Materials and methods

5.2.1 Chemicals and reagents

Culture media components were purchased from VWR, UK. BL21 D3 competent cells were purchased from New England Biolabs, UK. All other chemicals used were purchased from Merck, UK.

5.2.2 Microalgae strains and growth conditions

The microalgal strains used for the analysis included in this chapter were obtained from the culture collection of algae at Göttingen University (SAG) [135], Culture Collection of Algae and Protozoa (CCAP) [174], Culture Collection of Algae at the University of Texas at Austin (UTEX) [209] and included 2 *Chlorella variabilis*: SAG 211-6 and CCAP 211/84, 4 *Chlorella vulgaris*: SAG 211-11b, SAG 211-11p, UTEX 395 and Algenuity's proprietary strain 4TC3/16, previously identified with 18S-ITS2 sequencing and whole genome sequencing; and one strain of *Chlorella sorokiniana*, UTEX 1230. The strains were grown at 24 °C in TAP medium [136] with added vitamins as specified in paragraph 2.2.1, at 30 µE PAR in 250 mL flasks with 100mL of medium.

5.2.3 Infected cell extract preparation

Infected cell extract solution was prepared using the protocol available in literature [210] with modifications. *Chlorella variabilis* CCAP 211/84 was grown in

1L TAP medium until the culture reached about 10^7 cell*mL^{-1}. The culture was harvested via centrifugation at 6000 x g for 5 min, resuspended in 10 mL fresh medium and infected with 1 mL PBCV-1 virus stock and left mixing overnight or until complete lysis was observed. The lysed culture was sonicated to release the enzymes within the virus particles (Tekmar ultrasonic processor; 100 W model) in an ice bath for 2 min (5 s pulses for 24 pulses) and centrifuged at 4 °C for 15 min at 21,000 x g and the supernatant was filtered through a 0.2 µm filter. The final solution was aliquoted as 200 µL aliquots and stored at -20 °C. Processing of the entire lysate, as opposed to only the purified viruses as per the original protocol, included the enzymes produced within the cells (for virus release) rather than just the one stored in the virus capsid (A561L) used for virus entry.

5.2.4 Bacterial vector cloning and expression of the enzymes of interest

The coding sequences (CDS) of the PBCV-1 genes of interest were either produced by PCR using the virus genome as template or obtained from Twist Bioscience, with DNA sequence optimised for *E. coli* expression. Geneious v8.1.9 software (Dotmatics, USA) was used for *in silico* cloning planning, PCR primer design and DNA sequence verifications.

The only drawback of this strategy was that the full sequence needed to be screened for the presence of “illegal sites” - BsaI restriction endonuclease cut sites in addition to those that would be added for the cloning. If BsaI sites were identified within the respective CDS sequences the PCR was split in multiple fragments adjusting the sequence in order to eliminate these sites. Alternately,

the Twist sequence was ordered that removed the internal BsaI sites while preserving the primary encoded amino acid sequence.

In this instance, the genes A215L and A260R required these corrections ending up with 2 fragments for A215L and 3 fragments for A260R, one of which was 182 base pairs in length, therefore was added to the mix with a molarity five times higher than the backbone.

target template	direction	sequence (5' - 3')	annealing temperature (°C)
A094L	Forward	TAGGTCTCTTCACTCTCAAGTAG ACACCGTG	61
	Reverse	GAGGTCTCCGTCAATCGCGAAT GCCTG	59
A181-182R	Forward	TAGGTCTCTTCACGCGACCGTA CCAAG	59
	Reverse	GAGGTCTCCGTCACGCAAATGT GTTGAATATATTTGTG	60
A215L	Forward-1	TTGGTCTCTTCACAATGGAAACG ACAACTGG	60
	Reverse-1	TTGGTCTCTTCCACGGATCTTTT GTTTTAGATC	62
CviKI HAS	Forward-2	TTGGTCTCTTGGACTCGACCCC GAAGG	60
	Reverse-2	GAGGTCTCCGTCATTCGTATTTC TTCATTTGGAAATTCG	61
A260R	Forward-1	TTGGTCTCTTCACGCCCTTGCGA AAC	57
	Reverse-1	TTGGTCTCTTTTCATCAACGTTGA AGAATGC	61
	Forward-2	TTGGTCTCTGAAACCGGTAGGGT ATTC	59
	Reverse-2	TTGGTCTCTTCCTTTTTGGTGAAC AAAGTC	60
	Forward-3	TTGGTCTCTAGGACTCGGTGGTA TC	60
	Reverse-3	GAGGTCTCCGTCATTTCTTAGGC CAATCACAAG	60
A292L	Forward	TTGGTCTCTTCACTCAAACAAAAT AGAAATAACAGACG	59
	Reverse	GAGGTCTCCGTCATGAAATAACT ATGTTTTTACCCCAG	60
A561L^{d4}	Forward	ATGGTCTCATCACGCCGATGTTG AGGTTCC	63
	Reverse	GAGGTCTCCGTCAGGGCGACCA TTTAGAAATTTTTAC	62

Table 5.2. PCR oligonucleotide sequences used for the PCR amplification to use for Golden Gate cloning. From the top, A094L forward primer, A094L reverse primer, A181-182R forward primer, A181-182R reverse primer, A215L forward primer 1, A215L reverse primer 1, A215L forward primer 2, A215L reverse primer 2, A260R forward primer 1, A260R reverse primer 1, A260R forward primer 2, A260R reverse primer 2, A260R forward primer 3, A260R reverse primer 3, A292L forward primer, A292L reverse primer, A561L^{d4} forward primer, A561L^{d4} reverse primer.

For each sample, the golden gate mix was prepared with 1 µL of buffer G (ThermoFisher Scientific, UK), 1 µL of ATP solution 100 mM (ThermoFisher Scientific, UK), 0.5 µL of T4 ligase (ThermoFisher Scientific, UK), 0.5 µL of BsaI restriction enzyme (ThermoFisher Scientific, UK) and 2 µL of molecular grade water to which was added 5 µL of the PCR fragments (twice the molarity of the backbone) and the empty backbone (35 ng) making up to the desired volume (10 µL) with molecular grade water.

Once the mixes were ready, they were incubated in iCycler Thermal Cycler System with 96 Well Reaction Module (Bio-Rad Laboratories, UK) with the following protocol:

Ten min at 37˚C and ten min at 16˚C for three times after which the temperature of 16˚C was held until the samples were taken out for bacterial transformation.

Plasmids were transformed into chemically competent *E. coli* DH5α cells (New England Biolabs (NEB, UK) for plasmid production, incubated 5 µL of golden gate mix with 50 µL of cells in ice for 30 min, heat shocked at 42 °C for 30 s and incubated in ice for another 2 min. One mL of SOC medium (Merk, UK) was added to the cells and incubated at 37 °C for 1 h before 50 µL of each was plated on LB plates (Merk, UK) with carbenicillin 100 $mg*L^{-1}$ selection and incubated overnight at 37 °C. Single colonies were picked from selection plates and inoculated in 5 mL of LB medium with 100 $mg*L^{-1}$ carbenicillin and incubated overnight at 37 °C. Cultures were pelleted via centrifugation at 5,000 x g for 5 min and plasmids were extracted via miniprep kit (ThermoFisher Scientific, UK) following the supplier's protocol. At this step, the plasmids were sequenced with primers that flanked start and stop codons to confirm that the inserted sequence

was correct. One ng of each plasmid was used to transform BL21 DE3 (NEB, UK) following the protocol specified above. Single colonies were picked from selection plates and inoculated in 25 mL 2xYT medium (Merck, UK) and grown overnight at 37 °C. The next day, 1L cultures were inoculated, using the overnight cultures, at a starting OD 600 nm of 0.05. Once the OD 600 nm reached a value of 0.5-0.6, 1mM IPTG (final concentration) was added to the culture to induce the expression of the protein overnight at 30 °C. The next day, the biomass was harvested by centrifugation at 6000 x g for 5 min.

The wet weight of each pellet was measured and resuspended at 1 $g*mL^{-1}$ with PBS+5% glycerol and moved into 15mL tubes for easier processing. Lysis of the bacteria was achieved with sonication (Tekmar ultrasonic processor; 100 W model) in an ice bath 5 times 1 min sonication at 100% with intervals in between of 2 min.

After lysis, cell debris were centrifuged at 21000 x g for 10 min at 4 °C and the supernatants were filtered through 0.2 µm filters (Sartorius, UK), aliquoted in cryovials and flash frozen in liquid nitrogen before storage at −80 °C.

5.2.5 SDS-PAGE

Twenty-five µL of IPTG induced cultures were mixed with 25 µL of deionised water and 50 µL of 2x Laemmli buffer (Sigma-Aldrich, USA). Samples were incubated at 100 °C for 5 min before loading in NuPAGE 12% Bis-Tris gel (ThermoFisher Scientific, UK) with protein ladder (Color Prestained Protein Standard, Broad Range, P7719, New England Biolabs, UK) as the reference. The gel was run in NuPAGE MES SDS running buffer (ThermoFisher Scientific, UK)

at 150 V for 45 min. The staining of the proteins was performed with Coomassie stain (InstantBlue, Abcam, UK) incubating at room temperature with gentle shaking for 1 h.

5.2.6 Growth inhibition assay

Exponentially growing microalgal cells of the strains reported on paragraph 4.2.2 were harvested and resuspended in TAP medium at 4×10^8 cells*mL^{-1}. TAP medium soft agar was prepared adding 0.5% agarose to TAP medium, after cooling the medium at 50 °C, 3 mL were added to 0.3 mL of resuspended cells and plated immediately on the top of TAP agar plates (1.5% agarose). Once plates were cool and dry, 5 uL of infected cell extract or bacteria lysate expressing the enzyme of interest were spotted on the plates, using bacterial lysate expressing Venus fluorescent protein with no cell wall digestion activity as negative controls. Plates were imaged after 3 days and clear growth inhibition was visible with halos on plates where spots of infected cell extract or bacteria lysate were applied. Lysis activity of the virus was also tested by spotting virus lysate stocks on plate.

5.2.7 Cell wall digestion activity assay

Exponentially growing cells of the microalgal strains reported on paragraph 4.2.2 were harvested and resuspended in PBS at 1.25×10^8 cells*mL^{-1} (to achieve 10^8 cells in 0.8 mL). To 0.8 mL of cells, 0.2 mL of enzyme mix [204] from literature (N-Acetyl-β-D-Glucosaminidase, Merk, UK; Alginate lyase, Merk, UK; Lysozyme, Merk,UK; final concentration of 20 mg/L for each enzyme), or infected cell extract [3.2.3], or bacteria lysate expressing the enzyme of interest, single or in

combination, were added; for the negative control a bacterial lysate expressing Venus fluorescent protein with no cell wall digestion activity was used. Samples were incubated at room temperature mixing by inversion at 60 rpm overnight. The next day, 0.25 mL of 10% SDS was added to each sample and samples were incubated at room temperature for 30 min mixing by inversion, the centrifuged at 18000 x g for 5 min. OD 435 nm was measured of the supernatant with dilution in PBS if necessary. All conditions were tested with three biological replicates.

5.3 Results

5.3.1 Benchmarking cell wall digestion with enzyme preparation from PBCV-1 lysate against previously reported cell wall digestion protocol

The literature review on viruses infecting and lysing *Chlorella variabilis* for the production of HA (Chapter 2), indicated a close phylogenetic relationship between *Chlorella variabilis* and *Chlorella vulgaris*, which is a species of intense commercial relevance across multiple markets and of particular importance to Algenuity's commercial strategy.

Due to the specificity of the Chlorovirus infection towards *Chlorella variabilis* strains, most probably based on the recognition of cell wall polysaccharides [104], the current known Chloroviruses are unable to infect and lyse *Chlorella vulgaris* strains.

Crude enzyme preparations from the PBCV-1 virus were tested for cell wall degradation and growth inhibition activities against *Chlorella vulgaris* with *Chlorella variabilis* acting as a positive control.

Despite the fact that the specificity of infection and cell lysis from the virus infecting *Chlorella variabilis* cells has previously been described in the literature, growth inhibition was also observed in *Chlorella vulgaris*. As shown in Figure 5.1 the halo from the PBCV-1 enzyme preparation was visible for both *Chlorella variabilis* strains investigated and for the *Chlorella vulgaris* 4TC3/16 strain. As expected, there was no growth inhibition activity or cell lysis activity of the virus stock on the *Chlorella vulgaris* strain, the darker halo that can be noticed on the plate in Figure 5.1(c) was due to bacterial growth present in the viral stock. This result confirms that the cell wall digestion activity of the enzymes produced by the virus was not restricted to the host species, compared to the virus infection activity.

(a) (b) (c)

Figure 5.1. Growth inhibition assay. (a) SAG 211-6 *Chlorella variabilis*, (b) CCAP 211/84 *Chlorella variabilis*, (c) 4TC3/16 *Chlorella vulgaris*. PBS negative control, PBCV-1 virus, PBCV-1 enzyme preparation.

The enzyme preparation from PBCV-1 virus was then compared with the best previously reported enzyme mix for *Chlorella vulgaris* cell wall digestion and a control without the enzyme was included.

The digestion was performed overnight in order to give the enzymes enough time to completely digest the cell wall. After cell lysis with 2% SDS, the chlorophyll released was measured using OD 435nm.

As shown in Figure 5.2, when the cell wall is not digested, the chlorophyll release is very limited. Both the impacts of the enzyme mix from literature and the enzyme preparation from PBCV-1 lysate are statistically higher than the no enzyme control with a p-value lower than 0.01 showing a cell wall digestion activity. The impact of the Chlorovirus enzyme preparation is statistically higher than the enzyme mix, showing a value of chlorophyll released after cell wall digestion almost 8 times higher than the enzyme mix from literature [204].

This suggests that the enzyme preparation from the PBCV-1 virus is able to digest the *Chlorella vulgaris* cell wall more completely as compared to the established protocol [204].

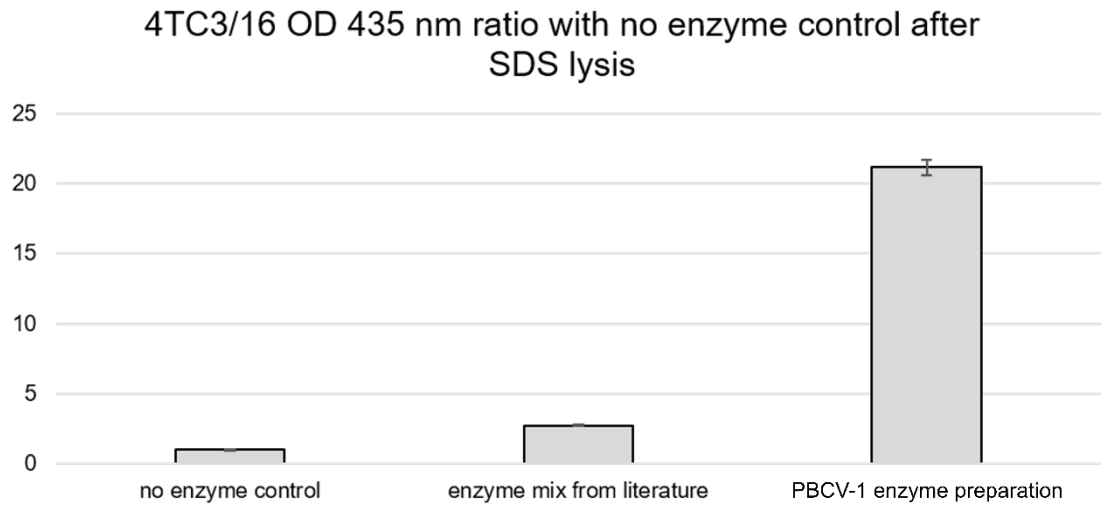

Figure 5.2. Chlorophyll released by lysed cells with 2% SDS following cell wall digestion. On the left the non-digested control sample, in the middle the sample digested with the protocol reported in literature [204] (N-Acetyl-β-D-Glucosaminidase, Merk, UK; Alginate lyase, Merk, UK; Lysozyme, Merk,UK), on the right the sample digested with PBCV-1 lysin preparation. The represented values are the average of 3 biological replicates with standard deviations.

Based upon this result it was investigated which enzymes are encoded by the virus with reported possible cell wall digestion activity.

Six genes are present in the PBCV-1 viral genome encoding enzymes with demonstrated polysaccharide degradation activity. It was decided to overexpress each of these recombinantly in bacteria to test the impact singly and in various combinations on *Chlorella vulgaris* and *Chlorella sorokiniana* strains.

5.3.2 Cloning strategy of cell wall digestion enzymes from PBCV-1 for production in bacteria

A Golden-gate cloning [211] protocol was chosen for the production of the plasmid constructs to express the selected cell wall digestion enzymes from PBCV-1 for recombinant protein production in bacteria.

The Golden Gate strategy relies on type II restriction enzymes and was chosen because an empty vector for protein expression was already available in Algenuity for this cloning strategy. Furthermore, with this protocol the cloning is scarless, requires minimum sequencing control just after the PCR step to confirm that the amplified sequence is correct, it is ideal for complicated directional assembly with multiple parts. In the present instance, a very simple plasmid was made with only one cloning step. This is one of the easiest and high-efficiency molecular cloning methods when compared to classical restriction enzyme cloning or the Gibson assembly [212] in terms of planning and hands-on time.

The only drawback using the Golden-gate strategy is that the full sequence has to be checked for the presence of “illegal sites” that in this case means BsaI sites in addition to those added for the cloning. If internal BsaI sites are present, they need to be domesticated, which can be achieved by splitting the PCR in multiple fragments, and adjusting the sequences to eliminate these sites.

These coding sequences were initially produced via PCR from the PBCV-1 genome and cloned into a vector for bacterial expression as outlined in the material and methods section. Venus protein expression was used as a positive control to verify the cloning strategy, the vector backbone and the induction protocol. The lysate of the induced culture expressing Venus protein was also used as a negative control for the growth inhibition assay and for the chlorophyll release assay. Venus is a yellow fluorescent protein commonly used for microalgae because the absorbance is different compared to chlorophylls and, therefore, does not have any interference in the chlorophyll release assay. With

regard to the A561L protein, a truncated protein representing the cell wall digestion catalytic domain (A561L^{d4}) [104,107], shown in Figure 5.3, was cloned.

For the A292L and A215L enzymes, induced products of the expected size were visible on SDS-PAGE and the, respective, bacterial lysates possessed growth inhibition activity. The constructs representing the other 4 enzymes, didn't produce any visible protein on SDS-PAGE and didn't have any activity, although the open-reading frame sequence was validated and confirmed to be in-frame within the context of the expression vector.

Optimised DNA sequences for the expression in *E. coli* with a reduced number of potentially problematic rare codons were designed, purchased and used for cloning in the same expression vector and in the same strain of *E. coli*.

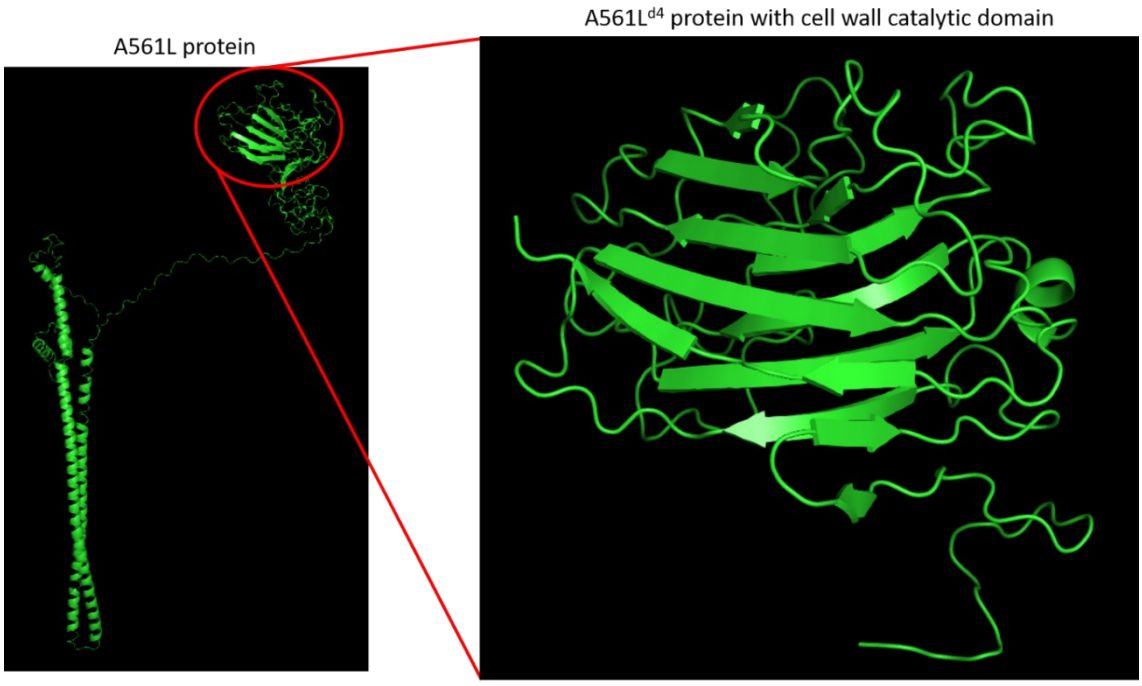

Figure 5.3. Structure prediction of A561L protein (left) and the truncated version A561L^{d4} (right).

In this instance, the A260R protein showed an induced protein of the expected size on the SDS-PAGE shown in Figure 5.4, but no induced product was visible for the A561L^{d4} protein, although bacterial lysates for both had reproducible growth inhibition activity (Figure 5.5). Still no expression and no activity were found for the remaining 2 proteins (A094L and A181-182R) so the focus for the remainder of the work was on those proteins that were successfully expressed and demonstrated to have relevant activity. Interestingly, of the two proteins that were not successfully expressed, the A181-182R enzyme was reported to have chitinase activity [207], while enzyme A094L is not reported to be related to cell wall degradation activity but probably to the “degradation of host storage polysaccharides releasing glucose as an energy source for the cell during viral assembly [205].

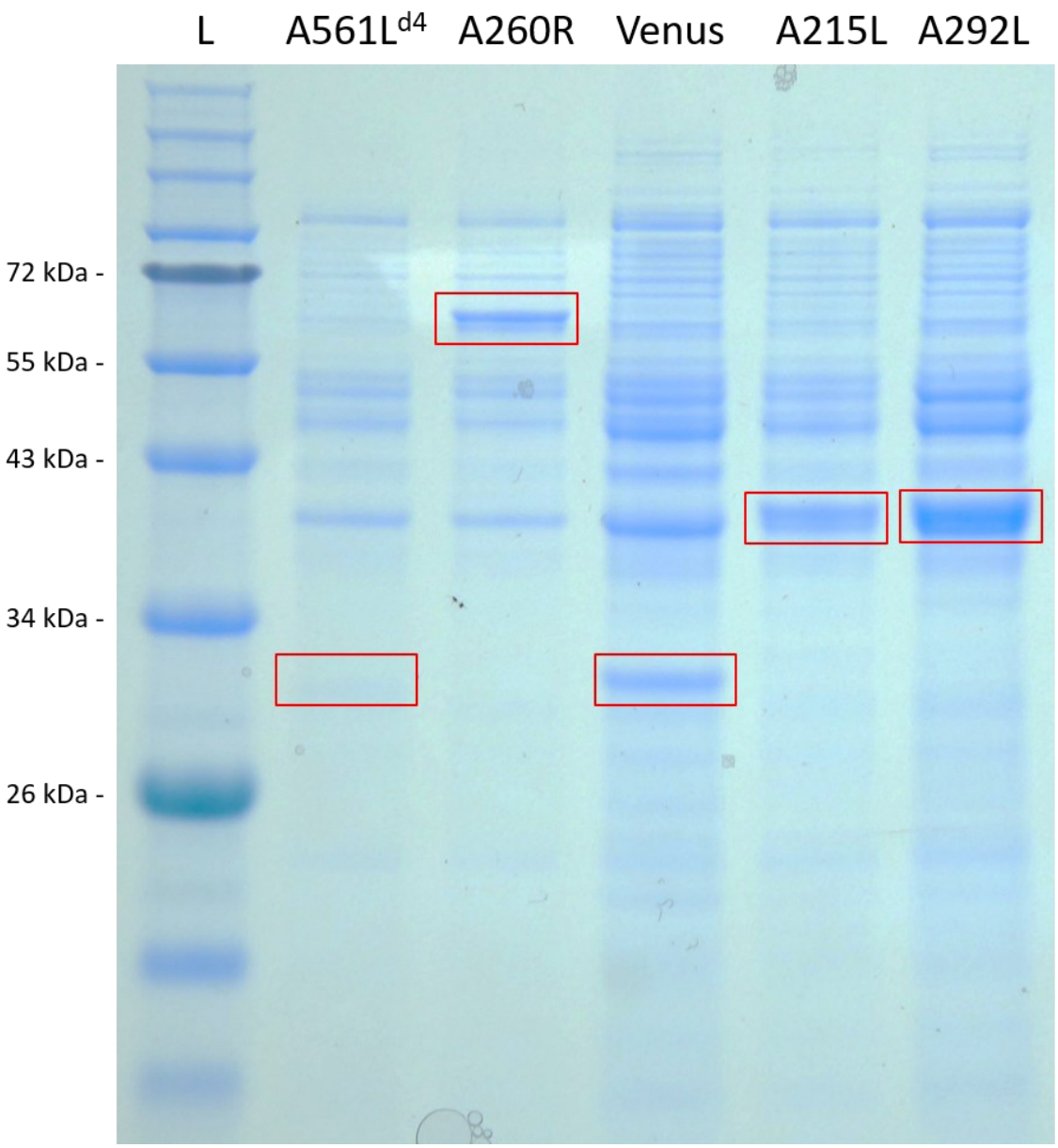

Figure 5.4. SDS-PAGE of IPTG induced bacterial cultures. First lane, protein ladder; second lane, protein from cells transformed with the plasmid for A561L^{d4} expression (28 kDa); third lane, protein from cells transformed with the plasmid for A260R expression (57 kDa); fourth lane, protein from cells transformed with the plasmid for the Venus expression (28 kDa); fifth lane, protein from cells transformed with the plasmid for the A215L expression (36 kDa); sixth lane, protein from cells transformed with the plasmid for the A292L expression (38 kDa). The bands in the red squares represent the protein induced in each sample.

The activities of the bacterial lysates were evaluated using a growth inhibition assay on a plate, spotting 10 µL of bacteria lysates with buffer control and Venus expressing bacteria lysate as negative controls. Growth inhibition was observed for the 4 enzymes produced, as shown on Figure 5.5, despite the fact that the A561L^{d4} polypeptide was not visible by eye on the stained SDS-PAGE.

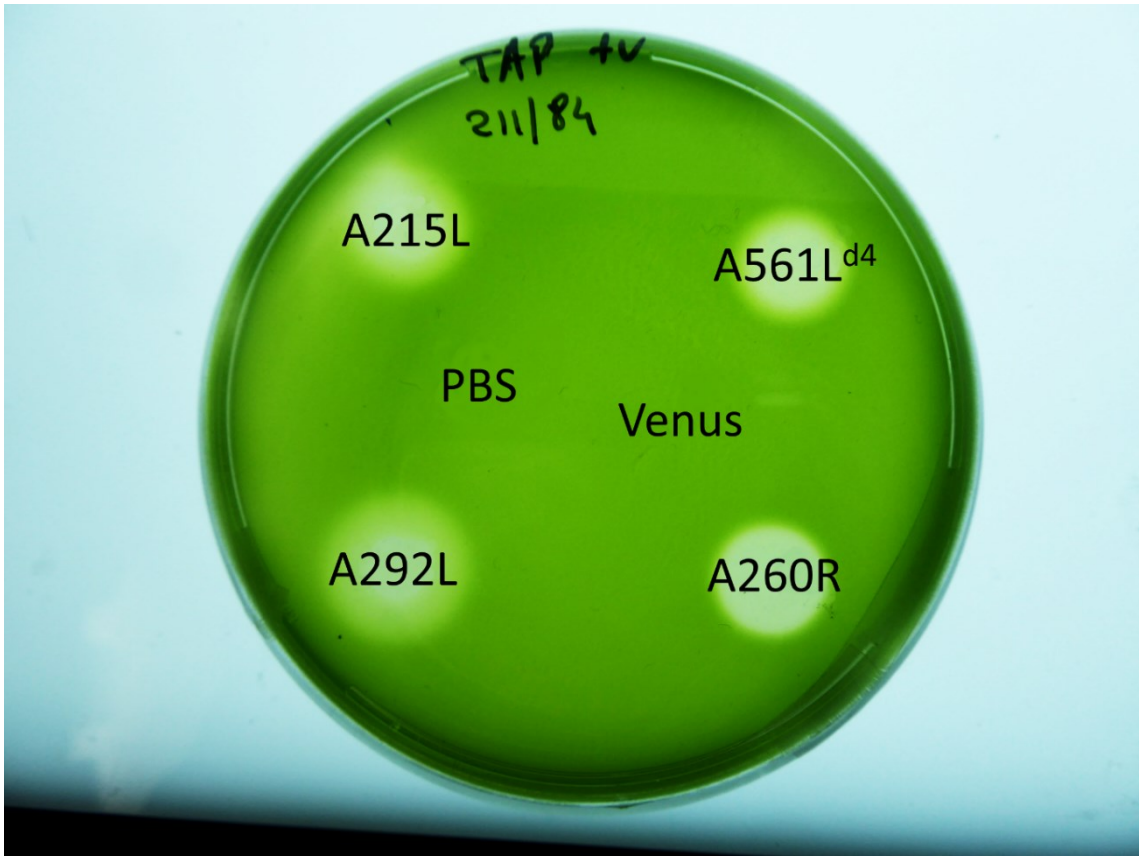

Figure 5.5. Growth inhibition assay. CCAP 211/84 *Chlorella variabilis*. PBS negative control, Venus negative control, A215L, A561L^{d4}, A292L and A260R.

5.3.3 Growth inhibition and cell wall digestion in related species

After the respective activities were demonstrated for growth inhibition on the *Chlorella variabilis* CCAP 211/84 strain, the same assay was used to evaluate the activity on other strains representing closely related *Chlorella* species based upon derived phylogeny (Figure 4.1).

The results, shown on Figure 5.6, were very similar for all *C. vulgaris* strains, except for the size of the halo and how defined the borders were. Regarding the *C. sorokiniana* strain tested, only the 2 enzymes with alginate lyase activity had an observed effect on the growth inhibition assay, suggesting that the cell wall architectures may be different for this species, for instance, and chitin or chitosan is not readily accessible to the chitinase enzymes or that chitin or chitosan is only a very minor part of the *C. sorokiniana* cell wall.

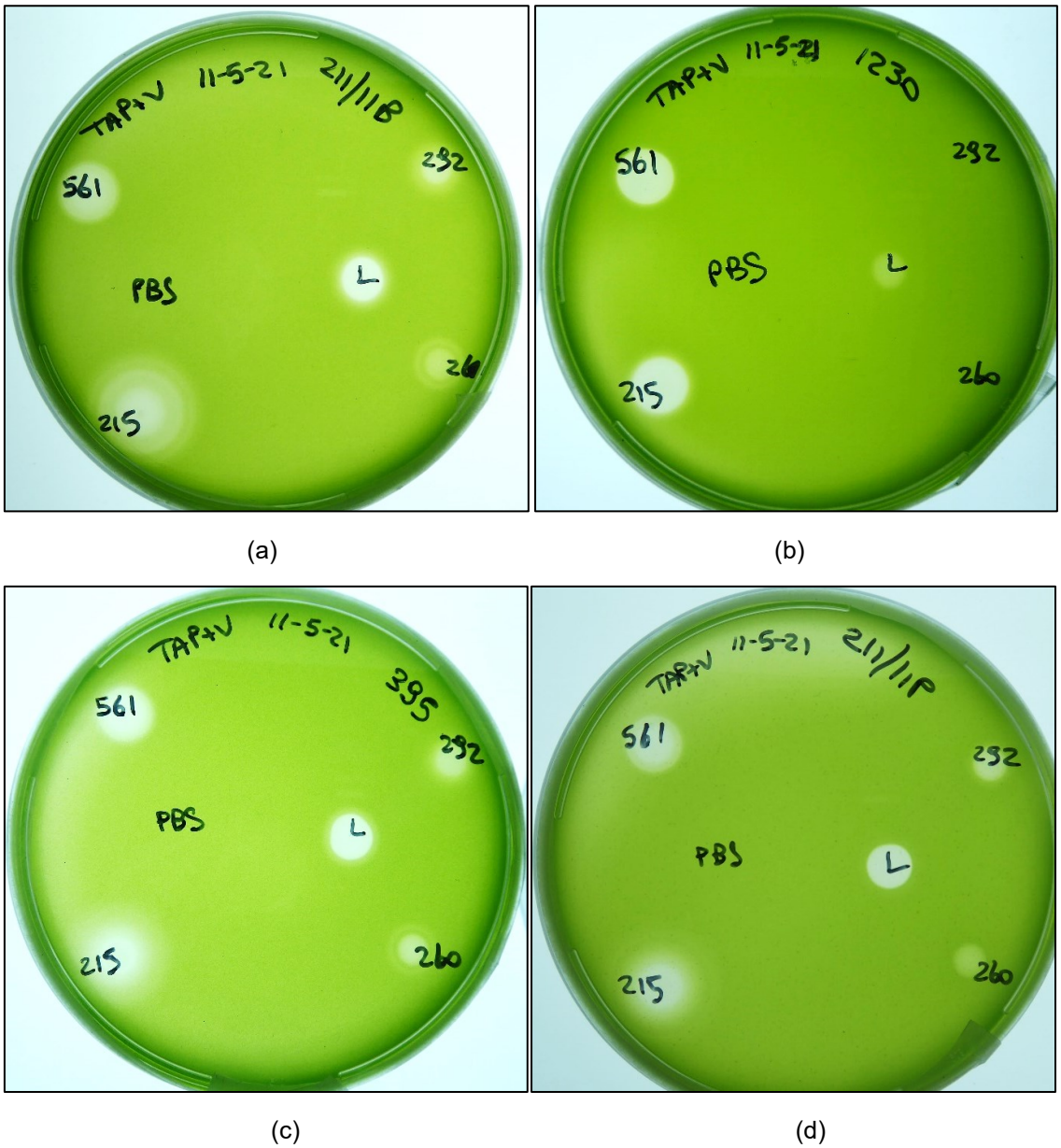

(a) (b)

(c) (d)

Figure 5.6. Growth inhibition assay. (a) SAG 211-11b *Chlorella vulgaris*, (b) UTEX 1230 *Chlorella sorokiniana*, (c) UTEX 395 *Chlorella vulgaris*, (d) SAG 211-11p *Chlorella vulgaris*. (PBS) negative control, (L) PBCV-1 enzyme preparation positive control, (215) A215L, (561) A561L^{d4}, (292) A292L and (260) A260R.

Following on from investigation of the growth inhibition activity of the respective enzymes on the related *Chlorella* species, the cell wall digesting activity was evaluated by measuring the absorbance of chlorophyll released after lysis with SDS (Figure 5.7). The enzymes in each lysate were not quantified, and the same

volume of lysate was used for all the enzymes in order to have a presumed excess of enzyme to cells in all reactions (tested multiple lysate volumes to cells number ratios), and the digestion was prolonged overnight, despite the fact that an observable effect was visible after 15 min of digestion.

For all strains of *C. vulgaris*, all enzymes produced values greater than the no-enzyme control, and they were all statistically significant with p-values less than 0.05 (Figure 5.7). The data were consistent with the observed result on the growth inhibition assay and suggest that the enzymes in question can directly permeabilise the cell walls of all *Chlorella vulgaris* strains tested with reproducible variations suggesting subtle changes in cell wall composition in specific *C. vulgaris* strains.

Despite *Chlorella sorokiniana* being a close relative to *Chlorella variabilis* based on the tree presented in Figure 4.1, the cell wall composition and/or macro-architecture of the two species must be significantly different. The digestions of *C. sorokiniana* showed values higher than the control for all four enzymes, which are statistically significant compared to the control without enzyme, with a p-value lower than 0.05, despite the fact that the chlorophyll released was very limited, implying a different structure of the cell wall or the presence of a further component not present in the cell wall of *C. vulgaris*.

According to [107] , the A561L^{d4} enzyme was tested on *C. sorokiniana* but had no effect. It was shown in this research that there is an effect, albeit reduced, on both chlorophyll release and growth inhibition. Assays using inactivated enzymes were carried out as negative controls (Figure 5.8).

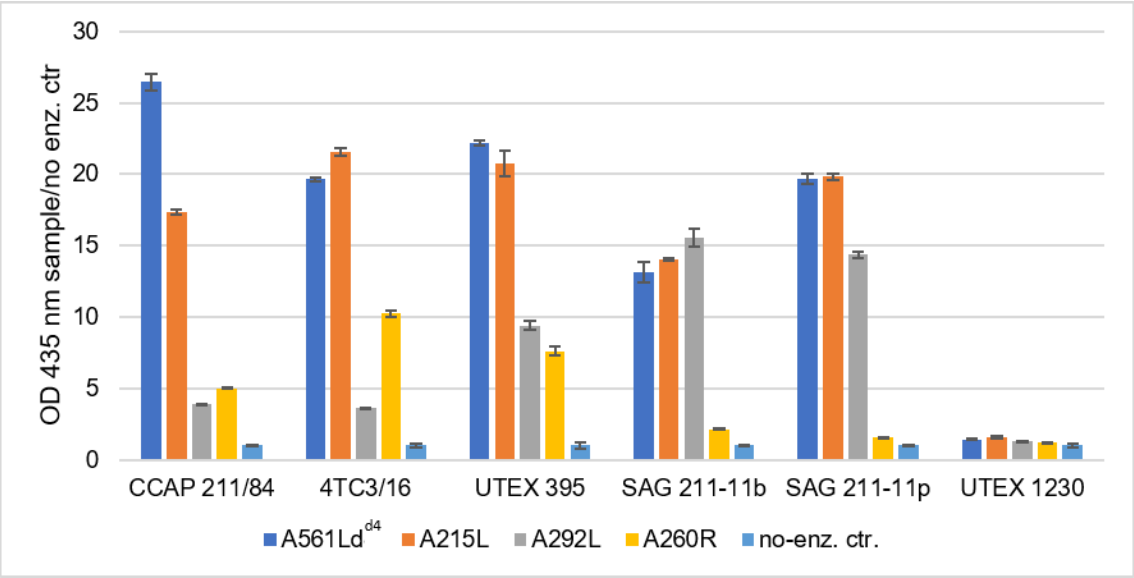

Figure 5.7. Histogram of chlorophyll released after cell wall digestion and lysis with SDS, normalised by the no-enzyme control with SDS.

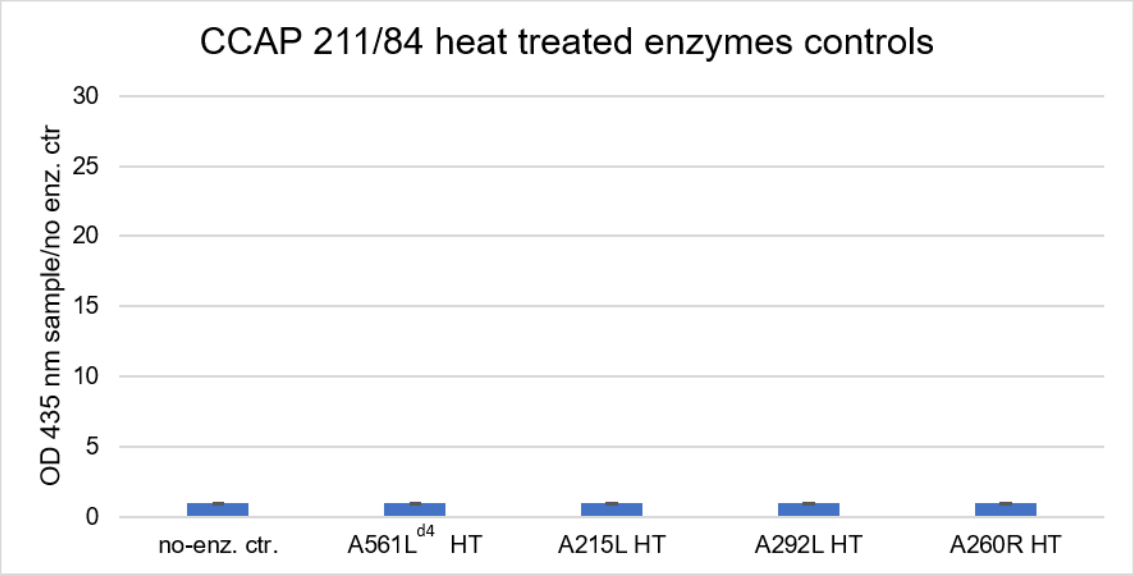

Figure 5.8. Histogram of chlorophyll released after cell wall digestion with heat treated (HT) enzymes and lysis with SDS, normalised by the no-enzyme control.

5.3.4 Evaluation of enzyme mixes on cell lysis

Isolated investigation of single expressed enzymes is useful to understand the respective activities alone, but it is highly likely that the viral genome directs

production of all or combinations of these proteins at any given time within the life cycle. For that reason, the relative effects of enzyme mixes were investigated.

CCAP 211/84 *C. variabilis* and 4TC3/16 *C. vulgaris* were used in this experiment. The combination of all four enzymes was tested on C. *sorokiniana*, but the results were no different from the single enzymes alone, confirming the strain cell wall's resistance to release chlorophylls.

In Figure 5.9 the results were normalised based on the 100 percent chlorophyll released achieved when all four enzymes were combined. Following digestion and lysis in SDS, no chlorophyll remained in the pellet after centrifugation under this condition as shown in Figure 5.10. A similar result to the combination of all 4 enzymes was obtained by combining only two enzymes: alginate lyase (A561L^{d4} or A215L) with either chitinase (A260R) or chitosanase (A292L) or both. A maximum chlorophyll release of 40% is achieved with a single enzyme.

The combination of the two alginate lyases did not increase the OD value of the chlorophylls released, indicating that both enzymes digest the same substrate.

The combination of A292L and A260R showed a higher value when compared to single enzyme digestions, indicating a synergistic effect likely due to the availability of more cell wall substrates, confirming that the two enzymes digest different substrates but not enough for complete lysis, most likely because chitin and chitosan are part of the same cell wall layer.

This study suggests that the cell walls of both *Chlorella variabilis* and *Chlorella vulgaris* have at least three components within their respective macro-molecular

architectures: one made of chitin, one composed of chitosan, and one made of alginate, although chitin and chitosan could be part of the same cell wall layer.

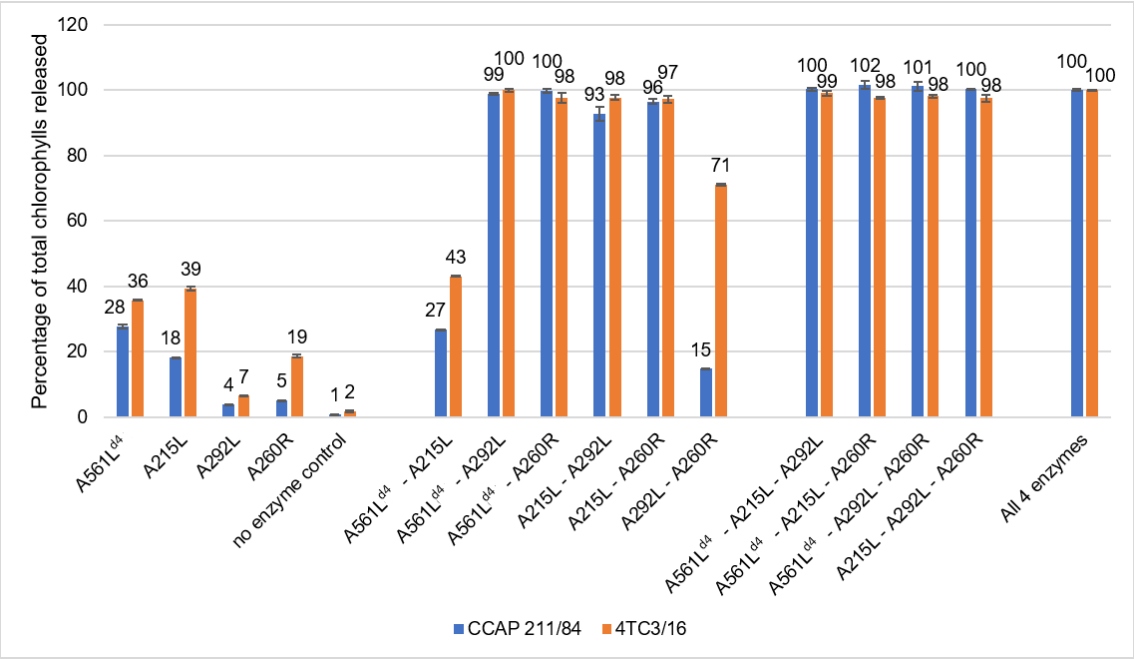

Figure 5.9. Histogram of chlorophyll released after cell wall digestion with a combination of the enzymes followed by lysis with SDS, normalised by the 100% lysis observed when cells were treated by a combination of all four enzymes. Single enzymes and combinations of enzymes are indicated.

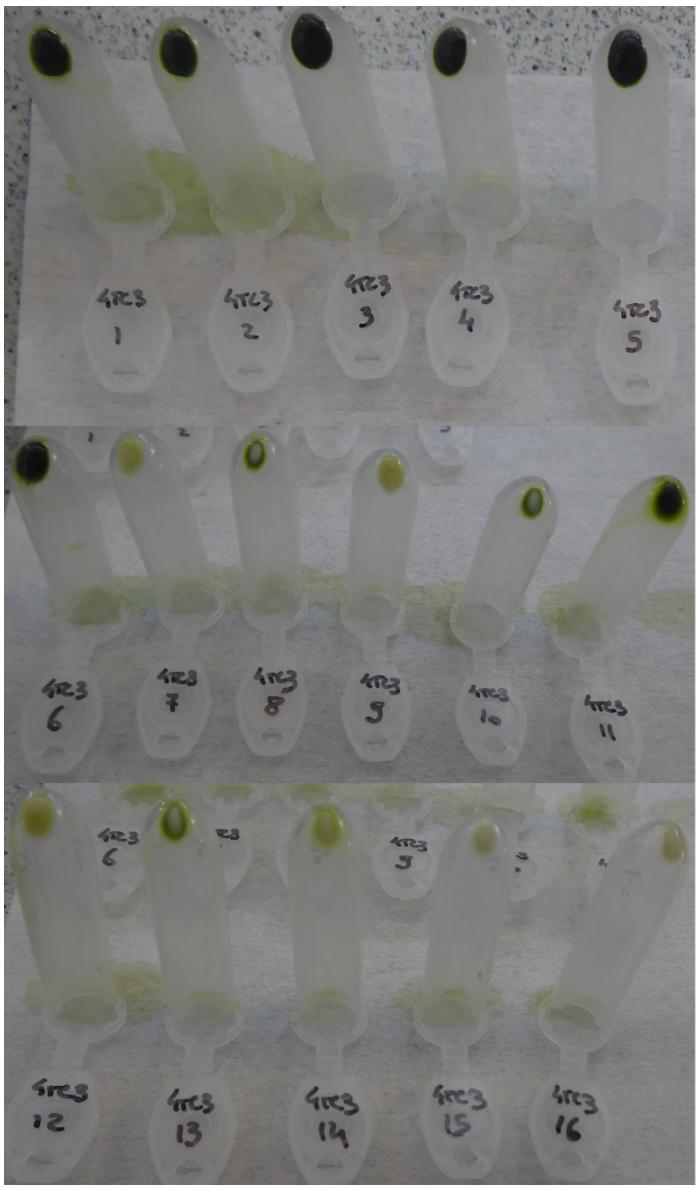

Figure 5.10. Pellets of cell debris of the 4TC3/16 samples digested with the combinations of the enzymes. On the right there is a list of the enzymes used for each sample related to the number of the sample.

5.4 Discussion

The cell wall composition and macro-molecular architecture of *Chlorella vulgaris* cell walls are still not fully determined [213].

In regards to the enzymatic degradation of microalgal cell walls, enzymes used in this manner are generally those that are commercially available and able to

degrade substrates similar to the ones that were theorised to be in *Chlorella vulgaris*, but probably due to the difference in the structure of the substrates, these enzymes have a limited observed effect (Figure 5.2).

Viruses infecting *Chlorella vulgaris* strains have yet to be found. *Chlorella vulgaris* is closely related to *Chlorella variabilis*, a species that gets infected by a large family of viruses called Chloroviruses. These viruses produce enzymes capable of degrading cell wall components as part of their life cycle including entrance into host cells and exit of newly assembled viruses from infected host cells.

Although infection of *Chlorella vulgaris* by these viruses is not possible due to the specificity of the spike protein of the virus in recognising a particular microalgae species (specific activity), the cell wall degrading enzymes produced by these viruses do have a reported effect on the cell wall of *Chlorella vulgaris* and other related species (non-specific activity) [208].

The enzymes' activities were evaluated on four distinct strains of *Chlorella vulgaris*, with diverse findings indicating heterogeneity across strains of the same species in terms of the relative proportions and compositions of the key, respective, cell wall components studied.

It has been reported that the A561L^{d4} enzyme has no observable effect on *Chlorella sorokiniana* [107]. Although there was very little but statistically significant chlorophyll released by all four enzymes tested, indicating a completely distinct cell wall composition in this species or a further encapsulation layer [214], growth suppression was seen when enzymes with alginate lyase activity were evaluated.

When combinations of the enzymes were tested, results confirmed that A561L^{d4} and A215L enzymes were acting upon the same substrate, reported in literature to be alginate [107,208] (a compound not fully characterised) although with different relative effectiveness depending on the strain that was tested.

When all three enzymes, digesting alginate, chitin (A260R enzyme), and chitosan (A292L enzyme), respectively, were combined, complete lysis was obtained for both *C. variabilis* and *C. vulgaris*. Future research should investigate the sugar content of the pellet after full lysis, which could be the starch component of the cells and the relative impact of enzyme treatments on the macro-molecular organisation of the cell walls for all three *Chlorella* species.

These enzymes have been previously identified and tested for activity [190,206–208,215], but no one has, to date, employed a combination of them for use in cell wall disruption.

Complete cell lysis following cell wall digestion has not been previously reported [127,202–204], even when combined with physical disruption. The results obtained through these studies potentially open up opportunities for applications including use of enzyme cocktails within a biorefinery cascade for release or isolation of higher value intracellular fractions of interest from *Chlorella*, though further improvements would be required to devise an approach that would be applicable and accessible for larger-scale applications due to the high cost of enzyme production and purification. Physically immobilised – fixed – enzymes could potentially be used.

5.5 Conclusions

A crude preparation of the enzymes from viral lysates was made and evaluated, with the activity compared to commercially available enzymes. The findings indicate that the viral enzymes are very effective, and as a result, they were produced independently in bacterial cells, and their activities were assessed using both growth inhibition and chlorophyll release assays.

When all three enzymes, digesting alginate (A561L^{d4} and A215L), chitin (A260R enzyme), and chitosan (A292L enzyme) were combined, complete lysis was obtained for *Chlorella vulgaris* and *Chlorella variabilis*. Future research should investigate the relative sugar content of the pellet after full lysis, which could be the un-soluble starch component of the cells. Furthermore, cell wall architectures as observable by transmission electron microscopy after treatment with single enzymes and selected combinations of enzymes would be fascinating to explore not just for *Chlorella vulgaris* but also for the related species, *Chlorella sorokiniana*.

General discussion

The general focus of the PhD thesis was on the production of HA from microalgae, with some insights on the cell wall degradation enzymes produced by Chloroviruses. The purpose of the study was initially to develop and build evidence in support of an economically and technically feasible scalable process for the production of hyaluronan (HA) in microalgae as a natural, non-GM, non-pathogenic, high molecular weight platform. According to the literature, there were two promising untapped platforms for the generation of HA in microalgae [118,133]. Initially, the study focused on a microalgae species that was reported to naturally produce HA, or closely related compound under specific stress conditions [133]. As exhaustively described earlier in the thesis the most suitable strain was chosen, growth and stress conditions were determined and extraction and purification protocols were developed for the isolation of the product. The glycosyl composition of the compound extracted from *L. segnis* was determined and N-acetylglucosamine was not detected in the sample, demonstrating the EPS produced was not HA as was previously suggested [133] and is also not a glycosaminoglycan, but rather a different compound with some similar characteristics. Despite this finding, rheological properties of the stressed cells and the isolated compound were tested and yielded relatively high values of viscosity [216]. Antioxidant activity was also assessed. *Lobochlamys segnis* EPS, being a novel compound produced from an organism that does not have any current approvals, would be considered a novel food ingredient if used within that market application. This would require extensive and costly testing, projected to cost between £350,000 and £500,000 before approval. Even for cosmetic and

medical applications, the substance must be examined and certified by the Scientific Committee on Consumer Safety (SCCS) before it may even be considered. For these reasons the further investigation and improvement of the platform was not pursued but the results of the investigation were published as a peer-reviewed manuscript [128].

Once it was determined that the substance generated by *Lobochlamys segnis* was not HA, the remaining option for HA production in microalgae was to evaluate strains following Chloroviral infection. Several papers [118,188,217,218] and a promising patent [219] on the investigation of HA production by infected *Chlorella variabilis* were available. The molecular weight of HA produced by infected *Chlorella* is reported to be 3–6 MDa [68], implying a potentially high market value, but yields were extremely low, possibly due to the low cell density achieved under non-ideal growth conditions and media [118,220]. It was hypothesised that by achieving high cell densities, the HA yield could become comparable to that of already established bacterial platforms [86]. During the course of the research, it became apparent that there were not adequately sensitive tools available to analyse *Chlorella*/virus interactions for industrial usage. As a result, Algem lab scale photobioreactor protocols were created to allow this work to be completed [158].

Four microalgae strains that could be infected by viruses producing HA were identified [190] and their growth was studied, with *Chlorella variabilis* CCAP 211/84 achieving the highest culture densities in both mixotroph and heterotrophic settings. Growth conditions and media were optimised for mixotrophic and heterotrophic growth under laboratory conditions, yielding (4.4 ±

0.1) g*L^{-1} DM in TAP+v with acetic acid feeding and (33.4 ± 1.6) g*L^{-1} DM in fermentation medium with glucose feeding, both of which far exceed those reported in the literature [220]. Six distinct virus isolates infecting the chosen microalgae strain and for which the genome was available [101] were evaluated, and their lysis times post-infection and amount of virus particles released per infected cell were found to be considerably diverse. Fresh insights into the biology of microalgal viruses and their potential environmental impacts were garnered as a result of this novel analytical technique [158]. The viral isolates were also examined in terms of the expression of the genes involved in HA production, with all isolates exhibiting prolonged gene expression when compared to the model virus PBCV-1. Flow cytometry studies of HA production revealed a probable greater production capacity in *Chlorella* cells infected by the MA-1D virus, albeit the result was not statistically significant. Despite best efforts, the HA production was still estimated to be substantially lower than the existing HA production platforms [90] and considered not to be sufficient for a possible commercial application at least under conditions assessed. Finding approaches to improve infection and viral propagation through dense *Chlorella* cultures would be potentially an unlock that could substantially improve the end-result and product yield.

Biomass downstream processing improvement is essential for biomolecular production in *Chlorella* strains with the energy needed for efficient cell lysis or disruption being a major obstacle for driving the cost down for lower value applications such as biofuel production [10]. Learning more about the Chloroviruses, it was fascinating to find enzymes produced by the viruses that could have a cell wall degradation activity. Cells digested with the enzyme

preparation from PBCV-1 virus released almost 8 times more chlorophylls compared to the enzyme combination reported in literature [204]. Expression of the genes in bacteria and verification of the activity of the single enzymes was achieved. The chlorophyll released was quantified for the combinations of enzymes on several microalgae strains. Subsequently, successful complete cell lysis was achieved without the implementation of mechanical disruption, a result that has never been reported in the literature before.

Conclusions

The hypothesis explored in this project about the feasibility of a microalgal platform to produce HA was validated, as shown in chapter 4. Unfortunately, it can't be exploited industrially yet, because of the lower yields and higher costs compared to bacterial platforms already established.

Bibliography

1. Https://Www.Unilever.Co.Uk/Sustainable-Living/ (Accessed on the 13th of November 2020).
2. Https://Www.Loreal.Com/Loreal-Sharing-Beauty-with-All.
3. Rösch, C.; Roßmann, M.; Weickert, S. Microalgae for Integrated Food and Fuel Production. *GCB Bioenergy* **2019**, *11*, 326–334, doi:10.1111/gcbb.12579.
4. Gifuni, I.; Pollio, A.; Safi, C.; Marzocchella, A.; Olivieri, G. Current Bottlenecks and Challenges of the Microalgal Biorefinery. *Trends in Biotechnology* **2019**, *37*, 242–252, doi:10.1016/j.tibtech.2018.09.006.
5. Schiano di Visconte, G.; Spicer, A.; Chuck, C.J.; Allen, M.J. The Microalgae Biorefinery: A Perspective on the Current Status and Future Opportunities Using Genetic Modification. *Applied Sciences* **2019**, *9*, 4793, doi:10.3390/app9224793.
6. Khan, M.I.; Shin, J.H.; Kim, J.D. The Promising Future of Microalgae: Current Status, Challenges, and Optimization of a Sustainable and Renewable Industry for Biofuels, Feed, and Other Products. *Microbial Cell Factories* **2018**, *17*, 36, doi:10.1186/s12934-018-0879-x.
7. Https://Www.Macrotrends.Net/1369/Crude-Oil-Price-History-Chart.

8. Https://Www.Greentechmedia.Com/Articles/Read/Lessons-from-the-Great-Algae-Biofuel-Bubble#gs.45l3sf.
9. Raikova, S.; Smith-Baedorf, H.; Bransgrove, R.; Barlow, O.; Santomauro, F.; Wagner, J.L.; Allen, M.J.; Bryan, C.G.; Sapsford, D.; Chuck, C.J. Assessing Hydrothermal Liquefaction for the Production of Bio-Oil and Enhanced Metal Recovery from Microalgae Cultivated on Acid Mine Drainage. *Fuel Processing Technology* **2016**, *142*, 219–227, doi:10.1016/j.fuproc.2015.10.017.
10. D'Adamo, S.; Kormelink, R.; Martens, D.; Barbosa, M.J.; Wijffels, R.H. Prospects for Viruses Infecting Eukaryotic Microalgae in Biotechnology. *Biotechnology Advances* **2022**, *54*, 107790, doi:10.1016/j.biotechadv.2021.107790.
11. Kumar, V.; Jain, S. Plants and Algae Species: Promising Renewable Energy Production Source. *Emir. J. Food Agric* **2014**, *26*, 679, doi:10.9755/ejfa.v26i8.18364.
12. de Vree, J.H.; Bosma, R.; Janssen, M.; Barbosa, M.J.; Wijffels, R.H. Comparison of Four Outdoor Pilot-Scale Photobioreactors. *Biotechnol Biofuels* **2015**, *8*, 215, doi:10.1186/s13068-015-0400-2.
13. Doucha, J.; Lívanský, K. Productivity, CO2/O2 Exchange and Hydraulics in Outdoor Open High Density Microalgal (Chlorella Sp.) Photobioreactors Operated in a Middle and Southern European Climate. *J Appl Phycol* **2006**, *18*, 811–826, doi:10.1007/s10811-006-9100-4.
14. Masojídek, J.; Torzillo, G. Mass Cultivation of Freshwater Microalgae. In *Encyclopedia of Ecology*; Jørgensen, S.E., Fath, B.D., Eds.; Academic Press: Oxford, 2008; pp. 2226–2235 ISBN 978-0-08-045405-4.
15. Gifuni, I.; Pollio, A.; Marzocchella, A.; Olivieri, G. New Ultra-Flat Photobioreactor for Intensive Microalgal Production: The Effect of Light Irradiance. *Algal Research* **2018**, *34*, 134–142, doi:10.1016/j.algal.2018.07.014.
16. Janoska, A.; Lamers, P.P.; Hamhuis, A.; van Eimeren, Y.; Wijffels, R.H.; Janssen, M. A Liquid Foam-Bed Photobioreactor for Microalgae Production. *Chemical Engineering Journal* **2017**, *313*, 1206–1214, doi:10.1016/j.cej.2016.11.022.
17. Https://Www.Variconaqua.Com/Products-Services/Phyco-Flow/ (Accessed on 20th June 2022).
18. Lindblad, P.; Fuente, D.; Borbe, F.; Cicchi, B.; Conejero, J.A.; Couto, N.; Čelešnik, H.; Diano, M.M.; Dolinar, M.; Esposito, S.; et al. CyanoFactory, a European Consortium to Develop Technologies Needed to Advance Cyanobacteria as Chassis for Production of Chemicals and Fuels. *Algal Research* **2019**, *41*, 101510, doi:10.1016/j.algal.2019.101510.
19. Jareonsin, S.; Pumas, C. Advantages of Heterotrophic Microalgae as a Host for Phytochemicals Production. *Front Bioeng Biotechnol* **2021**, *9*, 628597, doi:10.3389/fbioe.2021.628597.
20. Klamczynska, B.; Mooney, W.D. Chapter 20 - Heterotrophic Microalgae: A Scalable and Sustainable Protein Source. In *Sustainable Protein Sources*; Nadathur, S.R., Wanasundara, J.P.D., Scanlin, L., Eds.; Academic Press: San Diego, 2017; pp. 327–339 ISBN 978-0-12-802778-3.

21. Spain, O.; Funk, C. Detailed Characterization of the Cell Wall Structure and Composition of Nordic Green Microalgae. *J Agric Food Chem* **2022**, *70*, 9711–9721, doi:10.1021/acs.jafc.2c02783.
22. Michel, G.; Tonon, T.; Scornet, D.; Cock, J.M.; Kloareg, B. Central and Storage Carbon Metabolism of the Brown Alga Ectocarpus Siliculosus: Insights into the Origin and Evolution of Storage Carbohydrates in Eukaryotes. *New Phytologist* **2010**, *188*, 67–81, doi:10.1111/j.1469-8137.2010.03345.x.
23. Evolution and Function of the Plant Cell Wall Synthesis-Related Glycosyltransferase Family 8 | Plant Physiology | Oxford Academic Available online: https://academic.oup.com/plphys/article/153/4/1729/6111315 (accessed on 13 December 2022).
24. Saran, S.; Babu, V.; Chaubey, A. *A Handbook on High Value Fermentation Products, Volume 2: Human Welfare*; John Wiley & Sons, 2019; ISBN 978-1-119-55550-6.
25. de Jesus Raposo, M.; de Morais, A.; de Morais, R. Marine Polysaccharides from Algae with Potential Biomedical Applications. *Marine Drugs* **2015**, *13*, 2967–3028, doi:10.3390/md13052967.
26. What Is the Demand for Natural Ingredients for Cosmetics on the European Market? | CBI (Accessed the 13th of December 2022) Available online: https://www.cbi.eu/market-information/natural-ingredients-cosmetics/what-demand (accessed on 13 December 2022).
27. Moldes, A.; Vecino, X.; Rodríguez-López, L.; Rincón-Fontán, M.; Cruz, J.M. Chapter 8 - Biosurfactants: The Use of Biomolecules in Cosmetics and Detergents. In *New and Future Developments in Microbial Biotechnology and Bioengineering*; Rodrigues, A.G., Ed.; Elsevier, 2020; pp. 163–185 ISBN 978-0-444-64301-8.
28. hrom, zoe The Environmental Cost Of Synthetics (Accessed the 13th of December 2022). *Trail Runner Magazine* 2021.
29. Fashion's Impact On The World's Oceans (Accessed the 13th of December 2022) Available online: http://www.commonobjective.co/article/microfibres-what-to-know-and-do-beatplasticpollution (accessed on 13 December 2022).
30. Gubitosa, J.; Rizzi, V.; Fini, P.; Cosma, P. Hair Care Cosmetics: From Traditional Shampoo to Solid Clay and Herbal Shampoo, A Review. *Cosmetics* **2019**, *6*, 13, doi:10.3390/cosmetics6010013.
31. McIntosh, K.; Smith, A.; Young, L.K.; Leitch, M.A.; Tiwari, A.K.; Reddy, C.M.; O'Neil, G.W.; Liberatore, M.W.; Chandler, M.; Baki, G. Alkenones as a Promising Green Alternative for Waxes in Cosmetics and Personal Care Products. *Cosmetics* **2018**, *5*, 34, doi:10.3390/cosmetics5020034.
32. Pereira, L. Seaweeds as Source of Bioactive Substances and Skin Care Therapy—Cosmeceuticals, Algotheraphy, and Thalassotherapy. *Cosmetics* **2018**, *5*, 68, doi:10.3390/cosmetics5040068.
33. Weissmann, B.; Meyer, K. The Structure of Hyaluronic Acid and of Hyaluronic Acid from Umbilical Cord. *J. Am. Chem. Soc.* **1954**, *76*, 1753–1757, doi:10.1021/ja01636a010.
34. Http://Www.Medecine-Esthetique.Net/En/the-Secrets-of-Hyaluronic-Acid/ (Accessed on the 20th of June 2022).

35. Comstock, L.E.; Kasper, D.L. Bacterial Glycans: Key Mediators of Diverse Host Immune Responses. *Cell* **2006**, *126*, 847–850, doi:10.1016/j.cell.2006.08.021.
36. Https://Www.Grandviewresearch.Com/Press-Release/Global-Hyaluronic-Acid-Market (Accessed on 21st April 2020).
37. Meyer, K.; Palmer, J.W. The Polysaccharide of the Vitreous Humor. *J. Biol. Chem.* **1934**, *107*, 629–634.
38. Mo, Y.; Nishinari, K. Rheology of Hyaluronan Solutions under Extensional Flow. *Biorheology* **2001**, *38*, 379–387.
39. Dougados, M. Sodium Hyaluronate Therapy in Osteoarthritis: Arguments for a Potential Beneficial Structural Effect. *Seminars in Arthritis and Rheumatism* **2000**, *30*, 19–25, doi:10.1053/sarh.2000.0246.
40. Seluanov, A.; Gladyshev, V.N.; Vijg, J.; Gorbunova, V. Mechanisms of Cancer Resistance in Long-Lived Mammals. *Nat Rev Cancer* **2018**, *18*, 433–441, doi:10.1038/s41568-018-0004-9.
41. Moseley, R.; Leaver, M.; Walker, M.; Waddington, R.J.; Parsons, D.; Chen, W.Y.J.; Embery, G. Comparison of the Antioxidant Properties of HYAFF®-11p75, AQUACEL® and Hyaluronan towards Reactive Oxygen Species in Vitro. *Biomaterials* **2002**, *23*, 2255–2264, doi:10.1016/S0142-9612(01)00360-X.
42. Camenisch, T.D.; Spicer, A.P.; Brehm-Gibson, T.; Biesterfeldt, J.; Augustine, M.L.; Calabro, A.; Kubalak, S.; Klewer, S.E.; McDonald, J.A. Disruption of Hyaluronan Synthase-2 Abrogates Normal Cardiac Morphogenesis and Hyaluronan-Mediated Transformation of Epithelium to Mesenchyme. *J. Clin. Invest.* **2000**, *106*, 349–360, doi:10.1172/JCI10272.
43. Girish, K.S.; Kemparaju, K. The Magic Glue Hyaluronan and Its Eraser Hyaluronidase: A Biological Overview. *Life Sciences* **2007**, *80*, 1921–1943, doi:10.1016/j.lfs.2007.02.037.
44. Tian, X.; Azpurua, J.; Hine, C.; Vaidya, A.; Myakishev, M.; Ablaeva, J.; Mao, Z.; Nevo, E.; Gorbunova, V. High Molecular Weight Hyaluronan Mediates the Cancer Resistance of the Naked Mole-Rat. **2014**, 16.
45. Toole, B.P. Hyaluronan: From Extracellular Glue to Pericellular Cue. *Nat Rev Cancer* **2004**, *4*, 528–539, doi:10.1038/nrc1391.
46. Ramsden, C.A.; Bankier, A.; Brown, T.J.; Cowen, P.S.J.; Frost, G.I.; McCallum, D.D.; Studdert, V.P.; Fraser, J.R.E. A New Disorder of Hyaluronan Metabolism Associated with Generalized Folding and Thickening of the Skin. *THE JOURNAL OF PEDIATRICS* **2000**, *136*, 7.
47. Olsson, M.; Meadows, J.R.S.; Truvé, K.; Rosengren Pielberg, G.; Puppo, F.; Mauceli, E.; Quilez, J.; Tonomura, N.; Zanna, G.; Docampo, M.J.; et al. A Novel Unstable Duplication Upstream of HAS2 Predisposes to a Breed-Defining Skin Phenotype and a Periodic Fever Syndrome in Chinese Shar-Pei Dogs. *PLoS Genet* **2011**, *7*, e1001332, doi:10.1371/journal.pgen.1001332.
48. DeAngelis, P.L. Hyaluronan Synthases: Fascinating Glycosyltransferases from Vertebrates, Bacterial Pathogens, and Algal Viruses. *Cellular and Molecular Life Sciences (CMLS)* **1999**, *56*, 670–682, doi:10.1007/s000180050461.
49. Blackburn, M.R.; Hubbard, C.; Kiessling, V.; Bi, Y.; Kloss, B.; Tamm, L.K.; Zimmer, J. Distinct Reaction Mechanisms for Hyaluronan Biosynthesis in

Different Kingdoms of Life. *Glycobiology* **2018**, *28*, 108–121, doi:10.1093/glycob/cwx096.
50. Weigel, P.H. Hyaluronan Synthase: The Mechanism of Initiation at the Reducing End and a Pendulum Model for Polysaccharide Translocation to the Cell Exterior. *International Journal of Cell Biology* **2015**, *2015*, 1–15, doi:10.1155/2015/367579.
51. Weigel, P.H.; DeAngelis, P.L. Hyaluronan Synthases: A Decade-plus of Novel Glycosyltransferases. *J. Biol. Chem.* **2007**, *282*, 36777–36781, doi:10.1074/jbc.R700036200.
52. Agarwal, G.; K. V., K.; Prasad, S.B.; Bhaduri, A.; Jayaraman, G. Biosynthesis of Hyaluronic Acid Polymer: Dissecting the Role of Sub Structural Elements of Hyaluronan Synthase. *Sci Rep* **2019**, *9*, 12510, doi:10.1038/s41598-019-48878-8.
53. Weigel, P.H. Functional Characteristics and Catalytic Mechanisms of the Bacterial Hyaluronan Synthases. *IUBMB Life* **2002**, *54*, 201–211, doi:10.1080/15216540214931.
54. Kooy, F.K.; Beeftink, H.H.; Eppink, M.H.M.; Tramper, J.; Eggink, G.; Boeriu, C.G. Structural and Functional Evidence for Two Separate Oligosaccharide Binding Sites of Pasteurella Multocida Hyaluronan Synthase. *AER* **2013**, *01*, 97–111, doi:10.4236/aer.2013.14011.
55. DeAngelis, P.L.; Jing, W.; Drake, R.R.; Achyuthan, A.M. Identification and Molecular Cloning of a Unique Hyaluronan Synthase from *Pasteurella Multocida*. *J. Biol. Chem.* **1998**, *273*, 8454–8458, doi:10.1074/jbc.273.14.8454.
56. Kooy, F.K.; Beeftink, H.H.; Eppink, M.H.M.; Tramper, J.; Eggink, G.; Boeriu, C.G. Kinetic and Structural Analysis of Two Transferase Domains in Pasteurella Multocida Hyaluronan Synthase. *Journal of Molecular Catalysis B: Enzymatic* **2014**, *102*, 138–145, doi:10.1016/j.molcatb.2014.02.006.
57. Mandawe, J.; Infanzon, B.; Eisele, A.; Zaun, H.; Kuballa, J.; Davari, M.D.; Jakob, F.; Elling, L.; Schwaneberg, U. Directed Evolution of Hyaluronic Acid Synthase from *Pasteurella Multocida* towards High-Molecular-Weight Hyaluronic Acid. *ChemBioChem* **2018**, *19*, 1414–1423, doi:10.1002/cbic.201800093.
58. Cantarel, B.L.; Coutinho, P.M.; Rancurel, C.; Bernard, T.; Lombard, V.; Henrissat, B. The Carbohydrate-Active EnZymes Database (CAZy): An Expert Resource for Glycogenomics. *Nucleic Acids Research* **2009**, *37*, D233–D238, doi:10.1093/nar/gkn663.
59. Bart, G.; Vico, N.O.; Hassinen, A.; Pujol, F.M.; Deen, A.J.; Ruusala, A.; Tammi, R.H.; Squire, A.; Heldin, P.; Kellokumpu, S.; et al. Fluorescence Resonance Energy Transfer (FRET) and Proximity Ligation Assays Reveal Functionally Relevant Homo- and Heteromeric Complexes among Hyaluronan Synthases HAS1, HAS2, and HAS3. *J. Biol. Chem.* **2015**, *290*, 11479–11490, doi:10.1074/jbc.M115.640581.
60. Karousou, E.; Kamiryo, M.; Skandalis, S.S.; Ruusala, A.; Asteriou, T.; Passi, A.; Yamashita, H.; Hellman, U.; Heldin, C.-H.; Heldin, P. The Activity of Hyaluronan Synthase 2 Is Regulated by Dimerization and Ubiquitination. *J. Biol. Chem.* **2010**, *285*, 23647–23654, doi:10.1074/jbc.M110.127050.

61. Tien, J.Y.L.; Spicer, A.P. Three Vertebrate Hyaluronan Synthases Are Expressed during Mouse Development in Distinct Spatial and Temporal Patterns. *Dev. Dyn.* **2005**, *233*, 130–141, doi:10.1002/dvdy.20328.
62. Pummill, P.E.; Achyuthan, A.M.; DeAngelis, P.L. Enzymological Characterization of Recombinant *Xenopus* DG42, A Vertebrate Hyaluronan Synthase. *J. Biol. Chem.* **1998**, *273*, 4976–4981, doi:10.1074/jbc.273.9.4976.
63. Spicer, A.P.; Olson, J.S.; McDonald, J.A. Molecular Cloning and Characterization of a CDNA Encoding the Third Putative Mammalian Hyaluronan Synthase. *J. Biol. Chem.* **1997**, *272*, 8957–8961, doi:10.1074/jbc.272.14.8957.
64. Spicer, A.P.; McDonald, J.A. Characterization and Molecular Evolution of a Vertebrate Hyaluronan Synthase Gene Family. *J. Biol. Chem.* **1998**, *273*, 1923–1932, doi:10.1074/jbc.273.4.1923.
65. Itano, N.; Chanmee, T.; Kimata, K. Hyaluronan Synthase 1-3 (HAS1-3). In *Handbook of Glycosyltransferases and Related Genes*; Taniguchi, N., Honke, K., Fukuda, M., Narimatsu, H., Yamaguchi, Y., Angata, T., Eds.; Springer Japan: Tokyo, 2014; pp. 865–872 ISBN 978-4-431-54240-7.
66. Armstrong, D.C.; Johns, M.R. Culture Conditions Affect the Molecular Weight Properties of Hyaluronic Acid Produced by Streptococcus Zooepidemicus. *APPL. ENVIRON. MICROBIOL.* **1997**, *63*, 6.
67. Yang, L.; Zhang, X.; Tan, W.-S. Effect of Oxygen and Shear Stress on Molecular Weight of Hyaluronic Acid Produced by Streptococcus Zooepidemicus. 7.
68. DeAngelis, P.L.; Jing, W.; Graves, M.V.; Burbank, D.E.; Van Etten, J.L. Hyaluronan Synthase of Chlorella Virus PBCV-1. *Science* **1997**, *278*, 1800–1803, doi:10.1126/science.278.5344.1800.
69. Kojima, T.; Nagata, T.; Kudo, H.; Müller-Lierheim, W.G.K.; van Setten, G.-B.; Dogru, M.; Tsubota, K. The Effects of High Molecular Weight Hyaluronic Acid Eye Drop Application in Environmental Dry Eye Stress Model Mice. *Int J Mol Sci* **2020**, *21*, 3516, doi:10.3390/ijms21103516.
70. Salzillo, R.; Schiraldi, C.; Corsuto, L.; D'Agostino, A.; Filosa, R.; De Rosa, M.; La Gatta, A. Optimization of Hyaluronan-Based Eye Drop Formulations. *Carbohydrate Polymers* **2016**, *153*, 275–283, doi:10.1016/j.carbpol.2016.07.106.
71. Effects of Viscous Hyaluronate–Sodium Solutions on the Nasal Absorption of Vasopressin and An Analogue Available online: https://link.springer.com/article/10.1023/A:1015894910416 (accessed on 9 October 2019).
72. Pavicic, T.; Gauglitz, G.G.; Lersch, P.; Schwach-Abdellaoui, K.; Malle, B.; Korting, H.C.; Farwick, M. Efficacy of Cream-Based Novel Formulations of Hyaluronic Acid of Different Molecular Weights in Anti-Wrinkle Treatment. *J Drugs Dermatol* **2011**, *10*, 990–1000.
73. Price, R.D.; Myers, S.; Leigh, I.M.; Navsaria, H.A. The Role of Hyaluronic Acid in Wound Healing: Assessment of Clinical Evidence. *American Journal of Clinical Dermatology* **2005**, *6*, 393–402, doi:10.2165/00128071-200506060-00006.
74. Gariboldi, S.; Palazzo, M.; Zanobbio, L.; Selleri, S.; Sommariva, M.; Sfondrini, L.; Cavicchini, S.; Balsari, A.; Rumio, C. Low Molecular Weight

Hyaluronic Acid Increases the Self-Defense of Skin Epithelium by Induction of β-Defensin 2 via TLR2 and TLR4. *J Immunol* **2008**, *181*, 2103–2110, doi:10.4049/jimmunol.181.3.2103.
75. Kim, J.H.; Moon, M.J.; Kim, D.Y.; Heo, S.H.; Jeong, Y.Y. Hyaluronic Acid-Based Nanomaterials for Cancer Therapy. *Polymers* **2018**, *10*, 1133, doi:10.3390/polym10101133.
76. Mattheolabakis, G.; Milane, L.; Singh, A.; Amiji, M.M. Hyaluronic Acid Targeting of CD44 for Cancer Therapy: From Receptor Biology to Nanomedicine. *Journal of Drug Targeting* **2015**, *23*, 605–618, doi:10.3109/1061186X.2015.1052072.
77. Fallacara, A.; Baldini, E.; Manfredini, S.; Vertuani, S. Hyaluronic Acid in the 3rd Millennium. **2018**, doi:10.20944/preprints201805.0426.v1.
78. Bowman, S.; Awad, M.E.; Hamrick, M.W.; Hunter, M.; Fulzele, S. Recent Advances in Hyaluronic Acid Based Therapy for Osteoarthritis. *Clin Trans Med* **2018**, *7*, 6, doi:10.1186/s40169-017-0180-3.
79. Kawada, C.; Yoshida, T.; Yoshida, H.; Matsuoka, R.; Sakamoto, W.; Odanaka, W.; Sato, T.; Yamasaki, T.; Kanemitsu, T.; Masuda, Y.; et al. Ingested Hyaluronan Moisturizes Dry Skin. *Nutr J* **2014**, *13*, 70, doi:10.1186/1475-2891-13-70.
80. Sato, T.; Sakamoto, W.; Odanaka, W.; Yoshida, K.; Urushibata, O. Clinical Effects of Dietary Hyaluronic Acid on Dry, Rough Skin. *J. Aesthetic Dermatology* **2002**, *12*, 109–120.
81. Balogh, L.; Polyak, A.; Mathe, D.; Kiraly, R.; Thuroczy, J.; Terez, M.; Janoki, G.; Ting, Y.; Bucci, L.R.; Schauss, A.G. Absorption, Uptake and Tissue Affinity of High-Molecular-Weight Hyaluronan after Oral Administration in Rats and Dogs. *J. Agric. Food Chem.* **2008**, *56*, 10582–10593, doi:10.1021/jf8017029.
82. Kawada, C.; Kimura, M.; Masuda, Y.; Nomura, Y. Oral Administration of Hyaluronan Prevents Skin Dryness and Epidermal Thickening in Ultraviolet Irradiated Hairless Mice. *Journal of Photochemistry and Photobiology B: Biology* **2015**, *153*, 215–221, doi:10.1016/j.jphotobiol.2015.09.020.
83. Göllner, I.; Voss, W.; von Hehn, U.; Kammerer, S. Ingestion of an Oral Hyaluronan Solution Improves Skin Hydration, Wrinkle Reduction, Elasticity, and Skin Roughness: Results of a Clinical Study. *J Evid Based Complementary Altern Med* **2017**, *22*, 816–823, doi:10.1177/2156587217743640.
84. Oe, M.; Tashiro, T.; Yoshida, H.; Nishiyama, H.; Masuda, Y.; Maruyama, K.; Koikeda, T.; Maruya, R.; Fukui, N. Oral Hyaluronan Relieves Knee Pain: A Review. *Nutr J* **2015**, *15*, 11, doi:10.1186/s12937-016-0128-2.
85. Boeriu, C.G.; Springer, J.; Kooy, F.K.; van den Broek, L.A.M.; Eggink, G. Production Methods for Hyaluronan. *International Journal of Carbohydrate Chemistry* **2013**, *2013*, 1–14, doi:10.1155/2013/624967.
86. Shiedlin, A.; Bigelow, R.; Christopher, W.; Arbabi, S.; Yang, L.; Maier, R.V.; Wainwright, N.; Childs, A.; Miller, R.J. Evaluation of Hyaluronan from Different Sources: *Streptococcus Zooepidemicus* , Rooster Comb, Bovine Vitreous, and Human Umbilical Cord. *Biomacromolecules* **2004**, *5*, 2122–2127, doi:10.1021/bm0498427.
87. Rangaswamy, V.; Jain, D. An Efficient Process for Production and Purification of Hyaluronic Acid from Streptococcus Equi Subsp.

Zooepidemicus. *Biotechnol Lett* **2008**, *30*, 493–496, doi:10.1007/s10529-007-9562-8.
88. Yamada, T.; Kawasaki, T. Microbial Synthesis of Hyaluronan and Chitin: New Approaches. *Journal of Bioscience and Bioengineering* **2005**, *99*, 521–528, doi:10.1263/jbb.99.521.
89. Liu, L.; Liu, Y.; Li, J.; Du, G.; Chen, J. Microbial Production of Hyaluronic Acid: Current State, Challenges, and Perspectives. *Microbial Cell Factories* **2011**, *10*, 99, doi:10.1186/1475-2859-10-99.
90. Kaur, M.; Jayaraman, G. Hyaluronan Production and Molecular Weight Is Enhanced in Pathway-Engineered Strains of Lactate Dehydrogenase-Deficient Lactococcus Lactis. *Metabolic Engineering Communications* **2016**, *3*, 15–23, doi:10.1016/j.meteno.2016.01.003.
91. Yu, H.; Stephanopoulos, G. Metabolic Engineering of Escherichia Coli for Biosynthesis of Hyaluronic Acid. *Metabolic Engineering* **2008**, *10*, 24–32, doi:10.1016/j.ymben.2007.09.001.
92. Cheng, F.; Yu, H.; Stephanopoulos, G. Engineering Corynebacterium Glutamicum for High-Titer Biosynthesis of Hyaluronic Acid. *Metabolic Engineering* **2019**, S1096717619302095, doi:10.1016/j.ymben.2019.07.003.
93. Chien, L.-J.; Lee, C.-K. Enhanced Hyaluronic Acid Production in Bacillus Subtilis by Coexpressing Bacterial Hemoglobin. *Biotechnol. Prog.* **2007**, *0*, 0–0, doi:10.1021/bp070036w.
94. Widner, B.; Behr, R.; Von Dollen, S.; Tang, M.; Heu, T.; Sloma, A.; Sternberg, D.; DeAngelis, P.L.; Weigel, P.H.; Brown, S. Hyaluronic Acid Production in Bacillus Subtilis. *Applied and Environmental Microbiology* **2005**, *71*, 3747–3752, doi:10.1128/AEM.71.7.3747-3752.2005.
95. Rani, K.; Sandal, N.; Sahoo, P.K. A Comprehensive Review on Chlorella-Its Composition, Health Benefits, Market and Regulatory Scenario. *The Pharma Innovation Journal* **2018**, *7*, 584–589.
96. Blanc, G.; Duncan, G.; Agarkova, I.; Borodovsky, M.; Gurnon, J.; Kuo, A.; Lindquist, E.; Lucas, S.; Pangilinan, J.; Polle, J.; et al. The *Chlorella Variabilis* NC64A Genome Reveals Adaptation to Photosymbiosis, Coevolution with Viruses, and Cryptic Sex. *The Plant Cell* **2010**, *22*, 2943–2955, doi:10.1105/tpc.110.076406.
97. Ziesenisz, E.; Reisser, W.; Wiessner, W. Evidence of de Novo Synthesis of Maltose Excreted by the Endosymbiotic Chlorella from Paramecium Bursaria. *Planta* **1981**, *153*, 481–485, doi:10.1007/BF00394991.
98. Jeanniard, A.; Dunigan, D.D.; Gurnon, J.R.; Agarkova, I.V.; Kang, M.; Vitek, J.; Duncan, G.; McClung, O.; Larsen, M.; Claverie, J.-M.; et al. Towards Defining the Chloroviruses: A Genomic Journey through a Genus of Large DNA Viruses. *BMC Genomics* **2013**, *14*, 158, doi:10.1186/1471-2164-14-158.
99. Van Etten, J.L.; Dunigan, D.D. Chloroviruses: Not Your Everyday Plant Virus. *Trends Plant Sci* **2012**, *17*, 1–8, doi:10.1016/j.tplants.2011.10.005.
100. Rohozinski, J.; Girton, L.E.; Van Etten, J.L. Chlorella Viruses Contain Linear Nonpermuted Double-Stranded DNA Genomes with Covalently Closed Hairpin Ends. *Virology* **1989**, *168*, 363–369, doi:10.1016/0042-6822(89)90277-8.

101. Van Etten, J.; Agarkova, I.; Dunigan, D.; Tonetti, M.; De Castro, C.; Duncan, G. Chloroviruses Have a Sweet Tooth. *Viruses* **2017**, *9*, 88, doi:10.3390/v9040088.
102. Onimatsu, H.; Sugimoto, I.; Fujie, M.; Usami, S.; Yamada, T. Vp130, a Chloroviral Surface Protein That Interacts with the Host Chlorella Cell Wall. *Virology* **2004**, *319*, 71–80, doi:10.1016/j.virol.2003.10.030.
103. Etten, J.L.V.; Lane, L.C.; Meints, R.H. Viruses and Viruslike Particles of Eukaryotic Algae. *MICROBIOL. REV.* **1991**, *55*, 35.
104. Van Etten, J.L.; Agarkova, I.V.; Dunigan, D.D. Chloroviruses. *Viruses* **2019**, *12*, 20, doi:10.3390/v12010020.
105. Meints, R.H.; Burbank, D.E.; Van Etten, J.L.; Lamport, D.T.A. Properties of the Chlorella Receptor for the Virus PBCV-1. *Virology* **1988**, *164*, 15–21, doi:10.1016/0042-6822(88)90614-9.
106. Dunigan, D.D.; Cerny, R.L.; Bauman, A.T.; Roach, J.C.; Lane, L.C.; Agarkova, I.V.; Wulser, K.; Yanai-Balser, G.M.; Gurnon, J.R.; Vitek, J.C.; et al. Paramecium Bursaria Chlorella Virus 1 Proteome Reveals Novel Architectural and Regulatory Features of a Giant Virus. *J. Virol.* **2012**, *86*, 8821–8834, doi:10.1128/JVI.00907-12.
107. Agarkova, I.V.; Lane, L.C.; Dunigan, D.D.; Quispe, C.F.; Duncan, G.A.; Milrot, E.; Minsky, A.; Esmael, A.; Ghosh, J.S.; Van Etten, J.L. Identification of a Chlorovirus PBCV-1 Protein Involved in Degrading the Host Cell Wall during Virus Infection. *Viruses* **2021**, *13*, 782, doi:10.3390/v13050782.
108. Agarkova, I.; Hertel, B.; Zhang, X.; Lane, L.; Tchourbanov, A.; Dunigan, D.D.; Thiel, G.; Rossmann, M.G.; Van Etten, J.L. Dynamic Attachment of Chlorovirus PBCV-1 to Chlorella Variabilis. *Virology* **2014**, *466–467*, 95–102, doi:10.1016/j.virol.2014.07.002.
109. Milrot, E.; Shimoni, E.; Dadosh, T.; Rechav, K.; Unger, T.; Van Etten, J.L.; Minsky, A. Structural Studies Demonstrating a Bacteriophage-like Replication Cycle of the Eukaryote-Infecting Paramecium Bursaria Chlorella Virus-1. *PLoS Pathog* **2017**, *13*, e1006562, doi:10.1371/journal.ppat.1006562.
110. Meints, R.H.; Lee, K.; Burbank, D.E.; Van Etten, J.L. Infection of a Chlorella-like Alga with the Virus, PBCV-1: Ultrastructural Studies. *Virology* **1984**, *138*, 341–346, doi:10.1016/0042-6822(84)90358-1.
111. Romani, G.; Piotrowski, A.; Hillmer, S.; Gurnon, J.; Van Etten, J.L.; Moroni, A.; Thiel, G.; Hertel, B. A Virus-Encoded Potassium Ion Channel Is a Structural Protein in the Chlorovirus Paramecium Bursaria Chlorella Virus 1 Virion. *J Gen Virol* **2013**, *94*, 2549–2556, doi:10.1099/vir.0.055251-0.
112. Greiner, T.; Frohns, F.; Kang, M.; Van Etten, J.L.; Käsmann, A.; Moroni, A.; Hertel, B.; Thiel, G. 2009 Chlorella Viruses Prevent Multiple Infections by Depolarizing the Host Membrane. *Journal of General Virology 90*, 2033–2039, doi:10.1099/vir.0.010629-0.
113. Thiel, G.; Moroni, A.; Dunigan, D.; Van Etten, J.L. Initial Events Associated with Virus PBCV-1 Infection of Chlorella NC64A. *Prog Bot* **2010**, *71*, 169–183, doi:10.1007/978-3-642-02167-1_7.
114. McCulloh, D.H.; Lynn, J.W.; Chambers, E.L. Membrane Depolarization Facilitates Sperm Entry, Large Fertilization Cone Formation, and Prolonged Current Responses in Sea Urchin Oocytes. *Developmental Biology* **1987**, *124*, 177–190, doi:10.1016/0012-1606(87)90470-2.

115. Structural Insights of the Specificity and Catalysis of a Viral Histone H3 Lysine 27 Methyltransferase | Request PDF Available online: https://www.researchgate.net/publication/7177023_Structural_Insights_of_the_Specificity_and_Catalysis_of_a_Viral_Histone_H3_Lysine_27_Methyltransferase (accessed on 20 January 2022).
116. Mujtaba, S.; Manzur, K.L.; Gurnon, J.R.; Kang, M.; Van Etten, J.L.; Zhou, M.-M. Epigenetic Transcriptional Repression of Cellular Genes by a Viral SET Protein. *Nat Cell Biol* **2008**, *10*, 1114–1122, doi:10.1038/ncb1772.
117. Agarkova, I.V.; Dunigan, D.D.; Van Etten, J.L. Virion-Associated Restriction Endonucleases of Chloroviruses. *J Virol* **2006**, *80*, 8114–8123, doi:10.1128/JVI.00486-06.
118. Graves, M.V.; Burbank, D.E.; Roth, R.; Heuser, J.; DeAngelis, P.L.; Van Etten, J.L. Hyaluronan Synthesis in Virus PBCV-1-Infected Chlorella-like Green Algae. *Virology* **1999**, *257*, 15–23, doi:10.1006/viro.1999.9628.
119. Yanai-Balser, G.M.; Duncan, G.A.; Eudy, J.D.; Wang, D.; Li, X.; Agarkova, I.V.; Dunigan, D.D.; Van Etten, J.L. Microarray Analysis of Paramecium Bursaria Chlorella Virus 1 Transcription. *J Virol* **2010**, *84*, 532–542, doi:10.1128/JVI.01698-09.
120. Markine-Goriaynoff, N.; Gillet, L.; Van Etten, J.L.; Korres, H.; Verma, N.; Vanderplasschen, A. 2004 Glycosyltransferases Encoded by Viruses. *Journal of General Virology 85*, 2741–2754, doi:10.1099/vir.0.80320-0.
121. Landstein, D.; Graves, M.V.; Burbank, D.E.; DeAngelis, P.; Van Etten, J.L. ChlorellaVirus PBCV-1 Encodes Functional Glutamine: Fructose-6-Phosphate Amidotransferase and UDP-Glucose Dehydrogenase Enzymes. *Virology* **1998**, *250*, 388–396, doi:10.1006/viro.1998.9388.
122. Dunigan, D.D.; Al-Sammak, M.; Al-Ameeli, Z.; Agarkova, I.V.; DeLong, J.P.; Van Etten, J.L. Chloroviruses Lure Hosts through Long-Distance Chemical Signaling. *J Virol* **2019**, *93*, e01688-18, /jvi/93/7/JVI.01688-18.atom, doi:10.1128/JVI.01688-18.
123. D'Haeze, W.; Holsters, M. Nod Factor Structures, Responses, and Perception during Initiation of Nodule Development. *Glycobiology* **2002**, *12*, 79R-105R, doi:10.1093/glycob/12.6.79R.
124. Van Etten, J.L.; Burbank, D.E.; Joshi, J.; Meints, R.H. DNA Synthesis in a Chlorella-like Alga Following Infection with the Virus PBCV-1. *Virology* **1984**, *134*, 443–449, doi:10.1016/0042-6822(84)90311-8.
125. Milrot, E.; Mutsafi, Y.; Fridmann-Sirkis, Y.; Shimoni, E.; Rechav, K.; Gurnon, J.R.; Van Etten, J.L.; Minsky, A. Virus-Host Interactions: Insights from the Replication Cycle of the Large *Paramecium Bursaria Chlorella Virus*: Replication Factories of PBCV-1. *Cellular Microbiology* **2016**, *18*, 3–16, doi:10.1111/cmi.12486.
126. Van Etten, J.L.; Burbank, D.E.; Xia, Y.; Meints, R.H. Growth Cycle of a Virus, PBCV-1, That Infects Chlorella-like Algae. *Virology* **1983**, *126*, 117–125, doi:10.1016/0042-6822(83)90466-X.
127. Gerken, H.G.; Donohoe, B.; Knoshaug, E.P. Enzymatic Cell Wall Degradation of Chlorella Vulgaris and Other Microalgae for Biofuels Production. *Planta* **2013**, *237*, 239–253, doi:10.1007/s00425-012-1765-0.
128. Schiano di Visconte, G.; Allen, M.J.; Spicer, A. Novel Capsular Polysaccharide from *Lobochlamys Segnis*. *Polysaccharides* **2021**, *2*, 121–137, doi:10.3390/polysaccharides2010009.

129. Pröschold, T.; Marin, B.; Schlösser, U.G.; Melkonian, M. Molecular Phylogeny and Taxonomic Revision of *Chlamydomonas* (Chlorophyta). I. Emendation of *Chlamydomonas ehrenberg* and *Chloromonas gobi*, and Description of *Oogamochlamys* Gen. Nov. and *Lobochlamys* Gen. Nov. 36.
130. Lang, I.; Hodac, L.; Friedl, T.; Feussner, I. Fatty Acid Profiles and Their Distribution Patterns in Microalgae: A Comprehensive Analysis of More than 2000 Strains from the SAG Culture Collection. *BMC Plant Biol* **2011**, *11*, 124, doi:10.1186/1471-2229-11-124.
131. Allard, B.; Tazi, A. Influence of Growth Status on Composition of Extracellular Polysaccharides from Two *Chlamydomonas* Species. *Phytochemistry* **1992**, *32*, 41–47, doi:10.1016/0031-9422(92)80103-L.
132. Bafana, A. Characterization and Optimization of Production of Exopolysaccharide from *Chlamydomonas Reinhardtii*. *Carbohydrate Polymers* **2013**, *95*, 746–752, doi:10.1016/j.carbpol.2013.02.016.
133. Badour, S.S. Novel Hyaluronic Acid Produced from Algae 1999.
134. Gopalakrishnan, K. Isolation, Characterisation and Screening of New Zealand Alpine Algae for the Production of Secondary Metabolites in Photobioreactors. *PhD thesis* **2015**, *Department of Chemical and Process Engineering, University of Canterbury, Christchurch, New Zealand*, 287.
135. Culture Collection of Algae (SAG) - Georg-August-Universität Göttingen Available online: https://www.uni-goettingen.de/en/culture+collection+of+algae+%28sag%29/184982.html (accessed on 12 January 2021).
136. Gorman, D.S.; Levine, R.P. Cytochrome f and Plastocyanin: Their Sequence in the Photosynthetic Electron Transport Chain of *Chlamydomonas Reinhardtii*. *PNAS* **1965**, *54*, 1665–1669, doi:10.1073/pnas.54.6.1665.
137. Sueoka, N. Mitotic Replication of Deoxyribonucleic Acid in *Chlamydomonas Reinhardtii*. *Proc Natl Acad Sci U S A* **1960**, *46*, 83–91.
138. The Algem PRO and Algem HT24 Photobioreactors | Algenuity Available Online: Https://Www.Algenuity.Com/Algem (Accessed on 27 January 2022).
139. Santander, J.; Martin, T.; Loh, A.; Pohlenz, C.; Gatlin, D.M.; Curtiss, R. Mechanisms of Intrinsic Resistance to Antimicrobial Peptides of *Edwardsiella Ictaluri* and Its Influence on Fish Gut Inflammation and Virulence. *Microbiology* **2013**, *159*, 1471–1486, doi:10.1099/mic.0.066639-0.
140. Merkle, R.K.; Poppe, I. Carbohydrate Composition Analysis of Glycoconjugates by Gas-Liquid Chromatography/Mass Spectrometry. In *Methods in Enzymology*; Guide to Techniques in Glycobiology; Academic Press, 1994; Vol. 230, pp. 1–15.
141. Willis, L.M.; Stupak, J.; Richards, M.R.; Lowary, T.L.; Li, J.; Whitfield, C. Conserved Glycolipid Termini in Capsular Polysaccharides Synthesized by ATP-Binding Cassette Transporter-Dependent Pathways in Gram-Negative Pathogens. *Proceedings of the National Academy of Sciences* **2013**, *110*, 7868–7873, doi:10.1073/pnas.1222317110.
142. Anumula, K.R.; Taylor, P.B. A Comprehensive Procedure for Preparation of Partially Methylated Alditol Acetates from Glycoprotein Carbohydrates. *Analytical Biochemistry* **1992**, *203*, 101–108, doi:10.1016/0003-2697(92)90048-C.

143. Prieto, P.; Pineda, M.; Aguilar, M. Spectrophotometric Quantitation of Antioxidant Capacity through the Formation of a Phosphomolybdenum Complex: Specific Application to the Determination of Vitamin E. *Analytical Biochemistry* **1999**, *269*, 337–341, doi:10.1006/abio.1999.4019.
144. Oyaizu, M. Studies on Products of Browning Reaction. *The Japanese journal of nutrition and dietetics* **1986**, *44*, 307–315.
145. Xu, S.; Xu, X.; Zhang, L. Branching Structure and Chain Conformation of Water-Soluble Glucan Extracted from *Auricularia Auricula-Judae*. *J. Agric. Food Chem.* **2012**, *60*, 3498–3506, doi:10.1021/jf300423z.
146. Wu, D.-T.; Meng, L.-Z.; Wang, L.-Y.; Lv, G.-P.; Cheong, K.-L.; Hu, D.-J.; Guan, J.; Zhao, J.; Li, S.-P. Chain Conformation and Immunomodulatory Activity of a Hyperbranched Polysaccharide from *Cordyceps Sinensis*. *Carbohydrate Polymers* **2014**, *110*, 405–414, doi:10.1016/j.carbpol.2014.04.044.
147. Vinardell, M.P.; Ugartondo, V.; Mitjans, M. Potential Applications of Antioxidant Lignins from Different Sources. *Industrial Crops and Products* **2008**, *27*, 220–223, doi:10.1016/j.indcrop.2007.07.011.
148. Morganti, P.; Bruno, C.; Guarneri, F.; Cardillo, A.; Del Ciotto, P.; Valenzano, F. Role of Topical and Nutritional Supplement to Modify the Oxidative Stress. *Int J Cosmet Sci* **2002**, *24*, 331–339, doi:10.1046/j.1467-2494.2002.00159.x.
149. Rodrigues, F.; Palmeira-de-Oliveira, A.; das Neves, J.; Sarmento, B.; Amaral, M.H.; Oliveira, M.B. *Medicago Spp.* Extracts as Promising Ingredients for Skin Care Products. *Industrial Crops and Products* **2013**, *49*, 634–644, doi:10.1016/j.indcrop.2013.06.015.
150. Gülçin, İ. Antioxidant Activity of Food Constituents: An Overview. *Arch Toxicol* **2012**, *86*, 345–391, doi:10.1007/s00204-011-0774-2.
151. Pellegrini, N.; Colombi, B.; Salvatore, S.; Brenna, O.V.; Galaverna, G.; Del Rio, D.; Bianchi, M.; Bennett, R.N.; Brighenti, F. Evaluation of Antioxidant Capacity of Some Fruit and Vegetable Foods: Efficiency of Extraction of a Sequence of Solvents. *J. Sci. Food Agric.* **2007**, *87*, 103–111, doi:10.1002/jsfa.2682.
152. Sadhasivam, G.; Muthuvel, A.; Pachaiyappan, A.; Thangavel, B. Isolation and Characterization of Hyaluronic Acid from the Liver of Marine Stingray *Aetobatus Narinari*. *International Journal of Biological Macromolecules* **2013**, *54*, 84–89, doi:10.1016/j.ijbiomac.2012.11.028.
153. Gérin, S.; Mathy, G.; Franck, F. Modeling the Dependence of Respiration and Photosynthesis upon Light, Acetate, Carbon Dioxide, Nitrate and Ammonium in *Chlamydomonas Reinhardtii* Using Design of Experiments and Multiple Regression. *BMC Syst Biol* **2014**, *8*, 96, doi:10.1186/s12918-014-0096-0.
154. Smith, R.T.; Bangert, K.; Wilkinson, S.J.; Gilmour, D.J. Synergistic Carbon Metabolism in a Fast Growing Mixotrophic Freshwater Microalgal Species Micractinium Inermum. *Biomass and Bioenergy* **2015**, *82*, 73–86, doi:10.1016/j.biombioe.2015.04.023.
155. Kroen, W.K.; Rayburn, W.R. Influence of Growth Status and Nutrients on Extracellular Polysaccharide Synthesis by the Soil Alga *Chlamydomonas Mexicana* (Chlorophyceae). *Journal of Phycology* **1984**, *20*, 253–257, doi:10.1111/j.0022-3646.1984.00253.x.

156. Lee, H.G.; Cowman, M.K. An Agarose Gel Electrophoretic Method for Analysis of Hyaluronan Molecular Weight Distribution. *Analytical Biochemistry* **1994**, *219*, 278–287, doi:10.1006/abio.1994.1267.
157. Fisher, G.J. Cancer Resistance, High Molecular Weight Hyaluronic Acid, and Longevity. *J. Cell Commun. Signal.* **2015**, *9*, 91–92, doi:10.1007/s12079-015-0278-6.
158. Schiano di Visconte, G.; Allen, M.J.; Spicer, A. New Insights from the High-Resolution Monitoring of Microalgae–Virus Infection Dynamics. *Viruses* **2022**, *14*, 466, doi:10.3390/v14030466.
159. Cooper, P.D. The Plaque Assay of Animal Viruses. In *Advances in Virus Research*; Smith, K.M., Lauffer, M.A., Eds.; Academic Press, 1962; Vol. 8, pp. 319–378.
160. LaBarre, D.D.; Lowy, R.J. Improvements in Methods for Calculating Virus Titer Estimates from TCID50 and Plaque Assays. *Journal of Virological Methods* **2001**, *96*, 107–126, doi:10.1016/S0166-0934(01)00316-0.
161. Thiel, J.F.; Smith, K.O. Fluorescent Focus Assay of Viruses on Cell Monolayers in Plastic Petri Plates. *Proceedings of the Society for Experimental Biology and Medicine* **1967**, *125*, 892–895, doi:10.3181/00379727-125-32232.
162. Clark, D.A.; Ait-Khaled, M.; Wheeler, A.C.; Kidd, I.M.; McLaughlin, J.E.; Johnson, M.A.; Griffiths, P.D.; Emery, V.C. Quantification of Human Herpesvirus 6 in Immunocompetent Persons and Post-Mortem Tissues from AIDS Patients by PCR. *Journal of General Virology* **1996**, *77*, 2271–2275, doi:10.1099/0022-1317-77-9-2271.
163. Daisy, J.A.; Lief, F.S.; Friedman, H.M. Rapid Diagnosis of Influenza A Infection by Direct Immunofluorescence of Nasopharyngeal Aspirates in Adults. *Journal of Clinical Microbiology* **1979**, *9*, 688–692.
164. Fontaine-Rodriguez, E.C.; Taylor, T.J.; Olesky, M.; Knipe, D.M. Proteomics of Herpes Simplex Virus Infected Cell Protein 27: Association with Translation Initiation Factors. *Virology* **2004**, *330*, 487–492, doi:10.1016/j.virol.2004.10.002.
165. Edwards, M.L.; Cooper, J.I. Plant Virus Detection Using a New Form of Indirect ELISA. *Journal of Virological Methods* **1985**, *11*, 309–319, doi:10.1016/0166-0934(85)90024-2.
166. Chou, T.-C.; Hsu, W.; Wang, C.-H.; Chen, Y.-J.; Fang, J.-M. Rapid and Specific Influenza Virus Detection by Functionalized Magnetic Nanoparticles and Mass Spectrometry. *Journal of Nanobiotechnology* **2011**, *9*, 52, doi:10.1186/1477-3155-9-52.
167. Ho, T.; Tzanetakis, I.E. Development of a Virus Detection and Discovery Pipeline Using next Generation Sequencing. *Virology* **2014**, *471–473*, 54–60, doi:10.1016/j.virol.2014.09.019.
168. Kohl, C.; Brinkmann, A.; Dabrowski, P.W.; Radonić, A.; Nitsche, A.; Kurth, A. Protocol for Metagenomic Virus Detection in Clinical Specimens. *Emerg Infect Dis* **2015**, *21*, 48–57, doi:10.3201/eid2101.140766.
169. Brussaard, C.P.D.; Marie, D.; Bratbak, G. Flow Cytometric Detection of Viruses. *Journal of Virological Methods* **2000**, *85*, 175–182, doi:10.1016/S0166-0934(99)00167-6.

170. Debrick, K.S. Quantitative Assay for Plant Viruses Using Serologically Specific Electron Microscopy. *Virology* **1973**, *56*, 652–653, doi:10.1016/0042-6822(73)90068-8.
171. Kessler, M.K.; Collins, A.M.; Jones, H.; Timlin, J.A.; Carney, L.T.; Lane, T.W. Tracking Early Infection Events of the *Chlorella* Virus PBCV-1 with Hyperspectral Confocal Microscopy. *Microsc Microanal* **2012**, *18*, 226–227, doi:10.1017/S143192761200298X.
172. Van Etten, J.L.; Burbank, D.E.; Kuczmarski, D.; Meints, R.H. Virus Infection of Culturable *Chlorella*-Like Algae and Development of a Plaque Assay. *Science* **1983**, *219*, 994–996, doi:10.1126/science.219.4587.994.
173. Mojica, K.; Evans, C.; Brussaard, C. Flow Cytometric Enumeration of Marine Viral Populations at Low Abundances. *Aquat. Microb. Ecol.* **2014**, *71*, 203–209, doi:10.3354/ame01672.
174. Culture Collection of Algae and Protozoa (CCAP). Https://Www.Ccap.Ac.Uk/ (Accessed on 27 January 2022).
175. Nichols, H.W.; Bold, H.C. Trichosarcina Polymorpha Gen. et Sp. Nov. *Journal of Phycology* **1965**, *1*, 34–38, doi:10.1111/j.1529-8817.1965.tb04552.x.
176. The Algem Photobioreactor | Algenuity Available online: https://www.algenuity.com/algem (accessed on 12 January 2021).
177. Noel, E.A.; Weeks, D.P.; Van Etten, J.L. *Pursuit of Chlorovirus Genetic Transformation and CRISPR/Cas9-Mediated Gene Editing*; Molecular Biology, 2021;
178. Evans, C.; Pond, D.W.; Wilson, W.H. Changes in Emiliania Huxleyi Fatty Acid Profiles during Infection with E. Huxleyi Virus 86: Physiological and Ecological Implications. *Aquatic Microbial Ecology* **2009**, *55*, 219–228, doi:10.3354/ame01295.
179. Van Etten, J.L.; Burbank, D.E.; Schuster, A.M.; Meints, R.H. Lytic Viruses Infecting a *Chlorella*-like Alga. *Virology* **1985**, *140*, 135–143, doi:10.1016/0042-6822(85)90452-0.
180. Chen, B.J.; Lamb, R.A. Mechanisms for Enveloped Virus Budding: Can Some Viruses Do without an ESCRT? *Virology* **2008**, *372*, 221–232, doi:10.1016/j.virol.2007.11.008.
181. Vincent, F.; Sheyn, U.; Porat, Z.; Schatz, D.; Vardi, A. Visualizing Active Viral Infection Reveals Diverse Cell Fates in Synchronized Algal Bloom Demise. *PNAS* **2021**, *118*, doi:10.1073/pnas.2021586118.
182. Jover, L.F.; Effler, T.C.; Buchan, A.; Wilhelm, S.W.; Weitz, J.S. The Elemental Composition of Virus Particles: Implications for Marine Biogeochemical Cycles. *Nat Rev Microbiol* **2014**, *12*, 519–528, doi:10.1038/nrmicro3289.
183. Källberg, M.; Wang, H.; Wang, S.; Peng, J.; Wang, Z.; Lu, H.; Xu, J. Template-Based Protein Structure Modeling Using the RaptorX Web Server. *Nat Protoc* **2012**, *7*, 1511–1522, doi:10.1038/nprot.2012.085.
184. 1-Click-Docking by Mcule Https://Mcule.Com/about/ (Accessed on the 24th of February 2022).
185. Kozak, M. The Scanning Model for Translation: An Update. *Journal of Cell Biology* **1989**, *108*, 229–241, doi:10.1083/jcb.108.2.229.
186. PCI-Neo Mammalian Expression Vector, Https://Www.Promega.Com/-/Media/Files/Resources/Protocols/Technical-Bulletins/0/Pci-Neo-

Mammalian-Expression-Vector-Protocol.Pdf?La=en#:~:Text=The%20pCI%2Dneo%20Mammalian%20Expression,Selectable%20marker%20for%20mammalian%20cells (Accessed 1st of March 2022).
187. Kawasaki, T.; Tanaka, M.; Fujie, M.; Usami, S.; Sakai, K.; Yamada, T. Chitin Synthesis in Chlorovirus CVK2-Infected *Chlorella* Cells. *Virology* **2002**, *302*, 123–131, doi:10.1006/viro.2002.1572.
188. Rakkhumkaew, N.; Kawasaki, T.; Fujie, M.; Yamada, T. Prolonged Synthesis of Hyaluronan by *Chlorella* Cells Infected with Chloroviruses. *Journal of Bioscience and Bioengineering* **2013**, *115*, 527–531, doi:10.1016/j.jbiosc.2012.11.012.
189. Hyaluronan Quantification with StainsAll Purplejelley. Https://Www.Biocolor.Co.Uk/Site/Wp-Content/Uploads/2016/04/PurpleJelley-Manual-Webopt.Pdf (Accessed the Second of March 2022).
190. Chuchird, N.; Hiramatsu, S.; Sugimoto, I.; Fujie, M.; Usami, S.; Yamada, T. Digestion of *Chlorella* Cells by Chlorovirus-Encoded Polysaccharide Degrading Enzymes. *Microb. Environ.* **2001**, *16*, 206–212, doi:10.1264/jsme2.2001.206.
191. Darienko, T.; Gustavs, L.; Eggert, A.; Wolf, W.; Pröschold, T. Evaluating the Species Boundaries of Green Microalgae (Coccomyxa, Trebouxiophyceae, Chlorophyta) Using Integrative Taxonomy and DNA Barcoding with Further Implications for the Species Identification in Environmental Samples. *PLOS ONE* **2015**, *10*, e0127838, doi:10.1371/journal.pone.0127838.
192. Baldwin, B.G.; Sanderson, M.J.; Porter, J.M.; Wojciechowski, M.F.; Campbell, C.S.; Donoghue, M.J. The Its Region of Nuclear Ribosomal DNA: A Valuable Source of Evidence on Angiosperm Phylogeny. *Annals of the Missouri Botanical Garden* **1995**, *82*, 247–277, doi:10.2307/2399880.
193. Rakkhumkaew, N.; Kawasaki, T.; Fujie, M.; Yamada, T. Chitin Synthesis by *Chlorella* Cells Infected by Chloroviruses: Enhancement by Adopting a Slow-Growing Virus and Treatment with Aphidicolin. *Journal of Bioscience and Bioengineering* **2018**, *125*, 311–315, doi:10.1016/j.jbiosc.2017.10.002.
194. Faulkes, C.G.; Davies, K.T.J.; Rossiter, S.J.; Bennett, N.C. Molecular Evolution of the Hyaluronan Synthase 2 Gene in Mammals: Implications for Adaptations to the Subterranean Niche and Cancer Resistance. *Biol Lett* **2015**, *11*, doi:10.1098/rsbl.2015.0185.
195. Falaleeva, M.; Zurek, O.W.; Watkins, R.L.; Reed, R.W.; Ali, H.; Sumby, P.; Voyich, J.M.; Korotkova, N. Transcription of the Streptococcus Pyogenes Hyaluronic Acid Capsule Biosynthesis Operon Is Regulated by Previously Unknown Upstream Elements. *Infect Immun* **2014**, *82*, 5293–5307, doi:10.1128/IAI.02035-14.
196. Zhang, J.; Liu, L.; Chen, F. Production and Characterization of Exopolysaccharides from *Chlorella zofingiensis* and *Chlorella vulgaris* with Anti-Colorectal Cancer Activity. *International Journal of Biological Macromolecules* **2019**, *134*, 976–983, doi:10.1016/j.ijbiomac.2019.05.117.
197. Rossi, F.; De Philippis, R. Exocellular Polysaccharides in Microalgae and Cyanobacteria: Chemical Features, Role and Enzymes and Genes Involved in Their Biosynthesis. In *The Physiology of Microalgae*; Borowitzka, M.A.,

Beardall, J., Raven, J.A., Eds.; Developments in Applied Phycology; Springer International Publishing: Cham, 2016; pp. 565–590 ISBN 978-3-319-24945-2.
198. Im, J.-H.; Song, J.-M.; Kang, J.-H.; Kang, D.-J. Optimization of Medium Components for High-Molecular-Weight Hyaluronic Acid Production by Streptococcus Sp. ID9102 via a Statistical Approach. *J Ind Microbiol Biotechnol* **2009**, *36*, 1337–1344, doi:10.1007/s10295-009-0618-8.
199. Graydon, Ingredient Highlight: *Chlorella* Https://Graydonskincare.Com/Blogs/Mindfulbeauty/Ingredient-Highlight-*Chlorella* (Accessed on 17 February 2022).
200. Takeda, H. Sugar Composition of the Cell Wall and the Taxonomy of *Chlorella* (Chlorophyceae). *Journal of Phycology* **1991**, *27*, 224–232, doi:https://doi.org/10.1111/j.0022-3646.1991.00224.x.
201. Canelli, G.; Martínez, P.M.; Austin, S.; Ambühl, M.E.; Dionisi, F.; Bolten, C.J.; Carpine, R.; Neutsch, L.; Mathys, A. Biochemical and Morphological Characterization of Heterotrophic *Crypthecodinium cohnii* and *Chlorella vulgaris* Cell Walls. *J. Agric. Food Chem.* **2021**, 10.
202. Zheng, H.; Yin, J.; Gao, Z.; Huang, H.; Ji, X.; Dou, C. Disruption of *Chlorella vulgaris* Cells for the Release of Biodiesel-Producing Lipids: A Comparison of Grinding, Ultrasonication, Bead Milling, Enzymatic Lysis, and Microwaves. *Appl Biochem Biotechnol* **2011**, *164*, 1215–1224, doi:10.1007/s12010-011-9207-1.
203. Canelli, G.; Murciano Martínez, P.; Maude Hauser, B.; Kuster, I.; Rohfritsch, Z.; Dionisi, F.; Bolten, C.J.; Neutsch, L.; Mathys, A. Tailored Enzymatic Treatment of *Chlorella vulgaris* Cell Wall Leads to Effective Disruption While Preserving Oxidative Stability. *LWT* **2021**, *143*, 111157, doi:10.1016/j.lwt.2021.111157.
204. Coelho, D.; Lopes, P.A.; Cardoso, V.; Ponte, P.; Brás, J.; Madeira, M.S.; Alfaia, C.M.; Bandarra, N.M.; Gerken, H.G.; Fontes, C.M.G.A.; et al. Novel Combination of Feed Enzymes to Improve the Degradation of *Chlorella* Vulgaris Recalcitrant Cell Wall. *Sci Rep* **2019**, *9*, 5382, doi:10.1038/s41598-019-41775-0.
205. Sun, L.; Gurnon, J.R.; Adams, B.J.; Graves, M.V.; Etten, J.L.V. Characterization of a Beta-1,3-Glucanase Encoded by *Chlorella* Virus Pbcv-1. 10.
206. Sun, L.; Adams, B.; Gurnon, J.R.; Ye, Y.; Van Etten, J.L. Characterization of Two Chitinase Genes and One Chitosanase Gene Encoded by *Chlorella* Virus PBCV-1. *Virology* **1999**, *263*, 376–387, doi:10.1006/viro.1999.9958.
207. Ali, A.M.M.; Kawasaki, T.; Yamada, T. Characterization of a Chitinase Gene Encoded by Virus-Sensitive *Chlorella* Strains and Expressed during Virus Infection. **2007**, *10*, 16.
208. Sugimoto, I.; Hiramatsu, S.; Murakami, D.; Fujie, M.; Usami, S.; Yamada, T. Algal-Lytic Activities Encoded by *Chlorella* Virus CVK2. *Virology* **2000**, *277*, 119–126, doi:10.1006/viro.2000.0590.
209. Culture Collection of Algae at the University of Texas at Austin (UTEX). Https://Utex.Org/ (Archived on 21th of October 2021).
210. Agarkova, I.; Dunigan, D.; Gurnon, J.; Greiner, T.; Barres, J.; Thiel, G.; Van Etten, J.L. Chlorovirus-Mediated Membrane Depolarization of *Chlorella*

Alters Secondary Active Transport of Solutes. *JVI* **2008**, *82*, 12181–12190, doi:10.1128/JVI.01687-08.
211. Engler, C.; Marillonnet, S. Golden Gate Cloning. In *DNA Cloning and Assembly Methods*; Valla, S., Lale, R., Eds.; Methods in Molecular Biology; Humana Press: Totowa, NJ, 2014; Vol. 1116, pp. 119–131 ISBN 978-1-62703-763-1.
212. Gibson, D.G.; Young, L.; Chuang, R.-Y.; Venter, J.C.; Hutchison, C.A.; Smith, H.O. Enzymatic Assembly of DNA Molecules up to Several Hundred Kilobases. *Nat Methods* **2009**, *6*, 343–345, doi:10.1038/nmeth.1318.
213. Weber, S.; Grande, P.M.; Blank, L.M.; Klose, H. Insights into Cell Wall Disintegration of *Chlorella vulgaris*. *PLoS One* **2022**, *17*, e0262500, doi:10.1371/journal.pone.0262500.
214. Rosen, B.H.; Berliner, M.D.; Petro, M.J. Protoplast Induction in *Chlorella pyrenoidosa*. *Plant Science* **1985**, *41*, 23–30, doi:10.1016/0168-9452(85)90061-5.
215. Suda, K.; Tanji, Y.; Hori, K.; Unno, H. Evidence for a Novel *Chlorella* Virus-Encoded Alginate Lyase. *FEMS Microbiology Letters* 9.
216. Yu, F.; Zhang, F.; Luan, T.; Zhang, Z.; Zhang, H. Rheological Studies of Hyaluronan Solutions Based on the Scaling Law and Constitutive Models. *Polymer* **2014**, *55*, 295–301, doi:10.1016/j.polymer.2013.11.047.
217. Takashi Y. Production of hyaluronic acid and chitin by *Chlorella* culture 2007.
218. Sze, J.H.; Brownlie, J.C.; Love, C.A. Biotechnological Production of Hyaluronic Acid: A Mini Review. *3 Biotech* **2016**, *6*, 67, doi:10.1007/s13205-016-0379-9.
219. Yamada, T. Method for Separating/Purifying Hyaluronic Acid and/or Chitin 2004.
220. Loganathan, B.G.; Orsat, V.; Lefsrud, M. Evaluation and Interpretation of Growth, Biomass Productivity and Lutein Content of *Chlorella variabilis* on Various Media. *Journal of Environmental Chemical Engineering* **2020**, *8*, 103750, doi:10.1016/j.jece.2020.103750.